Department of Energy
Washington, DC 20585

QA: N/A
DOCKET NUMBER 63-001

June 9, 2009

ATTN: Document Control Desk
Christian Jacobs, Senior Project Manager
Project Management Branch Section B
Division of High-Level Waste Repository Safety
Office of Nuclear Material Safety and Safeguards
U.S. Nuclear Regulatory Commission
EBB-2B2
11545 Rockville Pike
Rockville, MD 20852-2738

YUCCA MOUNTAIN – REQUEST FOR ADDITIONAL INFORMATION –VOLUME 2, CHAPTER 2.1.1.4, SET 2 (DEPARTMENT OF ENERGY'S SAFETY ANALYSIS REPORT SECTION 1.7) – Passive Reliability of Containers – Submittal of Reference Document

Reference: Ltr, Jacobs to Williams, dtd 06/03/09, "Yucca Mountain - Request For Additional Information – Volume 2, Chapter 2.1.1.4, Set 2 & Set 3 (Department Of Energy's Safety Analysis Report Section 1.7)"

The purpose of this letter is to transmit the reference, *Seismic and Structural Container Analyses for the PCSA,* in response to Request for Additional Information (RAI) Number 1 of Set 2 of the above-referenced letter. The document, which is available on the Licensing Support Network, is provided in hard copy. A compact disk is also provided, which contains the electronic attachments to the document. The electronic attachments are not compatible with electronic information exchange (EIE) requirements, but are part of the reference requested by NRC. The electronic attachments will be made available to the public upon request.

There are no commitments identified in this submittal. If you have any questions regarding this letter, please contact me at (202) 586-9620, or by email to jeff.williams@rw.doe.gov.

Jeffrey R. Williams, Supervisor
Licensing Interactions Branch
Regulatory Affairs Division
Office of Technical Management

OTM: SEG-0803

NMSS25

Enclosure:
BSC (Bechtel SAIC Company) 2008. *Seismic and Structural Container Analyses for the PCSA.* 000-PSA-MGR0-02100-000-00A. Las Vegas, Nevada: Bechtel SAIC Company. ACC: ENG.20080220.0003. [Document in hard copy and Electronic Attachments on Compact Disk].

cc w/ encls:
Bob Brient, CNWRA, San Antonio, TX

cc w/o encls:
J. C. Chen, NRC, Rockville, MD
J. R. Davis, NRC, Rockville, MD
R. K. Johnson, NRC, Rockville, MD
A. S. Mohseni, NRC, Rockville, MD
N. K. Stablein, NRC, Rockville, MD
D. B. Spitzberg, NRC, Arlington, TX
J. D. Parrott, NRC, Las Vegas, NV
L. M. Willoughby, NRC, Las Vegas, NV
Jack Sulima, NRC, Rockville, MD
Christian Jacobs, NRC, Rockville, MD
Lola Gomez, NRC, Rockville, MD
W. C. Patrick, CNWRA, San Antonio, TX
Budhi Sagar, CNWRA, San Antonio, TX
Bob Brient, CNWRA, San Antonio, TX
Rod McCullum, NEI, Washington, DC
B. J. Garrick, NWTRB, Arlington, VA
Bruce Breslow, State of Nevada, Carson City, NV
Alan Kalt, Churchill County, Fallon, NV
Irene Navis, Clark County, Las Vegas, NV
Ed Mueller, Esmeralda County, Goldfield, NV
Ron Damele, Eureka County, Eureka, NV
Richard Cervantes, Inyo County, Independence, CA
Chuck Chapin, Lander County, Battle Mountain, NV
Connie Simkins, Lincoln County, Pioche, NV
Linda Mathias, Mineral County, Hawthorne, NV
Darrell Lacy, Nye County, Pahrump, NV
Jeff VanNeil, Nye County, Pahrump, NV
Joe Kennedy, Timbisha Shoshone Tribe, Death Valley, CA
Mike Simon, White Pine County, Ely, NV
K. W. Bell, California Energy Commission, Sacramento, CA
Barbara Byron, California Energy Commission, Sacramento, CA
Susan Durbin, California Attorney General's Office, Sacramento, CA
Charles Fitzpatrick, Egan, Fitzpatrick, Malsch, PLLC

BSC

Design Calculation or Analysis Cover Sheet

Complete only applicable items.

1. QA: QA
2. Page 1

3. System	4. Document Identifier
Monitored Geologic Repository	000-PSA-MGR0-02100-000-00A

5. Title

Seismic and Structural Container Analyses for the PCSA

6. Group

PCSA

7. Document Status Designation

☐ Preliminary ☒ Committed ☐ Confirmed ☐ Cancelled/Superseded

8. Notes/Comments

Steve Alves, under the supervision of Mike Gerhard, conducted the seismic analyses (Section 6.2).
Analysts Josh Wen, Gerry Mok, and Lisle Hagler conducted the LS-DYNA FEA calculations of the Max EPS of the canisters (Sections 6.3.1, 6.3.2, and 6.3.3), under the supervision of Ed Jones and of Mike Gerhard.
Analysts Souheil Ezzedine and Yun Duan conducted the MATLAB spreadsheet calculations for the probability of canister failure (Section 6.3.7).
Steven Carlson was the lead checker and checked the entire document. Steve Alves was supervised by, and assisted, Steve Carlson in the checking of Section 6.3.

Attachments	Total Number of Pages
Attachment 1: Reserved	1
Attachment 2: Files for Seismic Analyses of Emplaced Waste Packages	3
Attachment 3: Files for Structural Failure Analyses of Containers Subject to Drop-Impact Loads	2

RECORD OF REVISIONS

9. No.	10. Reason For Revision	11. Total # of Pgs.	12. Last Pg. #	13. Originator (Print/Sign/Date)	14. Checker (Print/Sign/Date)	15. EGS (Print/Sign/Date)	16. Approved/Accepted (Print/Sign/Date)
00A	Initial issue	111	111	Thomas A. Buscheck Thomas A. Buscheck 2/19/08	Steven R. Carlson Steven R Carlson 2/19/08	Michael V. Frank 2/19/08	Mark R. Wisenberg 2/19/2008

DISCLAIMER

The calculations contained in this document were developed by Bechtel SAIC Company, LLC (BSC) and are intended solely for the use of BSC in its work for the Yucca Mountain Project.

CONTENTS

Page

ACRONYMS 9
1. PURPOSE 11
1.1 RESERVED 11
1.2 SEISMIC ANALYSES OF EMPLACED WASTE PACKAGES 11
1.3 STRUCTURAL FAILURE ANALYSES OF CONTAINERS SUBJECT TO DROP-IMPACT LOADS 12
2. REFERENCES 13
2.1 PROJECT PROCEDURES/DIRECTIVES 13
2.2 DESIGN INPUTS 13
2.3 DESIGN CONSTRAINTS 16
2.4 DESIGN OUTPUTS 16
3. ASSUMPTIONS 17
3.1 ASSUMPTIONS REQUIRING VERIFICATION 17
3.2 ASSUMPTIONS NOT REQUIRING VERIFICATION 17
4. METHODOLOGY 20
4.1 QUALITY ASSURANCE 20
4.2 USE OF SOFTWARE 20
4.3 CALCULATION APPROACH 21
5. LIST OF ATTACHMENTS 29
6. BODY OF CALCULATION 30
6.1 RESERVED 30
6.2 SEISMIC ANALYSES OF EMPLACED WASTE PACKAGES 30
6.3 STRUCTURAL FAILURE ANALYSES OF CONTAINERS SUBJECT TO DROP-IMPACT LOADS 34
7. RESULTS AND CONCLUSIONS 104
7.1 RESERVED 104
7.2 SEISMIC ANALYSES OF EMPLACED WASTE PACKAGES 104
7.3 STRUCTURAL FAILURE ANALYSES OF CONTAINERS SUBJECT TO DROP-IMPACT LOADS 104
ATTACHMENT 1: RESERVED 106
ATTACHMENT 2: FILES FOR SEISMIC ANALYSES OF EMPLACED WASTE PACKAGES 107
ATTACHMENT 3: FILES FOR STRUCTURAL FAILURE ANALYSES OF CONTAINERS SUBJECT TO DROP-IMPACT LOADS 110

FIGURES

Page

6.3.1-1. The Structural Components of SNF Canister within Aging Overpack....38

6.3.1-2. Finite Element Analysis (FEA) Model Representation of Structural Components of SNF Canister within Aging Overpack....38

6.3.1-3. Max EPS for SNF Canister within Aging Overpack Resulting from a 3-ft Drop onto End with Vertical Orientation....39

6.3.1-4. Max EPS History for SNF Canister within Aging Overpack Resulting from a 3-ft Drop onto End with Vertical Orientation....40

6.3.1-5. Side View of Max EPS for SNF Canister within Aging Overpack Subjected to Slapdown Impact to Rigid Ground from a Vertical Orientation and 2.5-MPH Horizontal Velocity....41

6.3.1-6. Bottom View of Max EPS for SNF Canister within Aging Overpack Subjected to Slapdown Impact to Rigid Ground from a Vertical Orientation and 2.5-MPH Horizontal Velocity....42

6.3.1-7. Max EPS History for SNF Canister within Aging Overpack Subjected to Slapdown Impact to Rigid Ground from a Vertical Orientation and 2.5-MPH Horizontal Velocity....43

6.3.2-1. Structural Components of a SNF Canister inside a Transportation Cask....45

6.3.2-2. Finite Element Analysis (FEA) Model Representation of Structural Components of the SNF Canister inside a Transportation Cask....46

6.3.2.1-1. Max EPS for SNF Canister inside a Transportation Cask Subjected to 12-ft Drop with 4-degree Off-Vertical Orientation....47

6.3.2.1-2. Max EPS History for SNF Canister inside a Transportation Cask Subjected to a 12-ft Drop with 4-degree Off-Vertical Orientation....48

6.3.2.1-3. Max EPS for SNF Canister inside a Transportation Cask Subjected to 13.1-ft Drop with 4-degree Off-Vertical Orientation....49

6.3.2.1-4. Max EPS History for SNF Canister inside a Transportation Cask Subjected to a 13.1-ft Drop with 4-degree Off-Vertical Orientation....50

6.3.2.1-5. Max EPS for SNF Canister inside a Transportation Cask Subjected to 30-ft Drop with 4-degree Off-Vertical Orientation....51

6.3.2.1-6. Max EPS History for SNF Canister inside a Transportation Cask Subjected to a 30-ft Drop with 4-degree Off-Vertical Orientation....52

6.3.2.1-7. Max EPS for the Structural Body of the Transportation Cask Subjected to 30-ft Drop with 4-degree Off-Vertical Orientation....53

6.3.2.2-1. Max EPS for SNF Canister inside a Transportation Cask Subjected to 13.1-ft Drop with 4-degree Off-Vertical Orientation and Approximated Slapdown....54

6.3.2.2-2. Max EPS History for SNF Canister inside a Transportation Cask Subjected to a 13.1-ft Drop with 4-degree Off-Vertical Orientation and Approximated Slapdown....55

FIGURES (Continued)

Page

6.3.2.2-3. Max EPS for SNF Canister inside a Transportation Cask Subjected to an Approximated Slapdown 56

6.3.2.2-4. Max EPS History for SNF Canister inside a Transportation Cask Subjected to an Approximated Slapdown 57

6.3.2.3-1. Max EPS for SNF Canister inside a Transportation Cask Subjected to a 6-ft Drop onto Side with 3-degree Off-Horizontal Orientation 58

6.3.2.3-2. Max EPS History for SNF Canister inside a Transportation Cask Subjected to a 6-ft Drop onto Side with 3-degree Off-Horizontal Orientation 59

6.3.2.4-1. Max EPS for SNF Canister inside a Transportation Cask Subjected to a 10-ft Drop of a 10-metric-ton Load onto the Top of the Cask 60

6.3.2.4-2. Max EPS History for SNF Canister inside a Transportation Cask Subjected to a 10-ft Drop of a 10-metric-ton Load onto the Top of the Cask 61

6.3.2.5-1. Max EPS for SNF Canister inside a Transportation Cask Subjected to a 30-ft End Drop with Vertical Orientation 62

6.3.2.5-2. Max EPS History for SNF Canister inside a Transportation Cask Subjected to a 30-ft End Drop with Vertical Orientation 63

6.3.2.5-3. Max EPS for SNF Canister inside a Transportation Cask Subjected to a 30-ft End Drop with 45-degree Off-Vertical Orientation 64

6.3.2.5-4. Max EPS History for SNF Canister inside a Transportation Cask Subjected to a 30-ft End Drop with 45-degree Off-Vertical Orientation 65

6.3.2.5-5. Max EPS for SNF Canister inside a Transportation Cask Subjected to a 30-ft End Drop with the Center of Gravity over the Corner of Cask 66

6.3.2.5-6. Max EPS History for SNF Canister inside a Transportation Cask Subjected to a 30-ft End Drop with the Center of Gravity over the Corner of Cask 67

6.3.2.5-7. Max EPS for the Structural Body of the Transportation Cask Subjected to a 30-ft End Drop with 45-degree Off-Vertical Orientation 68

6.3.2.5-8. Max EPS for the Structural Body of the Transportation Cask Subjected to a 30-ft End Drop with the Center of Gravity over the Corner of Cask 69

6.3.3-1. Structural Components of the Dual Purpose Canister 71

6.3.3-2. Finite Element Analysis (FEA) Model Representation of Structural Components of the Dual Purpose Canister 72

6.3.3.1-1. Max EPS for Dual Purpose Canister Subjected to a 32.5-ft Drop onto End with Vertical Orientation 73

6.3.3.1-2. Max EPS History for Dual Purpose Canister Subjected to a 32.5-ft Drop onto End with Vertical Orientation 74

6.3.3.1-3. Max EPS for Dual Purpose Canister Subjected to a 32.5-ft Drop onto End with Vertical Orientation 75

6.3.3.1-4. Max EPS History for Dual Purpose Canister Subjected to a 40-ft Drop onto End with Vertical Orientation 76

FIGURES (Continued)

Page

6.3.3.2-1. Max EPS for Dual Purpose Canister Subjected to a 23-ft Drop onto End with 4-degree Off-Vertical Orientation 77

6.3.3.2-2. Max EPS History for Dual Purpose Canister Subjected to a 23-ft Drop onto End with 4-degree Off-Vertical Orientation 78

6.3.3.2-3. Max EPS for Dual Purpose Canister Subjected to a 10-ft Drop onto End with 4-degree Off-Vertical Orientation 79

6.3.3.2-4. Max EPS History for Dual Purpose Canister Subjected to a 10-ft Drop onto End with 4-degree Off-Vertical Orientation 80

6.3.3.2-5. Max EPS for Dual Purpose Canister Subjected to a 5-ft Drop onto End with 4-degree Off-Vertical Orientation 81

6.3.3.2-6. Max EPS History for Dual Purpose Canister Subjected to a 5-ft Drop onto End with 4-degree Off-Vertical Orientation 82

6.3.3.3-1. Max EPS for Dual Purpose Canister Subjected to a 40-ft/min Horizontal Collision with a Rigid Wall 83

6.3.3.3-2. Max EPS History for Dual Purpose Canister Subjected to a 40-ft/min Horizontal Collision with a Rigid Wall 84

6.3.3.4-1. Max EPS for Dual Purpose Canister (DPC) Subjected to a 10-ft Drop of a 10-metric-ton Load onto Top of Canister 85

6.3.3.4-2. Max EPS History for Dual Purpose Canister Subjected to the Impact from a 10-ft Drop of a 10-metric-ton Mass onto Top of Canister 86

6.3.3.6-1. Max EPS Plotted as a Function of Shell Thickness and Bottom Plate Thickness for Dual Purpose Canister Subjected to a 23-ft End Drop with 4-degree Off-Vertical Orientation 90

6.3.7-1. A Schematic of Relationship between Max EPS, Fragility Curve, and Probability of Failure 91

6.3.7-2. Histogram of Engineering Elongation Based on Ref. 2.2.23 94

6.3.7-3. Original and Shifted Cumulative Distribution Function (CDF) of Capacity (or Fragility) Curves Plotted as a Function of True Strain 95

TABLES

Page

4.3.3-1a. Container Configurations and Loading Conditions 24

4.3.3-1b. Sensitivity Studies of Hourglass Control, Friction Coefficient, and Mesh Density for Dual Purpose Canisters Subject to 23-ft End Drop, with 4-degree Off-Vertical Orientation 25

4.3.3-1c. Shell- and Bottom-Lid-Thickness Sensitivity Study Cases for Dual Purpose Canisters Subject to 23-ft End Drop with 4-degree Off-Vertical Orientation 25

4.3.3-2. Key Structural Features for Representative Canister and Typical Canisters 28

4.3.3-3. Key Structural Features for Representative Cask and Typical Casks 28

6.2-1. Probability of Damage for TAD-Bearing Waste Package as a Function of PGV and RST 31

6.2-2. Probability of Damage for Codisposal Waste Package as a Function of PGV and RST 31

6.2-3. Probability of Contact for TAD-Bearing and Codisposal Waste Packages as a Function of PGV, Determined for Individual Realizations 33

6.3-1. Static and Kinetic Coefficient of Friction for Contacting Surfaces for Aging Overpack 34

6.3-2. Static and Kinetic Coefficient of Friction for Contacting Surfaces for Transportation Cask 34

6.3-3. Static and Kinetic Coefficient of Friction for Contacting Surfaces for Dual Purpose Canister 35

6.3.1-1. Dimensions and Materials of the Structural Components of Aging Overpack 35

6.3.1-2. Material Properties of the Reinforcing Steel in the Concrete of the Aging Overpack (AO) Cell 36

6.3.1-3. Material Properties of the Concrete of the Aging Overpack (AO) Cell 36

6.3.1-4. Scale Factor vs. Effective Plastic Strain Curve 37

6.3.1-5. Pressure vs. Volumetric Strain Curve 37

6.3.2-1. Dimensions of Structural Components of the Transportation Cask 44

6.3.2-2. Material Properties of Structural Components of the Transportation Cask 44

6.3.2.5-1. Transportation Cask Contact Angle Sensitivity Study for a 30-ft End Drop 61

6.3.3-1. Dimensions and Materials of Structural Components of Dual Purpose Canister 70

6.3.3-2. Material Properties of Structural Components of Dual Purpose Canister 70

6.3.3.5-1. Summary of Sensitivity Cases for Impact Condition 2a: 23-ft End Drop, with 4-degree Off-Vertical Orientation 87

TABLES (Continued)

Page

6.3.3.6-1. Dual Purpose Canister Shell- and Bottom-Thickness Sensitivity Study for Impact Condition 2a: 23-ft End Drop, with 4-degree Off-Vertical Orientation 89

6.3.7.3-1. Probability of Failure versus True Strain Tabulated for Figure 6.3.7-3 96

6.3.7.6-1. Failure Probabilities with and without Triaxiality Factor, with and without the Fragility Curve Adjustment, for SNF Canister within Aging Overpack 99

6.3.7.6-2. Failure Probabilities with and without Triaxiality Factor, with and without the Fragility Curve Adjustment, for SNF Canister inside Transportation Cask 100

6.3.7.6-3. Failure Probabilities with and without Triaxiality Factor, with and without the Fragility Curve Adjustment, for Dual Purpose Canister 101

6.3.7.6-4. Failure Probabilities without Triaxiality Factor, with and without Fragility Curve Adjustment, for DOE Spent Nuclear Fuel (DSNF) Canisters, Analyzed by Ref. 2.2.37 102

6.3.7.6-5. Failure Probabilities without Triaxiality Factor, with and without Fragility Curve Adjustment, for the Multi-Canister Overpack (MCO), Analyzed by Ref. 2.2.37 103

ACRONYMS

AO	aging overpack
ASME	American Society of Mechanical Engineers
ASTM	American Society for Testing and Materials
BSC	Bechtel SAIC Company, LLC
CDF	cumulative distribution function
COTS	commercial, off-the-shelf (in reference to software)
CSNF	commercial spent nuclear fuel (waste package)
CTM	canister transfer machine
DHLW	defense high-level (radioactive) waste
DOE	U.S. Department of Energy
DPC	dual purpose canister
DR	ductility ratio
DSNF	DOE spent nuclear fuel
DTN	data tracking number
EBS	Engineered Barrier System
EPS	effective (or equivalent) plastic strain
FEA	finite element analysis (model)
IC	Impact Condition (with respect to a drop scenario)
INL	Idaho National Laboratory
LLNL	Lawrence Livermore National Laboratory
MCO	multi-canister overpack
NRC	Nuclear Regulatory Commission
NUREG	Nuclear Regulatory Commission technical report designation
OCB	outer corrosion barrier
PCSA	Preclosure Safety Analysis
PEEQ	peak equivalent plastic strain
PGV	peak ground velocity (refers to H1 horizontal component in each analysis)
QA	Quality Assurance
RST	residual stress threshold
SAE	Society of Automotive Engineers
SNF	spent nuclear fuel

ACRONYMS (Continued)

TAD	transportation, aging, and disposal (canister)
TC	transportation cask
TF	triaxiality factor
TSPA	total system performance assessment
TSPA-LA	total system performance assessment for the license application
WP	waste package
YMP	Yucca Mountain Project

1. PURPOSE

The purpose of these analyses, performed by staff at the Lawrence Livermore National Laboratory (LLNL), working to BSC procedures, is to support the ongoing Preclosure Safety Analysis (PCSA) for the Yucca Mountain Project (YMP). These analyses were performed in concert with the PCSA that quantifies the risk of operations at the multiple handling and transport facilities at the Yucca Mountain geologic repository. The scope of topics addresses potential seismic and structural load impacts on nuclear waste containers at the facilities. Although certain cask and canister designs have been evaluated and approved by the NRC for transportation purposes, and are likely to be handled at Yucca Mountain, the possible array of designs to be handled is not known with high certainty. Thus, the analyses address a representative variety of container configurations for the forms of nuclear waste containers likely to enter the site. As described in Sections 1.2 and 1.3, the purpose of these preclosure analyses falls under two tasks: (1) seismic analyses of emplaced waste packages, and (2) structural failure analyses of containers subject to drop-impact loads.

1.1 RESERVED

1.2 SEISMIC ANALYSES OF EMPLACED WASTE PACKAGES

The purpose of the preclosure seismic assessment presented in this report is to conservatively evaluate the effects of seismic events on emplaced waste packages during the first 100 years of repository life. The focus of the assessment is the probability of damage and the probability of rupture for the waste packages in emplacement drifts due to a seismic event. The probability that the waste packages and pallets will contact the drip shield, or the future location of the drip shield, is also determined. Note that the drip shields will not be emplaced until the end of the preclosure period. Work already performed for postclosure earthquake events is used, and assumptions and judgments are justified. The output is an assessment of the probability of damage, the probability of rupture, and the probability of contact with the drip shield for TAD-bearing and codisposal waste packages subject to a seismic event during the preclosure period of 100 years. Damage is defined as a residual tensile state that will lead to stress corrosion cracking. The probability of damage is based on annual exceedance frequencies from the bounded hazard curve and the probability that a seismic event of specific amplitude will cause damage. The probability of rupture is based on effective plastic strain (EPS) and deformation results from postclosure seismic analyses. The probability that waste packages and pallets will contact the drip shield, determined in the postclosure calculations, provides an estimate of the probability that the waste packages and pallets will be sufficiently displaced to interfere with the emplacement of the drip shield. Similar to the probability of damage, the probability of contact is based on annual exceedance frequencies from the bounded hazard curve and the probability that a seismic event of specific amplitude will cause contact.

These calculations do not assess the effects of rockfall on the waste packages during the portion of the preclosure period before the drip shield has been emplaced.

1.3 STRUCTURAL FAILURE ANALYSES OF CONTAINERS SUBJECT TO DROP-IMPACT LOADS

During various handling and storage activities, containers of spent nuclear fuel (SNF) or of other forms of nuclear waste could be subjected to drops or impacts that may lead to damage and leakage of fission products. The probability of containment failure (excessive leakage rate) for various container and event configurations is required by the PCSA. Currently, the possible array of container designs to be handled is not known with high certainty. Thus, failure analyses for the Yucca Mountain preclosure facilities address a representative array of container types, design parameters, drop parameters, and containment failure modes for the various nuclear waste containers likely to enter the site.

The purpose of the drop-impact-load analysis is to develop the relationship between container type/configuration/drop scenario and the probability of failure (loss of containment). For each identified drop scenario, described by a container type/configuration and drop type/height, a probabilistic response function is developed. For these scenario analyses, the independent variables are the container and drop parameters, and the response/dependent variable is the probability of failure for the given drop scenario. It is important to note that for the purpose of these analyses, containment is only provided by the SNF canister. For containers with an outer shell, such as aging overpack canisters and transportation casks, no containment credit is taken for the integrity of the outer container shell. Thus, the probability of container failure is always equivalent to the probability of SNF canister failure.

2. REFERENCES

2.1 PROJECT PROCEDURES/DIRECTIVES

2.1.1 EG-PRO-3DP-G04B-00037, Rev. 10. 2007. *Calculations and Analyses.* Las Vegas, Nevada. Bechtel SAIC Company. ACC: ENG.20071018.0001.

2.1.2 BSC 2005. *Q-List.* 000-30R-MGR0-00500-000-003. Rev. 003. Las Vegas, Nevada: Bechtel SAIC Company. ACC: ENG.20050929.0008.

2.1.3 BSC (Bechtel SAIC Company) 2007. *Quality Management Directive.* QA-DIR-10, Rev. 2. Las Vegas, Nevada: Bechtel SAIC Company. ACC: DOC.20080103.0002.

2.1.4 IT-PRO-0011, Rev. 7. 2007. *Software Management.* Las Vegas, Nevada: Bechtel SAIC Company. ACC: DOC.20070905.0007.

2.2 DESIGN INPUTS

2.2.1 Reserved.

2.2.2 Livermore Software Technology Corporation. 2003. *LS-DYNA Keyword User's Manual.* Version 970. Livermore, California: Livermore Software Technology Corporation. TIC: 254203. [DIRS 166841]

2.2.3 10 CFR 71. 2007. Energy: Packaging and Transportation of Radioactive Material. Internet Accessible. ACC: MOL.20070829.0114 [DIRS 181967].

2.2.4 Reserved.

2.2.5 Reserved.

2.2.6 Reserved.

2.2.7 Reserved.

2.2.8 Reserved.

2.2.9 Reserved.

2.2.10 Reserved.

2.2.11 Reserved.

2.2.12 Reserved.

2.2.13 Reserved.

2.2.14 Reserved.

2.2.15 Reserved.

2.2.16 Reserved.

2.2.17 Reserved.

2.2.18 Reserved.

2.2.19 Reserved.

2.2.20 Reserved.

2.2.21 Shigley, J.E., Mischke, C.R., and Budynas, R.G. 2004, *Mechanical Engineering Design.* McGraw-Hill, 7th Edition, ISBN: 0072520361. TIC: 259985. [DIRS 184700]

2.2.22 Reserved.

2.2.23 ASM (American Society for Metals) 1976. *Source Book on Stainless Steels (Section I: Stainless Types and their Characteristics).* Metals Park, OH, ASM, p. 3. TIC: 259927. [DIRS 184632]

2.2.24 BSC (Bechtel SAIC Company) 2008. *IED Seismic and Seismic Consequence Data.* 800-IED-MGR0-00701-000-00B. Las Vegas, Nevada: Bechtel SAIC Company. ACC: ENG.20080215.0004.

2.2.25 SNL 2007. *Mechanical Assessment of Degraded Waste Packages and Drip Shields Subject to Vibratory Ground Motion.* MDL-WIS-AC-000001 REV 00. Las Vegas, Nevada: Sandia National Laboratories. ACC: DOC.20070917.0006. [DIRS 178851]

2.2.26 SNL 2007. *Seismic Consequence Abstraction.* MDL-WIS-PA-000003 REV 03. Las Vegas, Nevada: Sandia National Laboratories. ACC: DOC.20070928.0011. [DIRS 176828]

2.2.27 MO0501BPVELEMP.001. Bounded Horizontal Peak Ground Velocity Hazard at the Repository Waste Emplacement Level. Submittal date: 01/11/2005. [DIRS 172682]

2.2.28 MO0703PASDSTAT.001. Statistical Analyses for Seismic Damage Abstractions. Submittal date: 09/21/2007. [DIRS 183148]

2.2.29 LL0704PA048SPC.023. LS-DYNA Kinematic Damaged Area Analyses for the TAD-Bearing Waste Package April 2007. Submittal date: 05/01/2007. [DIRS 180735]

2.2.30 LL0704PA049SPC.024. LS-DYNA Kinematic Damaged Area Analyses for the 5-DHLW/DOE SNF-Long Co-Disposal Waste Package April 2007. Submittal date: 05/01/2007. [DIRS 180736]

2.2.31 LL0703PA029SPC.014. Rupture Probability for the LS-DYNA Kinematic Analyses for the 5-DHLW/DOE SNF-Long Co-Disposal Waste Package and the TAD-Bearing Waste Package. Submittal date: 03/13/2007. [DIRS 179775]

2.2.32 Reserved.

2.2.33 Urquhart, L. 1940. *Civil Engineering Handbook.* 2nd Ed., McGraw-Hill, p. 797. TIC: 259987 [DIRS 184656]

2.2.34 Reserved.

2.2.35 Reserved.

2.2.36 Reserved.

2.2.37 Jones, E. 2008. "Fwd: Scanned Docs" E-mail from E.Jones to duan2@llnl.gov and buscheck1@llnl.gov, January 30, 2008, with attachment ACC: LLR.20080131.0028. [DIRS 184638] (transmittal e-mail for Snow, S.D 2007. *Structural Analysis Results of the DOE SNF Canisters Subjected to the 23-Foot Vertical Repository Drop Event to Support Probabilistic Risk Evaluations.* EDF-NSNF-085. Idaho Falls, ID: Idaho National Laboratory. 3 pages.)

2.2.38 Mendelson, A. 1968. *Plasticity; Theory and Application.* Macmillan, New York, New York. ISBN: 0608116106. 367 p.

2.2.39 Davis, E.A. and Connelly, F.M. 1959. "Stress Distribution and Plastic Deformation in Rotating Cylinders of Strain-Hardening Material," *Journal of Applied Mechanics, 26(1),* pp. 25-30, March 1959. TIC: 258873 [DIRS 178495]

2.2.40 Manjoine, M.J. 1983. "Damage and Failure at Elevated Temperature," *Transactions of the ASME, Journal of Pressure Vessel Technology*, Vol. 105, pp. 58-62, February 1983. TIC: 258853 [DIRS 178496]

2.2.41 DOE 2007. *Software Validation Report (SVR) for: LS-DYNA 971.7600.398-00.* Document ID: 10300-SVR-971.7600.398-00 Intel Itanium2 Redhat Linux 4. Las Vegas, Nevada: U.S. Department of Energy, Office of Repository Development. ACC: MOL.20070122.0233. [DIRS 178852]

2.2.42 LS-DYNA V971.7600.398-00. 2007. RedHat Linux Chaos 3.0. STN 10300-971.7600.398-00. [DIRS 178801]

2.2.43 Shapiro, S. S. and Wilk, M. B. 1965. "An analysis of variance test for normality (complete samples)", *Biometrika*, 52 (3 - 4), pages 591-611. TIC: 259992 [DIRS 184643]

2.2.44 Eadie, W.T., Drijard, D., James, F.E., Roos M., and Sadoulet, B. 1971. *Statistical Methods in Experimental Physics.* Amsterdam: North-Holland, ISBN-10: 0444101179, pp. 269-271.

2.2.45 Fischer, L.E., Chou, C.K., Gerhard, M.A., Kimura, C.Y., Martin, R.W., Mensing, R.W., Mount, M.E., and Witte, M.C. 1987. *Shipping Container Response to Severe Highway and Railway Accident Conditions.* NUREG/CR-4829. Volume 2. Washington, D.C.: U.S. Nuclear Regulatory Commission. ACC: NNA.19900827.0231. [DIRS 104775]

2.2.46 ASME (American Society of Mechanical Engineers) 2006. "Ferrous Material Specification." Section II, Part A of *ASME Boiler and Pressure Vessel Code.* New York, New York: American Society of Mechanical Engineers. TIC: 256479. [DIRS 184155]

2.3 DESIGN CONSTRAINTS

There are no specific design constraints for these analyses.

2.4 DESIGN OUTPUTS

There is no specific design output for these analyses. The analyses, however, support the Preclosure Safety Analysis (PCSA).

3. ASSUMPTIONS

3.1 ASSUMPTIONS REQUIRING VERIFICATION

3.1.1 Reserved

3.1.2 Seismic Analyses of Emplaced Waste Packages

There are no assumptions requiring verification.

3.1.3 Structural Failure Analyses of Containers Subject to Drop-Impact Loads

There are no assumptions requiring verification.

3.2 ASSUMPTIONS NOT REQUIRING VERIFICATION

3.2.1 Reserved

3.2.2 Seismic Analyses of Emplaced Waste Packages

The following assumptions are used in the seismic analyses of emplaced WPs.

3.2.2.1 Use of Postclosure Seismic Analyses for Preclosure Seismic Analyses

Assumption: The results from postclosure seismic analyses can be used to estimate preclosure behavior of WPs and pallets in drifts either with or without the drip shield present. This assumption is used in Section 6.2.

Rationale: The kinematic behavior of the WPs and pallets under a drip shield is analyzed in the postclosure seismic analyses (Ref. 2.2.25). This kinematic behavior is equally valid for the preclosure period after drip shield emplacement. Prior to drip shield emplacement, and for large enough ground motions, the WPs and pallets would have more freedom to separate and may be less likely to impact each other. Thus, analyses with a drip shield would tend to maximize the frequency and intensity of WP-to-WP and WP-to-pallet impacts. It directly follows that this would tend to maximize the estimates of damage and rupture, meaning that the postclosure analyses provide upper bound estimates for the preclosure period. However, it must be understood that the assessments in this document do not include the possibility of drift collapse directly onto WPs prior to drip shield emplacement.

3.2.2.2 Temperature of EBS Components

Assumption: A temperature of 60°C for evaluation of material properties of EBS components provides reasonable results for the preclosure period. This assumption is used in Section 6.2.

Rationale: A temperature of 60°C was used for the postclosure analyses. The repository will reach temperatures above 60°C during the preclosure period, and the relevant material properties, in general, show lower strength at elevated temperatures. However, sensitivity analyses with material properties at elevated temperatures (Section 6.3.2.2.2 of Ref. 2.2.25), demonstrate that

the damaged area of the outer corrosion barrier (OCB) is relatively insensitive to elevated temperature. Thus, using material properties at 60°C provides reasonable results for the preclosure period calculations.

3.2.2.3 Thickness Reduction of Outer Corrosion Barrier

Assumption: The thickness of the outer corrosion barrier is reduced by 2.4 mm. This assumption is used in Section 6.2.

Rationale: This approximation accounts for a reasonable amount of general corrosion during relatively early stages of the postclosure period (the first 10,000 years). For the preclosure period, this amount of general corrosion provides a lower bound for the resistance of the outer corrosion barrier to damage and rupture.

3.2.3 Structural Failure Analyses of Containers Subject to Drop-Impact Loads

3.2.3.1 Impact Surface Conditions

Assumption: The impact-surface conditions for all analyses were assumed to be infinitely stiff and unyielding. The impact surface includes the ground and the falling 10-metric-ton load (Impact Condition 4 in Table 4.3.3-1a). This assumption is used in Section 6.3.

Rationale: The assumed impact surface conditions are conservative, because they result in an upper-bound impact load, and facilitate simplicity and consistency in interpreting results.

3.2.3.2 Probability of Failure Based on a Single Finite Element Brick

Assumption: The probability of failure can be calculated based on the maximum strain for a single finite element brick, obtained from LS-DYNA simulations. This assumption is used in Section 6.3.

Rationale: Fracture propagation takes place on the milliseconds time-scale, and thus propagates across the canister wall thickness very quickly compared to the time-frame of the LS-DYNA simulations. Furthermore, the fragility curve is obtained from the maximum average strain over the thickness of the 2-in-long stainless steel 304 specimens. Although LS-DYNA results provide multiple values of the strain through the thickness of the canister wall (the wall thickness being represented by multiple finite element layers), it is more conservative to use the maximum strain value at a single finite element brick than the average of the multiple values across the wall thickness.

3.2.3.3 Structural Material Properties Evaluated at a Temperature of 100°F

Assumption: The material properties of the structural components of the canisters and casks are evaluated at a temperature of 100°F (37.8°C). This assumption is used in Section 6.3.

Rationale: Under normal operating conditions, temperatures can vary over the length of the canister and cask. For a wide range of temperatures, the properties of structural steels that are commonly used in casks and canisters do vary significantly. Moreover, this temperature is

consistent with the value per Section 71(b) of 10 CFR 71 (Ref. 2.2.3). Thus, it is reasonable to evaluate structural material properties at 100°F.

3.2.3.4 Ductility Ratio for Determining Probability of Structural Failure for Cases with Triaxiality Factor

Assumption: To account for the triaxiality factor in determining the probability of structural failure (Section 6.3.7.5), the ductility ratio is set to a value of 0.5. This is equivalent to assuming a triaxiality factor of 2, which corresponds to a state of biaxial tension. A ductility ratio of 0.5 is applied to cases that include the triaxiality factor for the aging overpack, transportation cask, and dual purpose canister. This assumption is used in Section 6.3.

Rationale: A ductility ratio of 0.5, equivalent to a triaxiality factor of 2, corresponds to a state of biaxial tension, which is reasonably conservative for the cylindrical-shell geometry of the respective containers. This assumption is conservative because it predicts an upper bound for the probability of structural failure.

4. METHODOLOGY

4.1 QUALITY ASSURANCE

This calculation was prepared in accordance with EG-PRO-3DP-G04B-00037, Calculations and Analyses (Ref. 2.1.1). These analyses support PCSA. Waste packages are classified as Safety Category items important to safety and important to waste isolation on the *Q-list* (Ref. 2.1.2, Table A-1, p. A-7). Therefore, this document is subject to the requirements of the BSC Quality Management Directive (Ref. 2.1.3), and the approved version of this document is designated as QA:QA.

4.2 USE OF SOFTWARE

4.2.1 Reserved

4.2.2 Seismic Analyses of Emplaced Waste Packages

Calculations supporting this report, which are from Ref. 2.2.25, used qualified software (LS-DYNA and KM_IMPACTS_PP), as documented in that reference. No controlled and baselined software was used in the additional seismic calculations for the preclosure period that are described in this report.

Commercial off-the-shelf software (COTS) was used for the seismic calculations described in this document. Microsoft Excel was used for presenting results in tabular form and for performing simple calculations, such as computing statistics for data sets. Microsoft Word was used for word processing of this document. Use of this software is exempt from the requirements for software qualification, as allowed under IT-PRO-0011 (Ref. 2.1.4, Section 4 and Attachment 12).

LS-PREPOST V. 2.0 was used for viewing time histories of resultant contact force. This software was used for graphical representation of data in this report. Information generated by this software was checked and approved in accordance with applicable procedures and was found to meet stated acceptance criteria. This software was run on the AMD Opteron Redhat Linux 4 and Intel Itanium2 Redhat Linux 4 systems. This software is exempt from the requirements for software qualification, as allowed under IT-PRO-0011 (Ref. 2.1.4, Section 4 and Attachment 12).

Numerical results from the use of commercial off-the-shelf (COTS) software in this report are not dependent on the software used. Documentation of each such use includes sufficient detail to allow an independent reviewer to reproduce or verify the results by visual inspection or hand calculation.

4.2.3 Structural Failure Analyses of Containers Subject to Drop-Impact Loads

LS-DYNA V971.7600.398-00 Intel Itanium2 Redhat Linux4 is a qualified, commercially available finite element code, which is identified by the Software Tracking Number 10300-971.7600.398-00 (Ref. 2.2.42). This code was selected for its capability to model structural mechanics in dynamic loading conditions. LS-DYNA was only used within the range of its

validation, as specified in the software validation report (Ref. 2.2.41). There are no known limitations on its outputs. LS-PREPOST V. 2.0 was used for viewing time histories of resultant impact scenarios. This software was used for graphical representation of data in this report. The analysis approach to process strain data in Section 6.3.7 was developed and encoded in a MATLAB script, which is COTS.

4.3 CALCULATION APPROACH

4.3.1 Reserved

Seismic Analyses of Emplaced Waste Packages

4.3.2.1 Probability of Damage for Waste Packages

Annual exceedance frequencies from the bounded hazard curve (Ref. 2.2.27) and probability of damage as a function of peak ground velocity (PGV) and residual stress threshold (RST) from the postclosure seismic analyses in Ref. 2.2.25 and Ref. 2.2.28, which is from the *Seismic Consequence Abstraction* (Ref. 2.2.26), are statistically combined using calculations performed in Microsoft Excel worksheets, provided in Attachment 2.

1. Using the bounded hazard curve, determine the probability that a single seismic event will occur during the 100-year preclosure period and determine intervals of conditional probability of hazard for 0.1 m/s PGV increments.

2. Using the probability of damage as a function of PGV and RST, determine the probability of damage in 0.1 m/s PGV increments.

3. Using the information determined in 1 and 2, determine the probability that a seismic event will occur and cause damage to WPs during the preclosure period by summing the contribution from each hazard interval and integrating over the RST range (see Eq. 6.2-4 in Section 6.2).

4.3.2.2 Probability of Rupture for Waste Packages

Results from the postclosure seismic analyses in Ref. 2.2.25, Ref. 2.2.29, and Ref. 2.2.30 are interpreted for the preclosure period. The results are summarized in a Microsoft Excel worksheet, provided in Attachment 2.

1. Using impact-force and velocity results from postclosure kinematic analyses, the most severe impact scenarios for ground motions considered in the preclosure period are determined.

2. Using the impact scenarios, bounding maximum effective strains are determined and compared to an effective strain limit of 0.285, documented in Appendix A2 in Ref. 2.2.25, to determine if rupture occurs.

3. A second more conservative approach (involving screening for rupture based on the occurrence of multiple large impacts causing severe deformations) is also applied to the WPs in the preclosure period, as it was in the postclosure analysis in Ref. 2.2.25.

4.3.2.3 Probability of Waste Packages and Pallets Contacting Drip Shield

The probability of contact between the WPs/pallets and the drip shield as a function of PGV is determined by analyzing output from postclosure seismic analyses. Annual exceedance frequencies from the bounded hazard curve (Ref. 2.2.27) and probability of contact as a function of PGV from the postclosure seismic analyses (Attachment 2) are statistically combined using calculations performed in Microsoft Excel worksheets, provided in Attachment 2. The following steps are followed in computing the probability of contact:

1. Time histories of resultant contact force for three WP-to-drip shield surfaces and three pallet-to-drip shield surfaces for each of the five central WPs are viewed for output of the postclosure seismic analyses using LS-PREPOST. Text files of the time histories are generated from the plots in LS-PREPOST.

2. Each set of six time histories is individually scrutinized for all 17 ground motion realizations at all 4 PGV levels to determine whether there is a nonzero contact force for a WP or its pallet with the drip shield at any time during an analysis. If there is a nonzero force, then that WP is recorded as contacting the drip shield for that realization and PGV level.

3. The probability of contact as a function of PGV level is computed by summing the total number of contacts and dividing by the total number of possible contacts (5 WPs × 17 realizations = 85 possible contacts).

4. Determine the PGV that corresponds to a zero probability of contact, by using linear extrapolation of the probabilities of contact for 0.40 m/s and 1.05 m/s PGV.

5. Using the bounded hazard curve, determine the probability that a single seismic event will occur during the 100-year preclosure period and determine intervals of conditional probability of hazard for 0.1 m/s PGV increments.

6. Using the probability of contact as a function of PGV, determine the probability of contact in 0.1 m/s PGV increments.

7. Using the information determined in 5 and 6, determine the probability that a seismic event will occur and cause contact between the WPs/pallets and the drip shield during the preclosure period by summing the contribution from each hazard interval.

4.3.3 Structural Failure Analyses of Containers Subject to Drop-Impact Loads

The analyses considered container configurations and values of key design variables and their relationships to probability of failure (loss of containment) that are associated with a safe facility. The container configurations and loading parameters used in the calculations are described in Table 4.3.3-1a. Tables 4.3.3-1b and 4.3.3-1c summarize the sensitivity cases that were analyzed.

The probabilistic method used to predict failure of a container for a specific drop scenario is described in Section 4.3.3.2. The selection of the representative canister and cask is discussed in Section 4.3.3.3.

4.3.3.1 Container Configurations and Loading Parameters

Owing to the number of configurations and parameter variations that needed to be considered, the analyses were conducted in the most efficient manner possible, while maintaining suitable accuracy. This was accomplished by consulting with BSC on combinations of container types, drop types/configurations, drop heights, and finite element analysis (FEA) modeling. After some iteration, a single representative description of each container type in Table 4.3.3-1a was used for the analyses. These representative descriptions were sufficiently flexible to accommodate various values of actual design parameters (e.g., changeable length, width, thickness, closure configurations, weights, etc.). The fleet of canisters and casks was reviewed and selected using a screening process similar to that used in the Modal Study NUREG/CR-4829 (Ref. 2.2.45), and with consultation with BSC. TAD drops were not directly simulated because they are represented by simulations conducted for the dual purpose canisters.

For simplicity and consistency in interpreting results, the impact-surface conditions for the analyses, including both the ground and the falling 10-metric-ton load (Impact Condition 4), were assumed to be infinitely stiff and unyielding (Assumption 3.2.3.1), which is a conservative assumption. The results of these cases are summarized in Table 6.3.7.6-1 through 6.3.7.6-5.

Existing commercial casks and canisters that would likely be used on the YMP were identified and characterized, as summarized in Section 4.3.3.3. Appropriate finite element models were developed for the representative cask, selected container types, configurations, and drop types. The level of detail for each model was selected to understand deformation and damage patterns, possible failure mode(s) in each structural element, and failure-related response. A consistent failure criterion for each case was identified as part of the detailed analyses. The maximum effective plastic strain (Max EPS), in combination with material ductility data, was used to predict the probability of failure.

Finite element analyses were performed for limited combinations of the container configurations and drop conditions. The analyses were performed with LS-DYNA. The meshing was simplified in order to expedite computational efforts in most areas, but used more detail in some areas depending on the sensitivity of certain structural areas to failure given a loading scenario. Special attention was required to properly model the closure region to ensure that the simplified model would capture failure related response with acceptable accuracy. As in the Modal Study (Ref 2.2.45), failure criteria were defined in terms of plastic strain for structural elements.

Table 4.3.3-1a. Container Configurations and Loading Conditions

Container	Configuration	Container Type/Impact Condition (CT.IC)[a]	Drop Height
• AO (Aging Overpack) cell with canister inside	Representative canister (Table 4.3.3-2) inside AO cell	A.IC 1: End with vertical orientation (Section 6.3.1.1)	3-ft vertical
		A.IC 2: Slapdown from a vertical orientation and 2.5-mph horizontal velocity (Section 6.3.1.2)	0-ft vertical
• Transportation Cask with Spent Nuclear Fuel (SNF) canister inside	Representative canister (Table 4.3.3-2) inside representative cask (Table 4.3.3-3)	T.IC 1a: End, with 4-degree off-vertical orientation (Section 6.3.2.1)	12-ft vertical
		T.IC 1b: Same as T.IC 1a	13.1-ft vertical
		T.IC 1c: Same as T.IC 1a	30-ft vertical
		T.IC 2a: End, with 4-degree off-vertical orientation, and approximated slapdown (Section 6.3.2.2)	13.1-ft vertical
		T.IC 2b: Same as IC 2a, with no free fall	0-ft vertical
		T.IC 3: Side, with 3-degree off-horizontal orientation (Section 6.3.2.3)	6-ft vertical
		T.IC 4: Drop of 10-metric-ton load onto top of cask (Section 6.3.2.4)	10-ft vertical
		T.IC 5a: End, with vertical orientation (Section 6.3.2.5)	30-ft vertical
		T.IC 5b: End, with 4-degree off-vertical (same as IC 1c)	
		T.IC 5c: End, with 45-degree off-vertical	
		T.IC 5d: End, with center of gravity over corner (i.e., point of impact)	
• DPC (Dual Purpose Canister) • TAD (Transportation, Aging, and Disposal) canister[b]	Representative canister (Table 4.3.3-2)	D.IC 1a: End, with vertical orientation (Section 6.3.3.1)	32.5-ft vertical
		D.IC 1b: Same as D.IC 1a	40-ft vertical
		D.IC 2a: End, with 4-degree off-vertical orientation (Section 6.3.3.2)	23-ft vertical
		D.IC 2b: Same as D.IC 2a	10-ft vertical
		D.IC 2c: Same as D.IC 2a	5-ft vertical
		D.IC 3: 40 ft/min horizontal side collision inside the Canister Transfer Machine (CTM) bell (Section 6.3.3.3)	NA[c]
		D.IC 4: Drop of 10-metric-ton load onto top of canister (Section 6.3.3.4)	10-ft vertical
		D.IC 2a: Hourglass-control study for end drop, with 4-degree off-vertical orientation (Section 6.3.3.5.1)	23-ft vertical
		D.IC 2a: Friction-coefficient sensitivity study for end drop, with 4-degree off-vertical orientation (Section 6.3.3.5.2)	23-ft vertical
		D.IC 2a: Mesh-density study for end drop, with 4-degree off-vertical orientation (Section 6.3.3.5.3)	23-ft vertical
		D.IC 2a: Shell- and bottom-lid-thickness sensitivity study for end drop, with 4-degree off-vertical orientation (Section 6.3.3.6)	23-ft vertical
• DSNF (DOE Spent Nuclear Fuel) Canister • MCO (Multi-Canister Overpack)	INL-analyzed case (Ref. 2.2.37)	O.IC 1: End, with 3-degree off-vertical orientation (Ref. 2.2.37) (Section 6.3.5)	23-ft vertical

NOTES: [a] CT.IC stands for impact condition; container types are designated by A (AO), T (transportation cask), and D (DPC). The letter "O" in the case label "O.IC 1" stands for DOE DSNF canister.

[b] TAD cases are represented by the results of the corresponding DPC cases (Section 6.3.3).

[c] Not applicable.

Table 4.3.3-1b. Sensitivity Studies of Hourglass Control, Friction Coefficient, and Mesh Density for Dual Purpose Canisters Subject to 23-ft End Drop, with 4-degree Off-Vertical Orientation

Container/ Configuration	Container Type/Impact Condition (CT.IC)[a]	Case Name	LS-DYNA Hour Glass Control Parameter	Friction Coefficient	Numerical Mesh Case	Notes
• DPC (Dual Purpose Canister) • TAD (Transportation, Aging, and Disposal) canister[b]	D.IC 2a: 23-ft end drop with 4-degree off-vertical orientation (Section 6.3.3.5)	H1-F1-M1	1	0.2	1	Original base[c]
		H2-F1-M1	9	0.2	1	
		H2-F2-M1	9	0.7	1	
		H2-F1-M2	9	0.2	2	
		H2-F1-M3	9	0.2	3	New base[d]
		H2-F1-M4	9	0.2	4	
		H2-F1-M5	9	0.2	5	

NOTE: [a] CT.IC stands for container type impact condition; container types are designated by A (AO), T (transportation cask), and D (DPC)
[b] TAD cases are represented by the results of the corresponding DPC cases (Section 6.3.3).
[c] The original base case is applied to all D.IC 1 (Section 6.3.3.1), D.IC3 (Section 6.3.3.3), and D.IC4 cases (Section 6.3.3.4).
[d] The new base case is applied to all of the D.IC 2 cases reported in Sections 6.3.3.2 and 6.3.3.6.

Table 4.3.3-1c. Shell- and Bottom-Lid-Thickness Sensitivity Study Cases for Dual Purpose Canisters Subject to 23-ft End Drop with 4-degree Off-Vertical Orientation

Container/Configuration	Container Type/Impact Condition (CT.IC)[a]	Case Name	Shell Thickness (in)	Bottom-Lid Thickness (in)
• DPC (Dual Purpose Canister) • TAD (Transportation, Aging, and Disposal) canister[b] Representative canister (Table 4.3.3-2) with following modifications to shell and base-plate thicknesses	D.IC 2a: 23-ft end drop with 4-degree off-vertical orientation (Sections 6.3.3.2 and 6.3.3.6)	S1-L1[c]	0.5	2.313
		S2-L1	0.75	2.313
		S3-L1	1.0	2.313
		S1-L2	0.5	0.75
		S1-L3	0.5	4.0
		S2-L3	0.75	4.0
		S3-L3	1.0	4.0
		S2-L4	0.75	8.0
		S3-L4	1.0	8.0

NOTE: [a] CT.IC stands for container type impact condition; container types are designated by A (AO), T (transportation cask), and D (DPC)
[b] TAD cases are represented by the results of the corresponding DPC cases (Section 6.3.3).
[c] This is the revised base case (Case H2-F1-M3 from Table 6.3.3.5-1).

4.3.3.2 Container Failure Probability

As discussed in Section 1.3, containment is only provided by the SNF canister in these analyses. For containers with an outer shell, such as aging overpack canisters and transportation casks, no credit is taken for the integrity of the outer container shell. Thus, the probability of container failure is always equivalent to the probability of SNF canister failure.

As discussed in Sections 4.3.3.1 and 4.3.3.3, representative container configurations and loading or impact conditions were selected for determining the conditional probability of container failure for each scenario. There are two fundamental steps in the determination of probability of failure. Given a numerical simulation impact analysis for a container type and impact condition, effective strain fields or distributions throughout the SNF canister are determined. Failure of containment can occur when there is a strain component of sufficient magnitude that a breakage or through-going puncture of the canister occurs. However, the distribution of strains in a canister calculated by LS-DYNA for a specific impact analysis will not indicate an obvious breach. Thus, the second step is to relate the strains obtained from a simulation to the probability of failure, which is accomplished through the use of a cumulative distribution function (CDF) of capacity or fragility curve (Figure 6.3.7-3). The fragility curve relates the magnitude of strain to the likelihood of failure of the canister steel material.

The highest likelihoods of failure are associated with the effective plastic strain (EPS) in regions ("hot zones") of the canister having high strain (and deformation) after an impact. These regions, which experience the maximum effective plastic strain (Max EPS), provide an upper bound for the probability of canister failure. Based on engineering judgment, the model meshing can be simplified in order to expedite computational efforts in most areas, while using more detail in others, depending on the sensitivity to failure for a loading scenario. Strains can be sampled within each of the selected regions according to degrees of resolution and conservatism. In this analysis effort, the probability of failure is calculated based on the Max EPS for a single element brick (with the greatest strain in the canister), obtained from a given LS-DYNA simulation. Fracture propagation takes place on the milliseconds time-scale, and thus propagates across the canister wall thickness very quickly compared to the time-frame of the LS-DYNA simulation. Although LS-DYNA results provide a distribution of strain values through the thickness of the canister wall (the wall thickness being represented by multiple finite element layers), it is more conservative to use the Max EPS value at a single finite element brick than the average of the values across a wall thickness.

Without comprehensive knowledge of the specific designs of these containers, the best that can be done on a practical basis is to make informed and reasonable judgments as to the important general design parameters of these containers; to estimate the margins in response-variable calculation; and to define a design space for which there is confidence in the probabilities of failure. Possible ranges of container designs are represented by values of key design variables selected by both LLNL and BSC.

Accuracy of the fragility curve is important for limiting the uncertainties associated with the probability of failure. Thus, it was decided to use an empirical set of 204 independent stainless steel 304 tensile failure tests (Ref. 2.2.23) for statistical analysis. The use of tensile elongation data is more conservative than the use of compressive strain data for determining structural fragility under both tensile and compressive strain conditions.

The tensile failure data were initially represented as a histogram of 2-in. coupon engineering elongation or strain at failure versus the number of specimens that failed at a particular strain value (i.e., frequency of failure). These data were evaluated for mean and standard deviation and for the uncertainties in mean and standard deviation. Both the data and their corresponding log-transform (to true strain) were found to be non-normally distributed by the Shapiro-Wilk test

(Ref. 2.2.43). However, these data were determined to be reasonably well-modeled as a sample from a probability density function (which was a weighted mixture of two normal distributions), with the goodness of fit to a 95% confidence level assessed by the Kolmogorov-Smirnov sample test (Ref. 2.2.44). This probability distribution function was then converted (by integration) to a cumulative distribution function that gives the probability of failure as a function of strain (either engineering or true strain). This fragility curve may have to be adjusted (e.g., by stochastic scaling) to account for variations in material properties, or weld effects that are not adequately represented in the native data set.

For a particular impact scenario (container type/impact condition), the Max EPS is obtained from the LS-DYNA simulation. For every finite element brick in the mesh model, the LS-DYNA simulation calculates an EPS, which is an accumulated true strain over the loading event. The global maximum value of all EPS values for an impact scenario is defined as the Max EPS. This calculated Max EPS value is set equal to the true strain in the fragility function (Figure 6.3.7-3) to determine the probability of canister failure for the container type/impact condition.

Another issue is that the fragility function is based on coupon tensile tests in uniaxial tension. Cracking of stainless steel may not be determined simply by comparing the calculated plastic strain to the true strain in the fragility function (Figure 6.3.7-3), because the EPS is calculated from a complex 3-D state of stress, while the true strain in the fragility function is based on a 1-D state of stress. A 3-D state of stress may condition plastic flow in the material and modify the value of EPS at which failure occurs. This change in ductility can be accounted for by the use of a triaxiality factor (TF), which is the ratio of normal stress to shear stress on the octahedral plane, normalized to unity for simple tension.

4.3.3.3 Selecting the Representative Containers

A representative cask and a representative canister were used as models for the structural analyses (Section 6.3). These representative models were developed using available information from existing spent nuclear fuel (SNF) transport casks and canisters. The models are simplified representations of the structural design of most existing transport casks and canisters. The models can be used to simulate various existing casks and canisters by simply adjusting the dimensions of the model components. Thus, the models are suitable for future parametric studies, if needed. Tables 4.3.3-2 and 4.3.3-3 list key structural design features of the representative models. The comparison indicates that the existing designs of the cask, and of the canister in particular, are very similar in geometry, dimension, and material. Thus, the representative model should be adequate for evaluating the structural performance of the existing designs. As indicated in Tables 4.3.3-2 and 4.3.3-3, the loaded weight, total length, and diameter of representative containers are chosen to be close to the average of the group. For the representative canister, the cylindrical shell thickness was chosen to be smaller than those of typical DPCs and TAD canisters (Table 4.3.3-2), which is conservative with respect to strain.

The representative canister is a hollow right cylinder closed by a circular plate welded to each of the cylinder's two ends. The contents of the canister are modeled as a solid composite cylinder, representing the fuel assembly and the supporting basket structure. The composite cylinder interacts with the canister by sliding contact with friction, where the friction coefficient is defined in Table 6.3-1. The stiffness of the composite is determined by the volume fraction of the

basket, and the mass density is determined from the volume of the composite cylinder and the mass of the fuel and the basket. The minimum yield strength and minimum tensile (ultimate) strength specified in the ASME material specification are used for the structural analysis (Ref. 2.2.46). Since LS-DYNA needs the input of a true stress-strain relation of the material, the material-specification values were converted from engineering stress to true stress, before they were used to determine a power-law true-stress-strain relation for the LS-DYNA structural analysis.

Table 4.3.3-2. Key Structural Features for Representative Canister and Typical Canisters

Design Feature		Representative Canister	Typical Horizontal DPC[a]	Typical Vertical DPC[a]	Typical Horizontal DPC[a]	Typical TAD[b] Canister
Maximum Weight (kips)	Fully Loaded	79.6	76.635	72.927	78.400	98.000[c]
Overall Dimension (in)	Total Length	190.31	182.30	164.15	186.50	210.00
	Outer Diameter	68.4	66.000	67.060	67.190	66.000
Component thickness (in)	Cylindrical Shell	0.500	0.625	0.625	0.625	1.000
	Top Plate	9.50	8.50	10.00	10.25	15.00
	Bottom Plate	2.313	5.880	1.750	8.750	3.500
Structural Material		S.S.[d] 304	S.S.[d]	S.S.[d]	S.S.[d]	S.S.[d]

NOTE: [a] DPC stands for dual purpose canister. Two different typical horizontal DPCs are listed. The specific identities of the typical canisters are withheld for proprietary reasons.
[b] TAD stands for transportation, aging, and disposal (canister). These specifications are based on a Naval SNF canister.
[c] Preliminary value.
[d] S.S. stands for stainless steel.

Source: The sources are withheld because they contain proprietary information.

Table 4.3.3-3. Key Structural Features for Representative Cask and Typical Casks

Design Feature		Representative Cask	Typical Transportation & Storage Cask[a]	Typical Transportation & Storage Cask[a]	Typical Vertical Storage (Transfer) Cask	Typical Horizontal Storage (Transfer) Cask	Typical Naval Cask
Maximum Weight w/o Impact Limiters (kips)	Fully Loaded	212.9	231.790	227.400	140.994	229.000	400.000
Overall Dimensions w/o Impact Limiters (in)	Total Length	200.56	193.000	197.250	162.800	197.100	305.900
	Outer Diameter	94.5	99.000	98.000	89.000	92.200	92.000
Component Thickness (in)	Cylindrical Shell	12.875	14.000	14.250	7.750	10.850	10.500[b]
	Closure Lid	4.25	14.250	9.500	10.500	3.000	28.000[b]
	Bottom Plate	6.0	13.650	9.750	2.000	5.000	31.200[b]
Bolted Closure	Total No. of Bolts	56	40	48	24	24	30[b]
	Bolt Diameter	1.625	1.500	1.875	0.750	1.500	NA[c]
Structural Material		Alloy Steel	S.S.[d]	Alloy Steel	Alloy Steel	S.S.[c]	S.S.[d]

NOTE: [a] Two different typical transportation and storage casks are listed. The identities of the typical casks are withheld for proprietary reasons.
[b] Preliminary value.
[c] Value not available.
[d] S.S. stands for stainless steel.

Source: The sources are withheld because they contain proprietary information.

5. LIST OF ATTACHMENTS

		Number of Pages
Attachment 1.	Reserved	1
Attachment 2.	Seismic Analyses of Emplaced Waste Packages	3
Attachment 3.	Structural Failure Analyses of Containers Subject to Drop-Impact Loads	2

6. BODY OF CALCULATION

6.1 RESERVED

6.2 SEISMIC ANALYSES OF EMPLACED WASTE PACKAGES

This calculation is an assessment of waste packages subjected to seismic ground motion during the preclosure time period of 100 years. This assessment utilizes the results from postclosure seismic analyses. The probability that a seismic event will cause damage leading to stress corrosion cracking of the waste package outer corrosion barrier is determined; and rupture of the waste package outer corrosion barrier is also considered. The probability that the waste packages and pallets will contact the drip shield during a seismic event is determined from the postclosure analyses. This determination provides an estimate of the probability that displacement of the waste packages and/or pallets during the preclosure period before the drip shield is present will cause drip shield emplacement difficulties.

Postclosure seismic analyses were performed at four PGV levels for horizontal ground motion in Ref. 2.2.25. The four PGV levels are 0.40 m/s, 1.05 m/s, 2.44 m/s, and 4.07 m/s. These PGV levels correspond to mean annual exceedance frequencies of 1.0×10^{-4}, 1.0×10^{-5}, 4.5×10^{-7}, and 1.0×10^{-8}, respectively, on the bounded hazard curve for horizontal PGV (Ref. 2.2.27). Only ground motions with an annual exceedance frequency of 1.0×10^{-6} or greater need to be considered for the preclosure period. This corresponds to a probability of approximately 1.0×10^{-4} that an event will exceed that PGV level once in 100 years. The 2.44 m/s PGV level provides bounding ground motions, and the 4.07 m/s PGV level does not require consideration.

The postclosure analyses were performed for the TAD-bearing waste package and the codisposal waste package. Analyses were performed with 2.4 mm removed from the outer corrosion barrier thickness (Assumption 3.2.2.3), and with the inner vessel and its contents intact. This serves as a bounding assumption for the general corrosion that could occur in the 100-year preclosure period.

Damaged area leading to stress corrosion cracking is defined as an area with residual tensile stress exceeding a threshold value. The threshold value is defined as a uniform distribution between 90% and 105% of the yield strength of the outer corrosion barrier material (Alloy 22). Areas with residual tensile stress above 90%, 100%, and 105% of yield strength were determined from the postclosure analyses.

The probabilities of damage at each PGV value and residual stress threshold (RST) for the TAD-bearing waste package and the codisposal waste package are given in Table 6.2-1 and Table 6.2-2, respectively. For the codisposal waste package, the probability of damage is extrapolated to zero at 0.364 m/s PGV. Even though only ground motions up to 2.44 m/s PGV need to be considered for preclosure, ground motion at 4.07 m/s PGV is included in the calculation of damaged area probability. The contribution of ground motion at 4.07 m/s PGV to the total probability of a seismic event that causes damage is small, because the likelihood of an event of that amplitude occurring in 100 years is very small. Inclusion of ground motion at 4.07 m/s PGV provides a bounding result.

Table 6.2-1. Probability of Damage for TAD-Bearing Waste Package as a Function of PGV and RST

PGV (m/s)	90% of yield strength	100% of yield strength	105% of yield strength
0.40	0	0	0
1.05	0	0	0
2.44	0	0	0
4.07	0.118	0	0

Source: Ref. 2.2.28

Table 6.2-2. Probability of Damage for Codisposal Waste Package as a Function of PGV and RST

PGV (m/s)	90% of yield strength	100% of yield strength	105% of yield strength
0.364	0	0	0
0.40	0.029	0	0
1.05	0.559	0	0
2.44	0.941	0.147	0
4.07	1	0.412	0

Source: Ref. 2.2.28

The probability that a single seismic event will occur during the 100-year period is 4.1×10^{-2}, which is calculated from:

$$P(1 \mid \Delta\lambda, t) = 100(\Delta\lambda)e^{-100(\Delta\lambda)} \quad \text{(Eq. 6.2-1)}$$

where $\Delta\lambda$ is the difference in annual exceedance frequencies at 0.219 m/s PGV and 4.07 m/s PGV. The PGV value of 0.219 m/s is an extrapolated point on the bounded hazard curve (Ref. 2.2.27), which provides a value below 0.40 m/s PGV. The annual exceedance frequency at 0.219 m/s PGV is 4.3×10^{-4}.

The probability of damage (Table 6.2-1 and Table 6.2-2) is linearly interpolated to PGV levels in 0.1 m/s increments, and intervals of the conditional probability of hazard ($\delta\lambda$) are determined at the same 0.1 m/s PGV increments. The intervals of the conditional probability of hazard are determined by computing interpolated values of annual exceedance frequency at 0.05 m/s PGV increments, and then calculating the difference in the annual exceedance frequencies around each 0.1 m/s increment. The annual exceedance frequency values are interpolated assuming a power law fit between adjacent points:

$$\lambda = a(PGV)^b \quad \text{(Eq. 6.2-2)}$$

where a and b are determined for each point on the bounded hazard curve. From these values, the product of the probability of damage and the probability that a seismic event lies within an interval on the hazard curve is calculated. The probability that a seismic event lies within an interval on the hazard curve is calculated from:

$$\frac{P(1 \mid \Delta\lambda, t)\delta\lambda}{\Delta\lambda} \quad \text{(Eq. 6.2-3)}$$

The probability that a seismic event will occur and cause damage to the waste package outer corrosion barrier is computed by summing the individual products of the probability of damage and the probability that a seismic event lies within an interval on the hazard curve. Up to this point, the calculation only considered a single RST level for the definition of damage, and the calculation was done for each RST level individually. The final probability that a seismic event will occur and cause damage to the outer corrosion barrier is computed by integrating the probability over the three RST levels, which is computed by:

$$P = \frac{P_{90} + P_{100}}{2} \frac{100-90}{105-90} + \frac{P_{100} + P_{105}}{2} \frac{105-100}{105-90} \qquad \text{(Eq. 6.2-4)}$$

where P is the final probability and P_i is the probability for RST level i.

The probabilities that a TAD-bearing waste package and a codisposal waste package will be damaged by a seismic event during the 100-year period are 5.0×10^{-7} and 7.3×10^{-4}, respectively. The spreadsheets detailing these calculations are in Attachment 2.

The probability of rupture caused by a seismic event during the 100-year preclosure period is determined separately from damage. As described in Ref. 2.2.25, an effective strain threshold of 0.285 was determined as a value below which rupture of the Alloy 22 outer corrosion barrier is not considered. The value of 0.285 includes an 11% reduction for strain rate effects and a reduction factor of 2 for a worst case biaxial state of stress.

Two types of impacts were considered in the postclosure seismic analyses: waste package-to-waste package and waste package-to-pallet (Ref. 2.2.25). For ground motion with PGV up to 2.44 m/s, the maximum impact velocity for waste package-to-waste package impacts is 4.711 m/s for TAD-bearing waste packages and 4.165 m/s for codisposal waste packages. Detailed waste-package-to-waste-package impact analyses for the TAD-bearing and codisposal waste packages compute maximum effective strains of 0.166 and 0.188, respectively, for waste-package-to-waste-package impacts up to 6 m/s. The maximum effective strains computed for all waste package-to-pallet impacts are 0.064 and 0.076 for the TAD-bearing and codisposal waste packages, respectively. The data described here are found in Attachment 2. These maximum effective strains are below the threshold value of 0.285. A second approach for assessing rupture was utilized in the postclosure analyses. This approach involves estimating the probability of rupture based on multiple impacts causing large deformations (Ref. 2.2.31). However, since the inner vessel and its contents remain intact during the preclosure period, the deformations will be small and no probability of rupture would be estimated. Based on the above discussion, rupture of the outer corrosion barrier of the waste packages is not predicted by the analyses for seismic events occurring in the 100-year preclosure period.

The probability that the waste packages and pallets will contact the drip shield during a seismic event was calculated in a manner similar to the probability of damage. First, the probability of contact was determined based on PGV level. This was done for three TAD-bearing waste packages and two codisposal waste packages. The five pallets associated with these waste packages were also considered. Time histories of resultant contact force between waste packages/pallets and the drip shield (Attachment 2) were analyzed for this purpose. For each analysis there are five files, one for each waste package, where each file contains six separate

time histories. Three time histories are for the contact definitions between the waste package and three drip shield surfaces, and three time histories are for the contact definitions between the pallet and three drip shield surfaces. The drip shield was separated into three separate contact surfaces: top, negative X side, and positive X side (the X-coordinate of the finite element representation is oriented in the cross-drift direction). Note that contact surfaces are defined between the pallets and the top of the drip shield even though contact between those components is unlikely. If any of the six time histories associated with a waste package become non-zero at any time during an analysis, then contact is recorded for that waste package. The number of recorded contacts and the probability of contact as a function of PGV are summarized in Table 6.2-3. The probability of contact as a function of PGV is a combination of the probabilities for the TAD-bearing and codisposal waste packages, weighted by the quantity of each type of waste package in the group of five waste packages being analyzed.

Table 6.2-3. Probability of Contact for TAD-Bearing and Codisposal Waste Packages as a Function of PGV, Determined for Individual Realizations

	0.4 m/s PGV		1.05 m/s PGV		2.44 m/s PGV		4.07 m/s PGV	
Realization	TAD-bearing	Codisposal	TAD-bearing	Codisposal	TAD-bearing	Codisposal	TAD-bearing	Codisposal
1	0	0	0	0	3	2	3	2
2	0	0	0	0	3	2	3	2
3	1	0	3	2	3	2	3	2
4	0	0	3	2	3	2	3	2
5	0	0	3	2	3	2	3	2
6	0	0	1	0	3	2	3	2
7	0	0	1	1	3	2	3	2
8	0	0	3	2	3	2	3	2
9	0	0	0	0	3	2	3	2
10	2	2	3	2	3	2	3	2
11	0	1	3	2	3	2	3	2
12	0	0	3	2	3	2	3	2
13	0	0	0	0	3	2	3	2
14	0	0	2	2	3	2	3	2
15	0	0	2	1	3	2	3	2
16	0	0	0	0	3	2	3	2
17	0	0	2	2	3	2	3	2
Probability of Contact	0.059	0.088	0.569	0.588	1.000	1.000	1.000	1.000
	0.071		**0.576**		**1.000**		**1.000**	

Source: Attachment 2

The probability of contact as a function of PGV is extrapolated to zero at 0.309 m/s PGV. Utilizing an identical approach for determining the total probability of damage for each individual RST level (described above), the total probability of contact between the waste packages/pallets and the drip shield during the 100-year period is computed to be 2.6×10^{-3}. The spreadsheets detailing these calculations are in Attachment 2.

The value of 2.6×10^{-3} is a reasonable upper bound for the probability that a seismic event prior to drip shield emplacement would displace the waste packages and pallets such that drip shield emplacement at a later time would be affected. The value is an upper bound because the occurrence of relatively large displacement during a seismic event does not necessarily mean that the final state would include significant displacement in every case.

6.3 STRUCTURAL FAILURE ANALYSES OF CONTAINERS SUBJECT TO DROP-IMPACT LOADS

Tables 4.3.3-1a through 4.3.3-1c summarize the container types, "Impact Conditions," and sensitivity cases considered in these analyses. The results are summarized in Tables 6.3.7.6-1 through 6.3.7.6-3. The maximum effective plastic strain (Max EPS) is the largest value throughout the canister.

Tables 6.3-1 through 6.3-3 summarize the assumed static and kinetic coefficients of friction for the aging overpack, transportation cask, and dual purpose canister, respectively. These coefficient of friction values for the canister-to-SNF, spacer-to-canister, and cask-to-canister are typical for metal-to-metal contacting surfaces and for metal-to-concrete contacting surfaces (Table XVI on page 797 of Ref. 2.2.33) when dirt or oils may be present on the contacting surfaces. The cask-to-ground friction values are at the upper end of frictional coefficients for dry masonry and brickwork (Table XVI on page 797 of Ref. 2.2.33). They are appropriate for representing the ground, which is likely to be some form of pavement surface. The (concrete) overpack-to-canister friction values are similar to those for dry masonry and brickwork (Table XVI on page 797 of Ref. 2.2.33).

Table 6.3-1. Static and Kinetic Coefficient of Friction for Contacting Surfaces for Aging Overpack

Impact Condition	Canister to SNF Surfaces		Spacer to Canister		Spacer to Overpack		Overpack to Canister		Overpack to Rigid Ground	
	Static	Kinetic	Static	Kinetic	Static	Kinetic	Static	Kinetic	Static	Kinetic
1	0.3	0.15	0.3	0.2	0.3	0.2	0.7	0.5	0.7	0.7
2	0.3	0.15	0.3	0.2	0.3	0.2	0.7	0.5	0.7	0.7

NOTE: Impact Condition cases are defined in Table 4.3.3-1a.

Table 6.3-2. Static and Kinetic Coefficient of Friction for Contacting Surfaces for Transportation Cask

Impact Condition	Cask to Canister Surfaces		Canister to SNF Surfaces		Cask to Rigid Ground		Falling Object to Cask	
	Static	Kinetic	Static	Kinetic	Static	Kinetic	Static	Kinetic
1	0.3	0.15	0.3	0.15	0.2	0.2	NA	NA
2	0.3	0.15	0.3	0.15	0.2	0.2	NA	NA
3	0.3	0.15	0.3	0.15	0.2	0.2	NA	NA
4	0.3	0.15	0.3	0.15	0.2	0.2	0.8	0.8
5	0.3	0.15	0.3	0.15	0.2	0.2	NA	NA

NOTE: Impact Condition cases are defined in Table 4.3.3-1a.

Table 6.3-3. Static and Kinetic Coefficient of Friction for Contacting Surfaces for Dual Purpose Canister

Impact Condition	Canister to SNF Surfaces		Canister to Rigid Ground		Falling Object to Canister	
	Static	Kinetic	Static	Kinetic	Static	Kinetic
1	0.3	0.15	0.2	0.2	NA	NA
2	0.3	0.15	0.2	0.2	NA	NA
3	0.3	0.15	0.2	0.2	NA	NA
4	0.3	0.15	0.2	0.2	0.8	0.8

NOTE: Impact Condition cases are defined in Table 4.3.3-1a.

6.3.1 Aging Overpack Canisters

The structural components of the model of the aging overpack (AO) cell with a spent nuclear fuel (SNF) canister used in the dynamic impact analyses are shown in Figure 6.3.1-1, with the dimensions summarized in Table 6.3.1-1. These components consist of a ribbed mass to simulate the SNF, plus the basket containing the SNF, a thin-walled canister containing this ribbed mass, and a concrete aging overpack (AO) cell that holds the SNF canister. The corresponding finite element analysis (FEA) model is shown in Figure 6.3.1-2. The SNF canister is the same as that of the dual purpose canister, described in Section 6.3.3. The units used in the simulations of the AO canisters are: [L] mm, [M] kg, [t] milliseconds, [F] kN, and [P] GPa.

Table 6.3.1-1. Dimensions and Materials of the Structural Components of Aging Overpack

Structural Component	Outer Radius		Length		Wall Thickness		Material
	in	mm	in	mm	in	mm	
Aging Overpack	69.50	1765.3	258.00	6553.2	31.50	800.1	Concrete with Steel Rebar
Cavity in the AO Cell	38.00	965.2	214.50	5448.3	N/A	N/A	N/A
Guide Rail	38.00	965.2	177.2	4500.0	N/A	N/A	Stainless Steel (hollow)
Spacer	29.5	750.	11.27	286.2	1.00	25.4	Stainless Steel
Cover	42.000	1066.8	12.00	304.8	N/A	N/A	Stainless Steel

NOTE: The SNF canister dimensions are those of the representative canister in Table 4.3.3-2. The material properties of the SNF canister are given in Table 6.3.3-2.

Source: Attachment 3

The purpose of this calculation is to determine the damage to an SNF canister contained within an AO cell as a result of a 3-ft vertical drop and as a result of slapdown of the AO cell. Two distinct "Impact Condition" cases are considered for the AO cell, which impose unique loads that affect different portions of the canister (Table 4.3.3-1a). For Impact Condition 1, the AO cell drops 3 feet to the rigid (unyielding) ground. For Impact Condition 2, the AO is subjected to slapdown from an upright position with 2.5-mph horizontal velocity. Because these two impact conditions impose loads and create maximum strains in different portions of the canister, it was deemed reasonable to start Impact Condition 2 from a pristine state, rather than starting it from the end state of Impact Condition 1.

The total mass of the aging overpack is 143,000 kg. The concrete, with reinforcing steel, is modeled as LS-DYNA Mat type 16–II.B (Ref. 2.2.2), and includes 5% steel rebar by volume, with the steel properties smeared with those of the concrete. This results in an effective composite material that is 95% concrete and 5% steel rebar. The material properties of the reinforcing steel are summarized in Table 6.3.1-2.

Table 6.3.1-2. Material Properties of the Reinforcing Steel in the Concrete of the Aging Overpack (AO) Cell

Young's Modulus			Initial Yield Stress	
psi	GPa	ν^a	psi	GPa
2.90×10^7	200	0.3	49,900	0.344

NOTE: [a] Poisson's Ratio

Source: Attachment 3

The LS-DYNA material model used for the concrete has several modes. The mode used to model the AO is mode II.B, tensile failure plus plastic strain scaling. Material properties for the concrete are given in Table 6.3.1-3 and the remaining required input is described below.

Table 6.3.1-3. Material Properties of the Concrete of the Aging Overpack (AO) Cell

Density			Shear Modulus		Tensile Cutoff Stress	
lb/ft^3	kg/mm^3	ν^a	psi	GPa	psi	GPa
125	2.00×10^{-6}	0.22	9.50×10^5	6.55	870	0.00599

NOTE: [a] Poisson's Ratio

Source: Attachment 3

The yield stress, σ_{yield} of concrete is calculated by LS-DYNA from two user-input curves, the σ_{max}-P, and the σ_{failed}-P curves, where P is the pressure:

$$\sigma_{yield} = \sigma_{failed} + \eta(\sigma_{max} - \sigma_{failed}) \quad \text{(Eq. 6.3.1-1)}$$

The σ_{max}-P curve is defined as:

$$\sigma_{max} = a_0 + \frac{P}{a_1 + a_2 P}, \quad \text{(Eq. 6.3.1-2)}$$

where:

Cohesion, $a_0 = 0.0138$ GPa (2000 psi)

Pressure hardening coefficient, $a_1 = 0.418$

Pressure hardening coefficient, $a_2 = 12.11$ GPa^{-1} (8.35×10^{-5} psi^{-1})

The σ_{failed}-P curve is defined as:

$$\sigma_{failed} = a_{of} + \frac{P}{a_{1f} + a_2 P} \qquad \text{(Eq. 6.3.1-3)}$$

where:

Cohesion for failed material, $a_{0f} = 0.0$ GPa (0.0 psi)

Pressure hardening coefficient for failed material, $a_{1f} = 0.385$

Table 6.3.1-4 defines the scale factor, η, vs. the effective plastic strain, ε, curve. The Equation-of-State (Type 9) defining pressure vs. volumetric strain is defined in Table 6.3.1-5.

Table 6.3.1-4. Scale Factor vs. Effective Plastic Strain Curve

Effective Plastic Strain (ε)	0.0	0.00094	0.00296	0.00837	0.01317	0.0234	0.04034	1.0
Scale Factor (η)	1.0	0.711	0.535	0.371	0.226	0.107	0.0	0.0

Source: Attachment 3

Table 6.3.1-5. Pressure vs. Volumetric Strain Curve

Volumetric Strain	0.0	-0.006	-0.0075	-0.01	-0.012	-0.02	-0.038	-0.06	-0.0755	-0.097
Pressure (GPa)	0.0	0.0317	0.0372	0.0427	0.0455	0.0538	0.0689	0.0869	0.1034	0.1289
Pressure (psi)	0.0	4600	5400	6200	6600	7800	10000	12600	15000	18700

Source: Attachment 3

6.3.1.1 Impact Condition 1: 3-ft Vertical Drop onto End with Vertical Orientation

The aging overpack has an impact velocity of 13.88 ft/sec (4.233 m/sec) in the vertical direction for the 3-ft drop. Accordingly, the calculation starts close to the ground with an initial vertical velocity of 4.233 m/sec. The static and kinetic (dynamic) friction coefficients between the AO cell and the rigid floor are 0.7 (Table 6.3-1). The static and kinetic (dynamic) friction coefficients are 0.7 and 0.5, respectively, for the contacting surfaces between the concrete overpack and SNF canister (Table 6.3-1). The canister-to-SNF contacting surfaces are represented with static and dynamic friction coefficients of 0.3 and 0.15, respectively (Table 6.3-1). The surfaces for the spacer contacting the canister and the overpack are represented with static and kinetic (dynamic) friction coefficients of 0.3 and 0.2, respectively (Table 6.3-1). Note that the spacer is located between the top of the canister and the bottom of the AO cover (Figure 6.3.1-1).

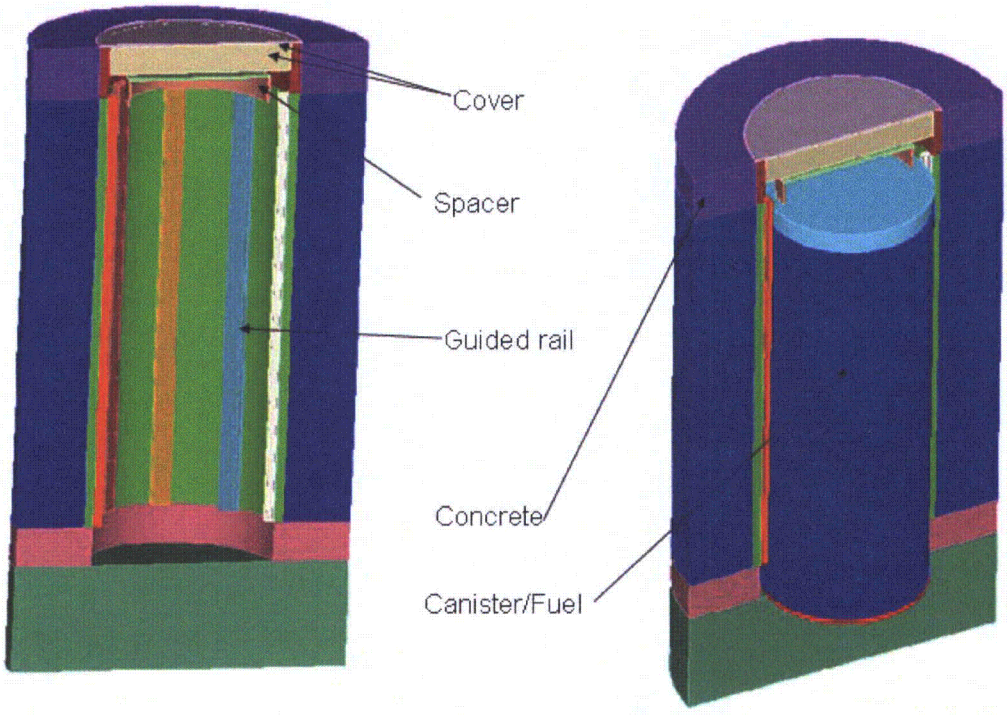

NOTE: The spacer is located between the top of the canister and the bottom of the AO cover.

Figure 6.3.1-1. The Structural Components of SNF Canister within Aging Overpack

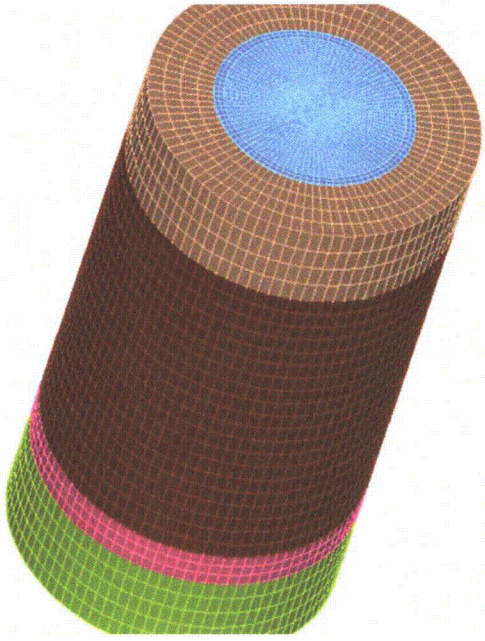

Figure 6.3.1-2. Finite Element Analysis (FEA) Model Representation of Structural Components of SNF Canister within Aging Overpack

Figure 6.3.1-3 shows the maximum plastic strain in the SNF canister. The maximum effective plastic strain (Max EPS) for Impact Condition 1 (A.IC 1) for the SNF canister inside the AO cell is 0.16% (Figure 6.3.1-4 and Table 6.3.7.6-1).

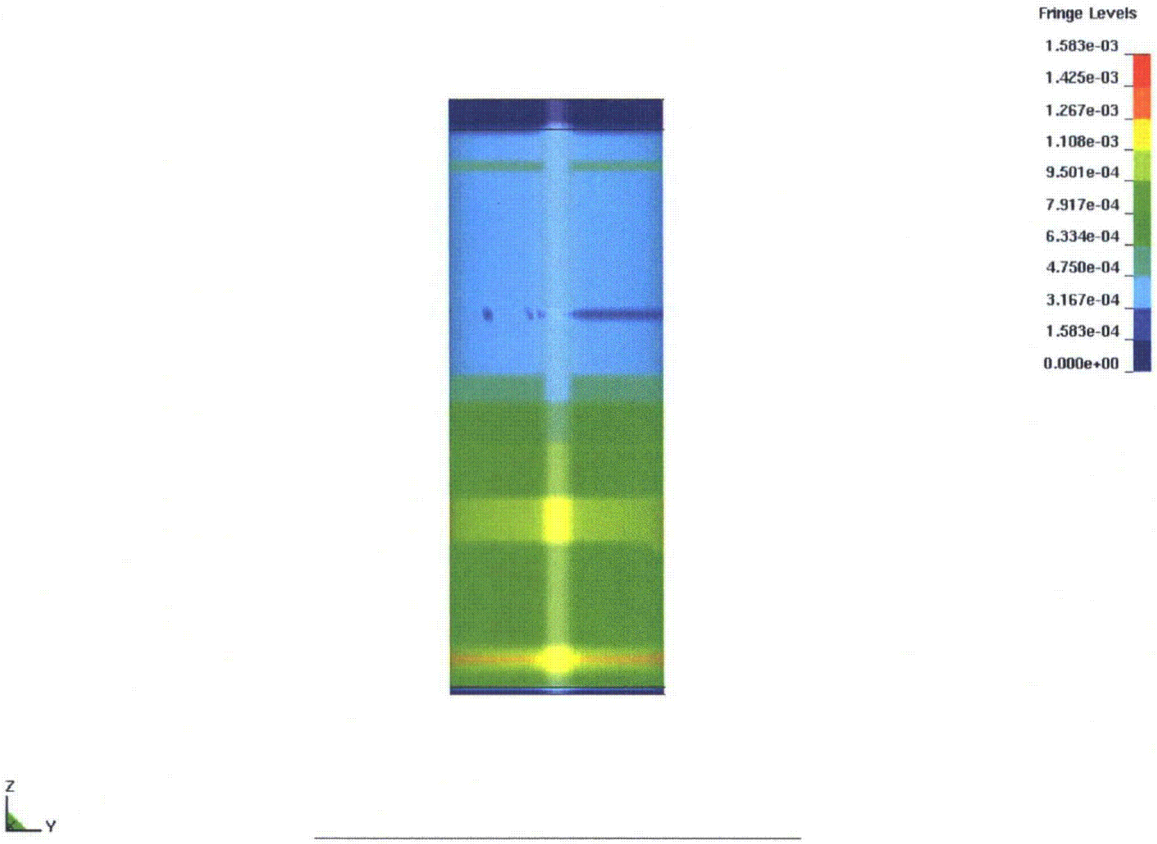

Figure 6.3.1-3. Max EPS for SNF Canister within Aging Overpack Resulting from a 3-ft Drop onto End with Vertical Orientation

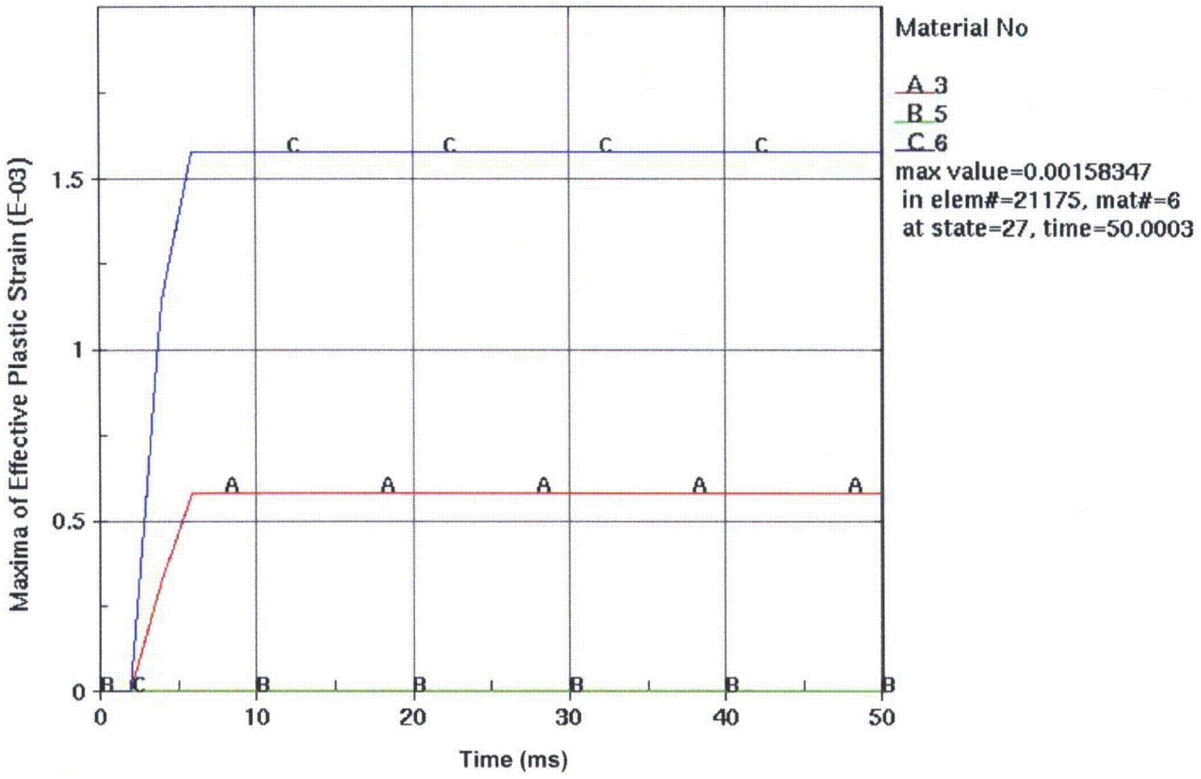

NOTE: The Max EPS histories are plotted for all structural components of the canister. Time is in milliseconds (ms). The simulation starts a few milliseconds before the time of impact.

Figure 6.3.1-4. Max EPS History for SNF Canister within Aging Overpack Resulting from a 3-ft Drop onto End with Vertical Orientation

6.3.1.2 Impact Condition 2: Slapdown from a Vertical Orientation and 2.5-MPH Horizontal Velocity

The geometry, contact surfaces, and materials of the aging overpack for Impact Condition 2 (A.IC 2) are the same as for Impact Condition 1 (A.IC 1). Initially, the overpack has a 2-degree off-horizontal orientation with respect to the rigid ground. The overpack is rotating about one bottom corner. The initial angular velocity is 1.32×10^{-3} rad/ms, which is calculated by equating the change in the potential energy from the vertical to the horizontal position and the translational kinetic energy in the horizontal velocity of 2.5 mph to the initial kinetic energy of rotation.

Figure 6.3.1-5 is a side view of the Max EPS in the canister. Because the maximum strains occur at the bottom of the canister, Figure 6.3.1-5 does not show the area of maximum strain. Figure 6.3.1-6 shows that the maximum plastic strain in the canister occurs at the bottom, interacting with guide rails inside the aging overpack cell. The maximum effective plastic strain (Max EPS) for A.IC 2 for the SNF canister inside the AO cell is 0.82% (Figure 6.3.1-7 and Table 6.3.7.6-1).

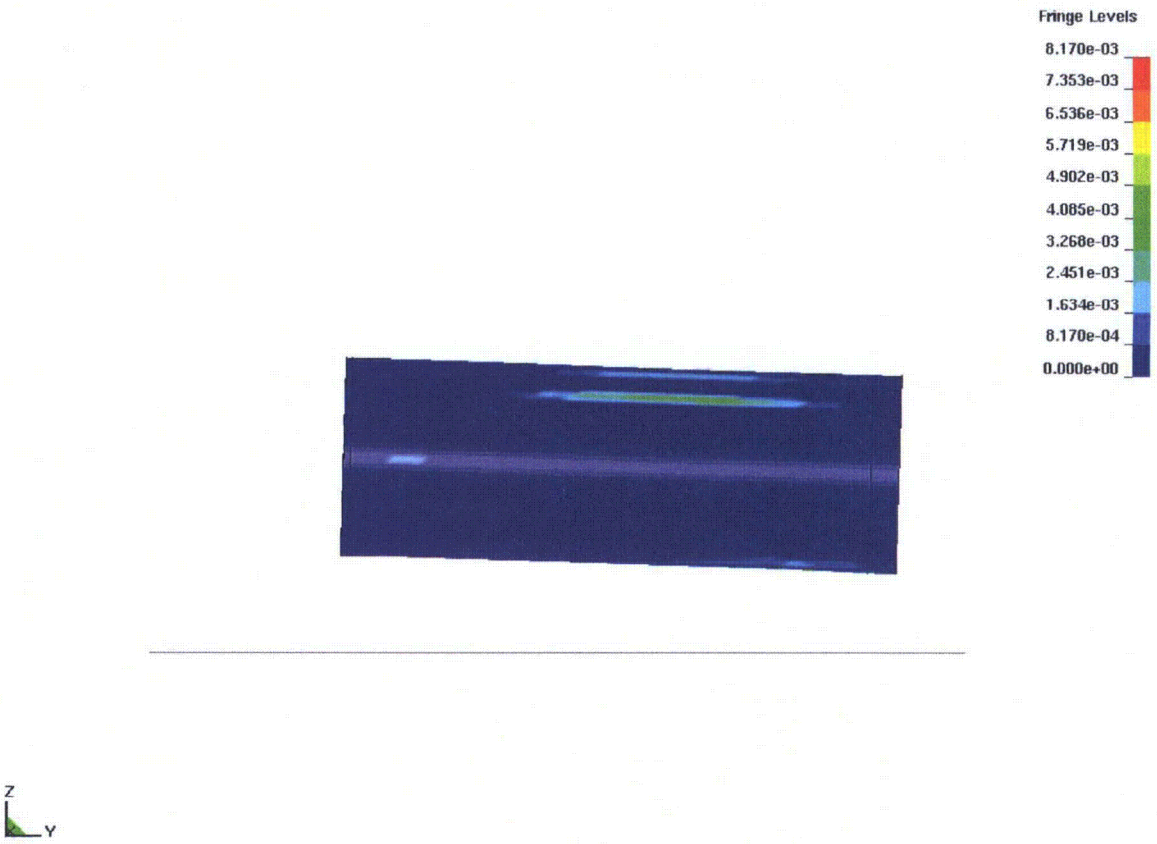

Figure 6.3.1-5. Side View of Max EPS for SNF Canister within Aging Overpack Subjected to Slapdown Impact to Rigid Ground from a Vertical Orientation and 2.5-MPH Horizontal Velocity

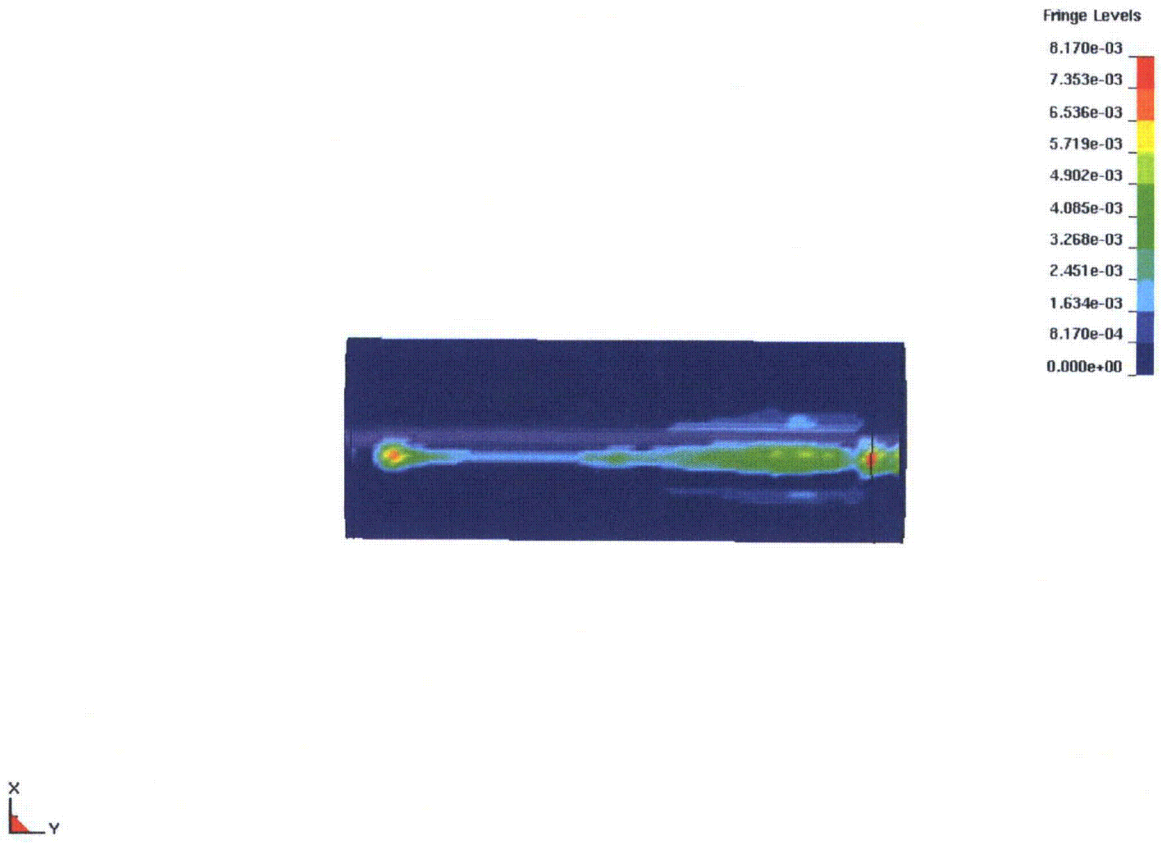

Figure 6.3.1-6. Bottom View of Max EPS for SNF Canister within Aging Overpack Subjected to Slapdown Impact to Rigid Ground from a Vertical Orientation and 2.5-MPH Horizontal Velocity

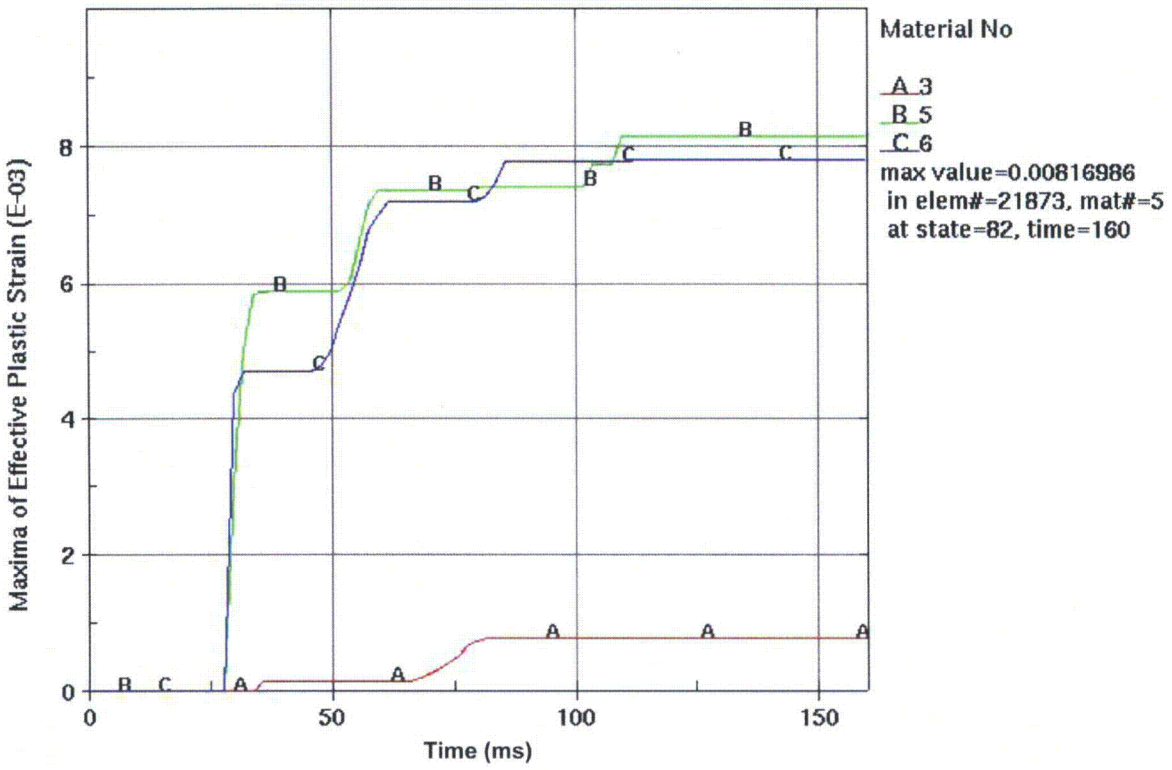

NOTE: The Max EPS histories are plotted for all structural components of the canister. Time is in milliseconds (ms). The simulation starts a few milliseconds before the time of impact.

Figure 6.3.1-7. Max EPS History for SNF Canister within Aging Overpack Subjected to Slapdown Impact to Rigid Ground from a Vertical Orientation and 2.5-MPH Horizontal Velocity

6.3.2 Transportation Casks with SNF Canisters

The study of transportation casks with spent nuclear fuel (SNF) canisters considered several drop types, or impact conditions, as indicated in Table 4.3.3-1a. The cask has dynamic mechanical responses to the impact loading conditions, and forces are propagated to the inner fuel canister, with its own dynamic response. The mechanical behaviors of the two containers are coupled, and of ultimate interest are the resultant strains of the inner canister. The container 'system' is not considered breached unless the SNF canister material fails. The study addressed a range of modeling approaches and variables, such as cask and canister design features, finite element meshing strategies, and contact surfaces' interface or matching conditions. The objective was to find a combination of modeling attributes to reach a conservative estimate of the plastic strains most important to potential failure of the transportation cask system.

The structural components of the model of the transportation cask with a SNF canister used in the dynamic impact analyses are shown in Figure 6.3.2-1. The dimensions and materials of the structural components are given in Table 6.3.2-1, and the material properties are listed in Table 6.3.2-2. These components consist of a ribbed mass to simulate the SNF, plus the basket containing the SNF, a thin-walled canister containing this ribbed mass, and a bolted-lid

transportation cask and shielding, which, in turn, holds the SNF canister. The corresponding finite element analysis (FEA) model is shown in Figure 6.3.2-2. The model represents all structural components with a minimum of three elements through the thickness of the respective components. Note that the cask closure bolts are modeled as beam elements, while the other structural components are modeled as solid elements. The beam elements, which represent the bolts, are modeled using the LS-DYNA bi-linear elastic-plastic material model, Material 3 (Ref 2.2.2). The solid elements, which represent the remaining structural components, are modeled using the LS-DYNA power-law plasticity material model, Material 18 (Ref 2.2.2).

Table 6.3.2-1. Dimensions of Structural Components of the Transportation Cask

Structural Component	Outer Radius		Length		Wall Thickness	
	in	mm	in	mm	in	mm
Cask	41.625	1057.3	200.563	5094.30	1.15625	29.3688
Closure Lid	38.4375	976.313	4.25	108.	N/A	N/A
Inner Shell	42.125	1070.0	170.0	4318.	0.50	12.7
Outer Shell	47.250	1200.2	173.688	4411.68	0.50	12.7
Gamma Shield	41.625	1057.3	173.688	4411.68	6.09	155
Neutron Shield	46.750	1187.5	170.0	4318.	4.625	117.5
Closure Bolts	0.8125	20.64	7.2	183.	N/A	N/A

Source: Attachment 3

Table 6.3.2-2. Material Properties of Structural Components of the Transportation Cask

Structural Component	Density		Young's Modulus		ν^a	Strength Coefficient[b] (K)		Hardening Exponent[b] (n)
	lb/in^3	kg/mm^3	psi	GPa		psi	GPa	
Cask	0.282	7.81×10^{-6}	2.760×10^7	190.3	0.3	118107.4	0.8143269	0.20076
Closure Lid	0.282	7.81×10^{-6}	2.760×10^7	190.3	0.3	118107.4	0.8143269	0.20076
Inner Shell	0.282	7.81×10^{-6}	2.760×10^7	190.3	0.3	115286.4	0.7948767	0.186042
Outer Shell	0.282	7.81×10^{-6}	2.930×10^7	202.0	0.3	117324.9	0.8089317	0.19664
Gamma Shield	0.282	7.81×10^{-6}	2.930×10^7	202.0	0.3	117324.9	0.8089317	0.19664
Neutron Shield	0.0703	1.95×10^{-6}	1.29×10^6	8.89	3×10^{-6}	5141.76	0.035451	0.19664
Closure Bolts	0.286	7.91×10^{-6}	2.90×10^7	199.9	0.3	N/A	N/A	N/A

NOTE: [a] Poisson's Ratio

[b] The power-law equation and parameters K and n are described on pages 20.76 and 20.77 of the LS-DYNA Keyword User's Manual (Ref. 2.2.2).

Source: Attachment 3

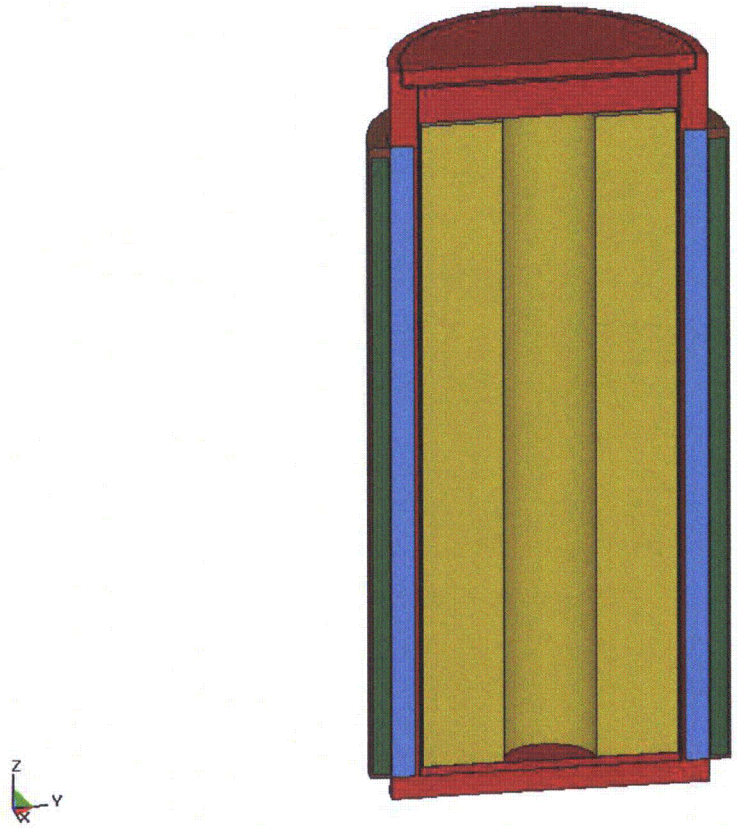

Figure 6.3.2-1. Structural Components of a SNF Canister inside a Transportation Cask

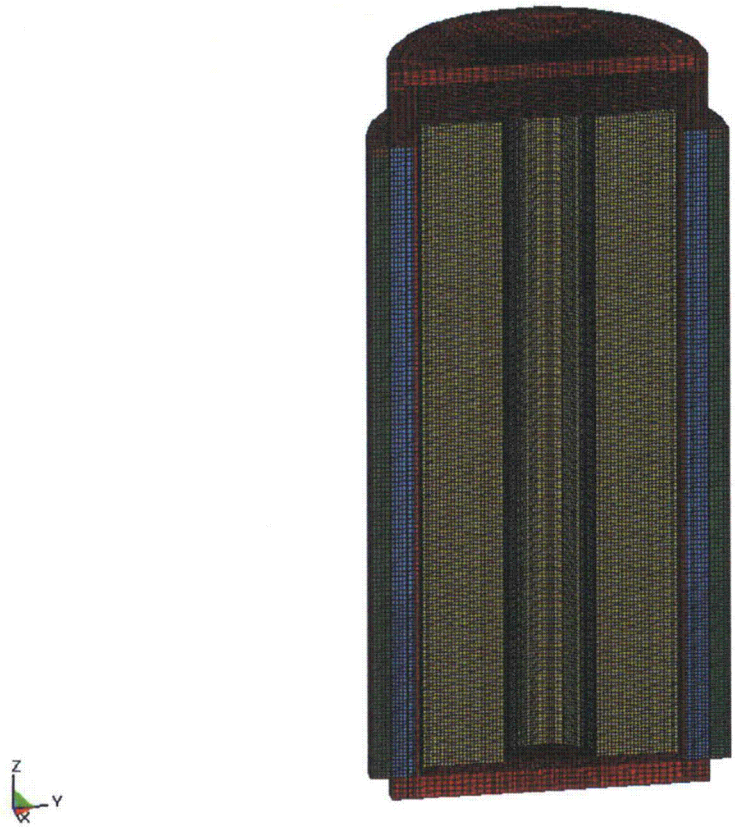

Figure 6.3.2-2. Finite Element Analysis (FEA) Model Representation of Structural Components of the SNF Canister inside a Transportation Cask

6.3.2.1 Impact Conditions 1a, 1b, and 1c: 12-, 13.1-, and 30-ft Drops with 4-degree Off-Vertical Orientation

Three different drop heights are considered: 12, 13.1, and 30 ft, with a 4-degree off-vertical orientation (Table 4.3.3-1a). Figure 6.3.2.1-1 plots maximum effective plastic strain (Max EPS) resulting from Impact Condition T.IC 1a, with a 12-ft drop. Figure 6.3.2.1-2, which is a history plot of maximum effective plastic strain (Max EPS) for T.IC 1a, shows that the Max EPS is 3.53% for the SNF canister (Table 6.3.7.6-2). For T.IC 1a, the cask closure bolt strains remain purely elastic, and the Max EPS is 9.20% for the structural body of the cask (Table 6.3.7.6-2).

Figure 6.3.2.1-3 plots Max EPS in the canister, resulting from T.IC 1b, with a 13.1-ft drop. Figure 6.3.2.1-4, which is a history plot of Max EPS for T.IC 1b, shows that the Max EPS is 4.06% for the SNF canister (Table 6.3.7.6-2). For T.IC 1b, the cask closure bolt strains remain purely elastic, and the Max EPS is 9.37% for the structural body of the cask (Table 6.3.7.6-2).

Figure 6.3.2.1-5 plots Max EPS in the canister, resulting from T.IC 1c, with a 30-ft drop. Figure 6.3.2.1-6, which is a history plot of Max EPS for T.IC 1c, shows that the Max EPS is 5.77% for the SNF canister (Table 6.3.7.6-2). For T.IC 1c, the cask closure bolt strains remain purely elastic, and the Max EPS is 11.25% for the structural body of the cask (Figure 6.3.2.1-7

and Table 6.3.7.6-2). A close inspection of Figure 6.3.2.1-7 reveals that the region of highest strains is localized to the outer corner of the bottom plate (which is the initial point of impact) and that the maximum strain values away from the corner of the bottom lid are comparable to the Max EPS for the SNF canister itself.

Figure 6.3.2.1-1. Max EPS for SNF Canister inside a Transportation Cask Subjected to 12-ft Drop with 4-degree Off-Vertical Orientation

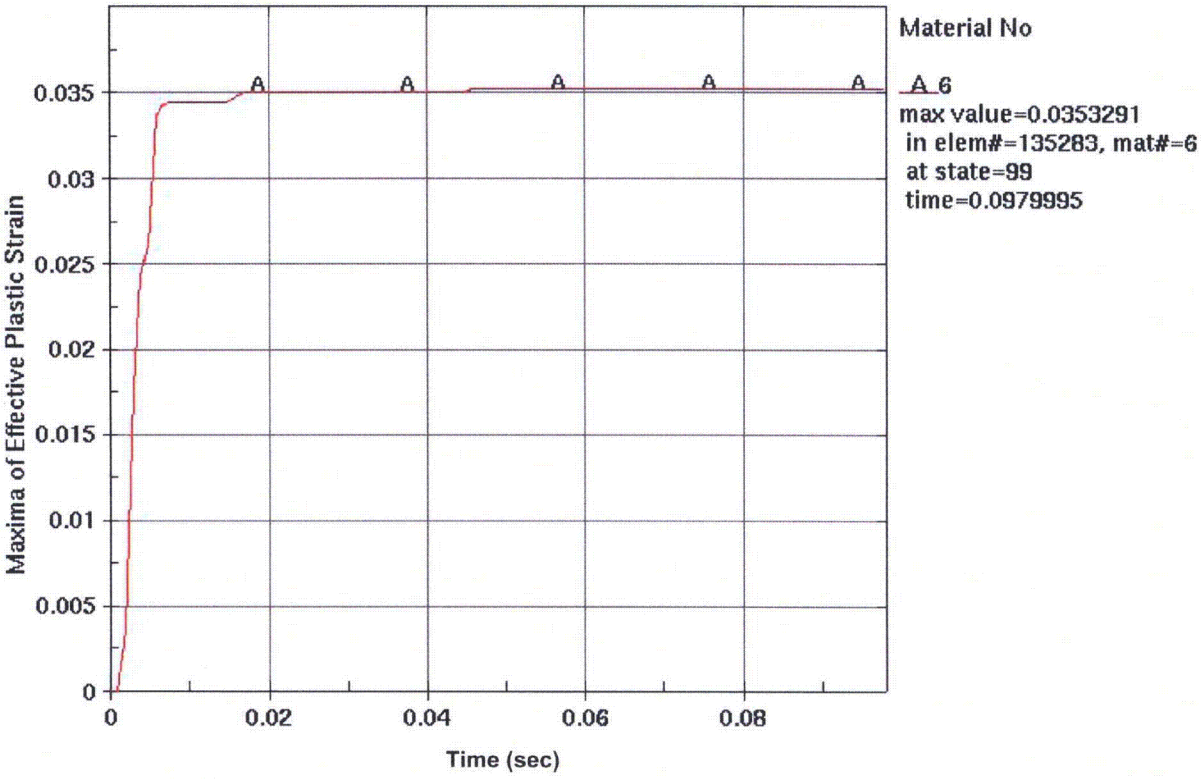

NOTE: The Max EPS history is plotted for the canister. Time is plotted in seconds (sec). The simulation starts a few milliseconds before the time of impact.

Figure 6.3.2.1-2. Max EPS History for SNF Canister inside a Transportation Cask Subjected to a 12-ft Drop with 4-degree Off-Vertical Orientation

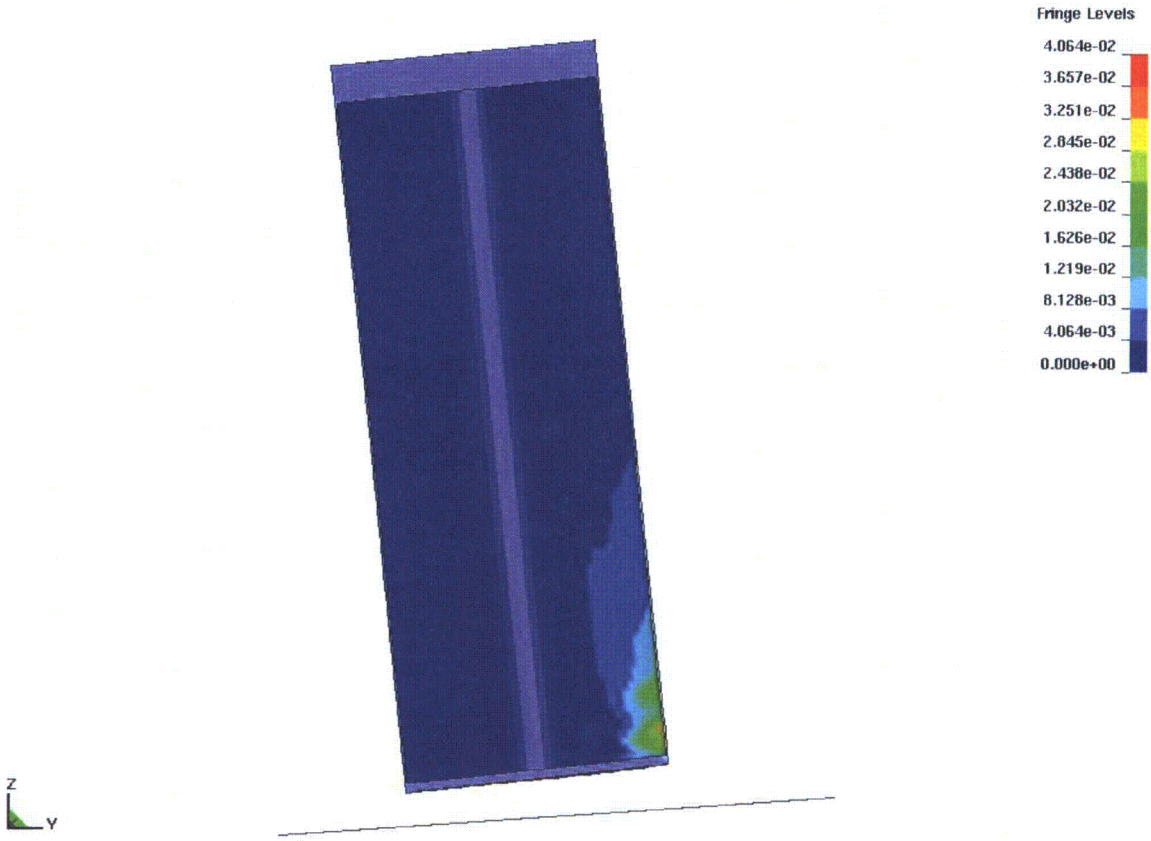

Figure 6.3.2.1-3. Max EPS for SNF Canister inside a Transportation Cask Subjected to 13.1-ft Drop with 4-degree Off-Vertical Orientation

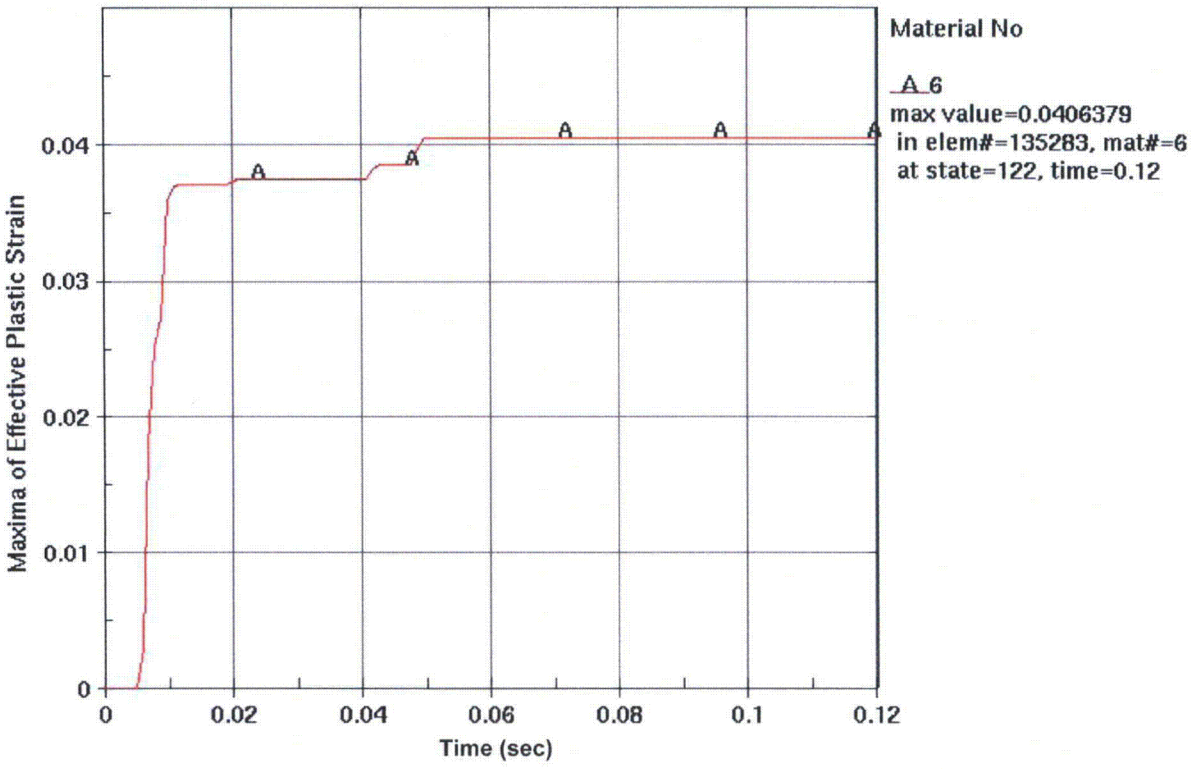

NOTE: The Max EPS history is plotted for the canister. Time is plotted in seconds (sec). The simulation starts a few milliseconds before the time of impact.

Figure 6.3.2.1-4. Max EPS History for SNF Canister inside a Transportation Cask Subjected to a 13.1-ft Drop with 4-degree Off-Vertical Orientation

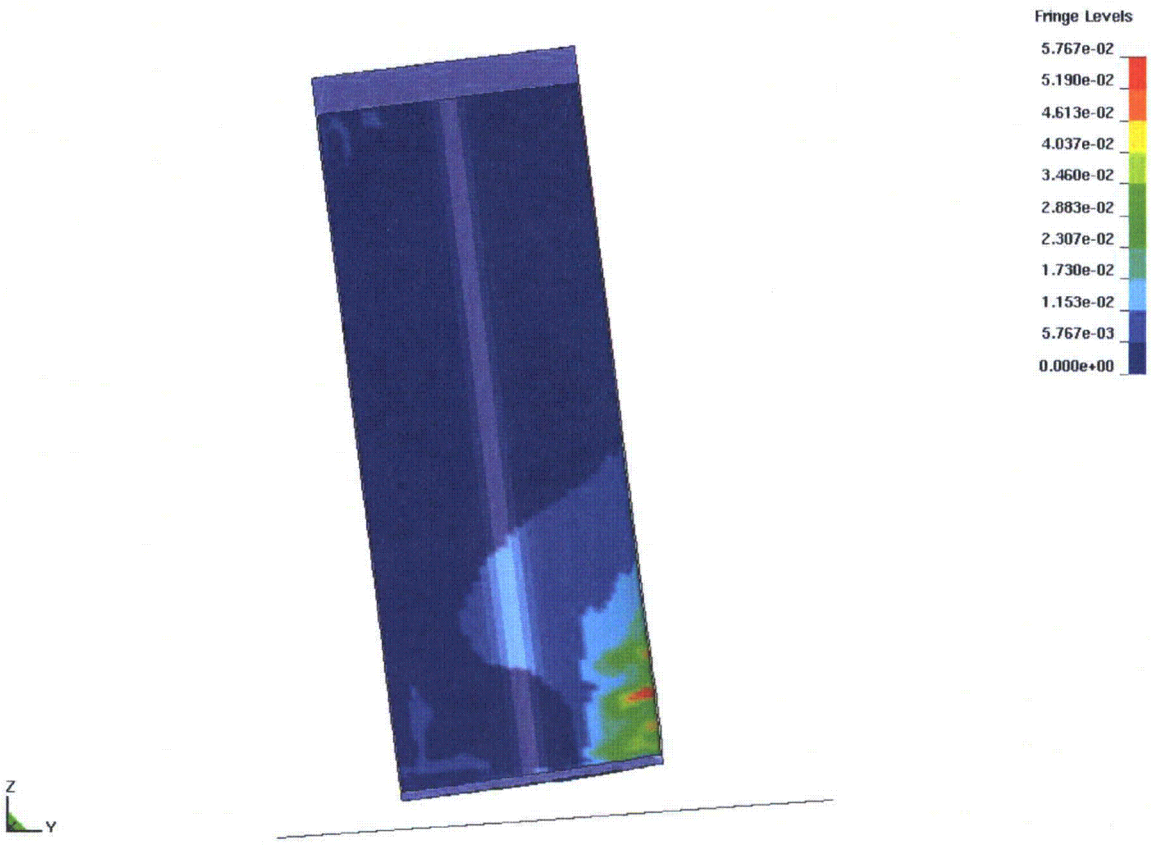

Figure 6.3.2.1-5. Max EPS for SNF Canister inside a Transportation Cask Subjected to 30-ft Drop with 4-degree Off-Vertical Orientation

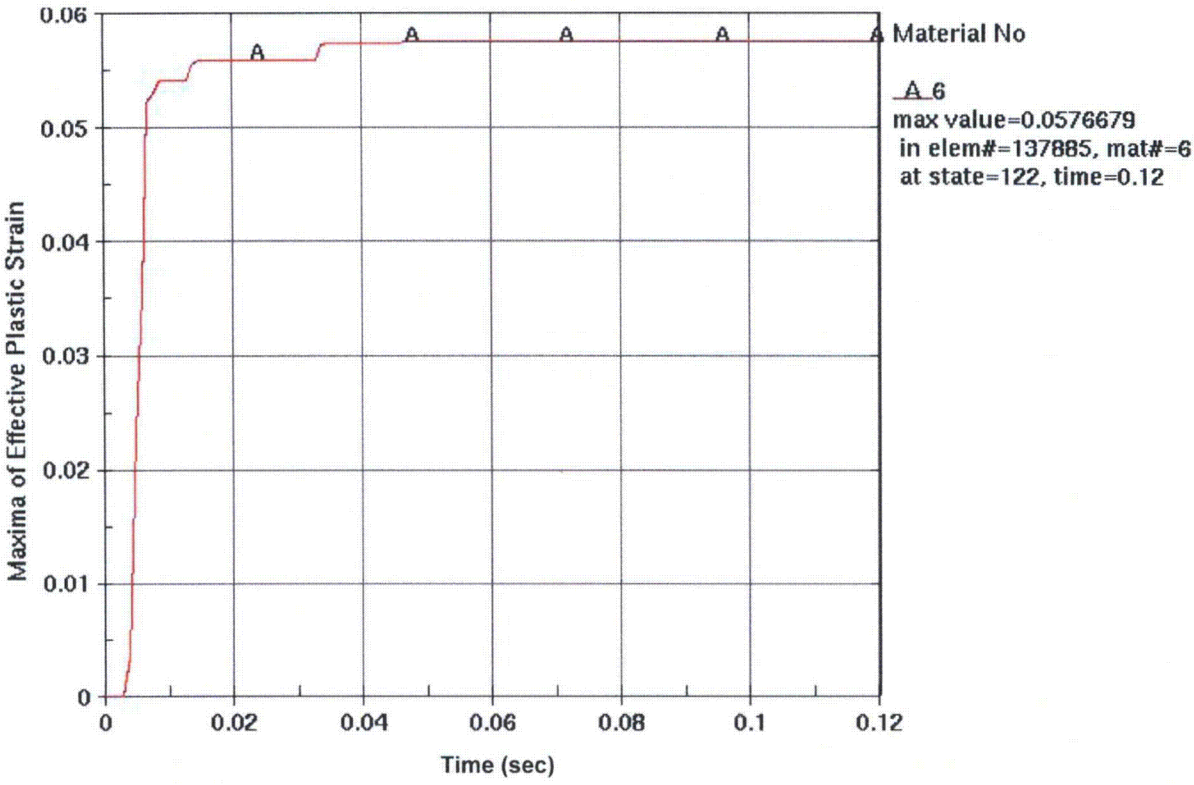

NOTE: The Max EPS history is plotted for the canister. Time is plotted in seconds (sec). The simulation starts a few milliseconds before the time of impact.

Figure 6.3.2.1-6. Max EPS History for SNF Canister inside a Transportation Cask Subjected to a 30-ft Drop with 4-degree Off-Vertical Orientation

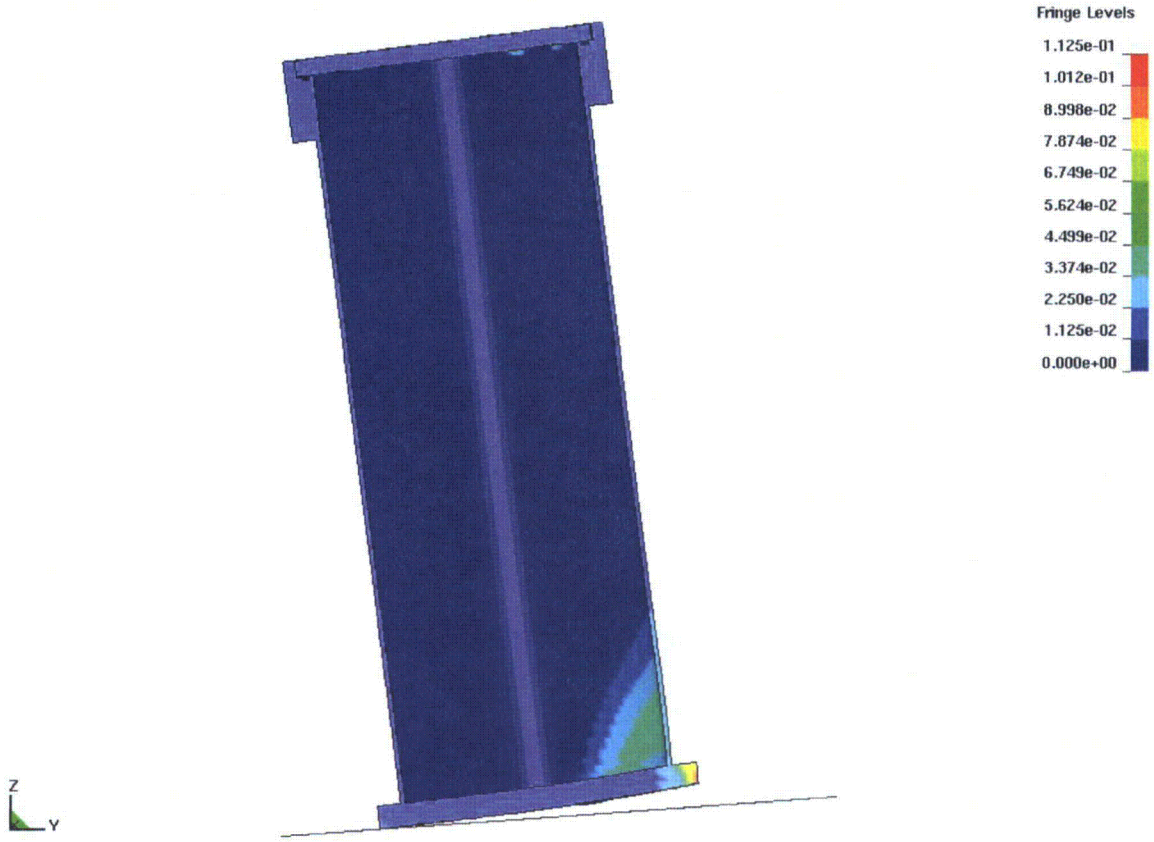

NOTE: The fringe plot shows the transportation cask at the instant of the second impact. The first impact occurred at the lower right corner of the bottom plate, which is the region of largest strain values.

Figure 6.3.2.1-7. Max EPS for the Structural Body of the Transportation Cask Subjected to 30-ft Drop with 4-degree Off-Vertical Orientation

6.3.2.2 Impact Conditions 2a and 2b: 13.1-ft and 0-ft Drop onto End with 4-degree Off-Vertical Orientation and Approximated Slapdown

Transportation cask Impact Condition (T.IC) 2a is similar to T.IC 1b, except that there is an approximated slapdown in T.IC 2a. Figure 6.3.2.2-1 plots Max EPS in the canister resulting from T.IC 2a, with a 13.1-ft drop and approximated slapdown. Figure 6.3.2.2-2, which is a history plot of Max EPS for T.IC 2a, shows that the Max EPS is 4.35% for the SNF canister (Table 6.3.7.6-2), which is slightly greater than the value of Max EPS (4.06%) for T.IC 1b. For T.IC 2a, the cask closure bolt strains remain purely elastic, and the Max EPS is 9.94% for the structural body of the cask (Table 6.3.7.6-2).

Impact Condition T.IC 2b is similar to IC 2a, except that T.IC 2b has no free fall prior to the approximated slapdown. Figure 6.3.2.2-3 plots Max EPS in the canister, resulting from IC 2b, with an approximated slapdown from an initial upright position. Figure 6.3.2.2-4, which is a history plot of Max EPS for T.IC 2b, shows that the Max EPS is 1.25% for the SNF canister (Table 6.3.7.6-2). For T.IC 2b, the cask closure bolt strains remain purely elastic, and the Max EPS is 5.30% for the structural body of the cask (Table 6.3.7.6-2).

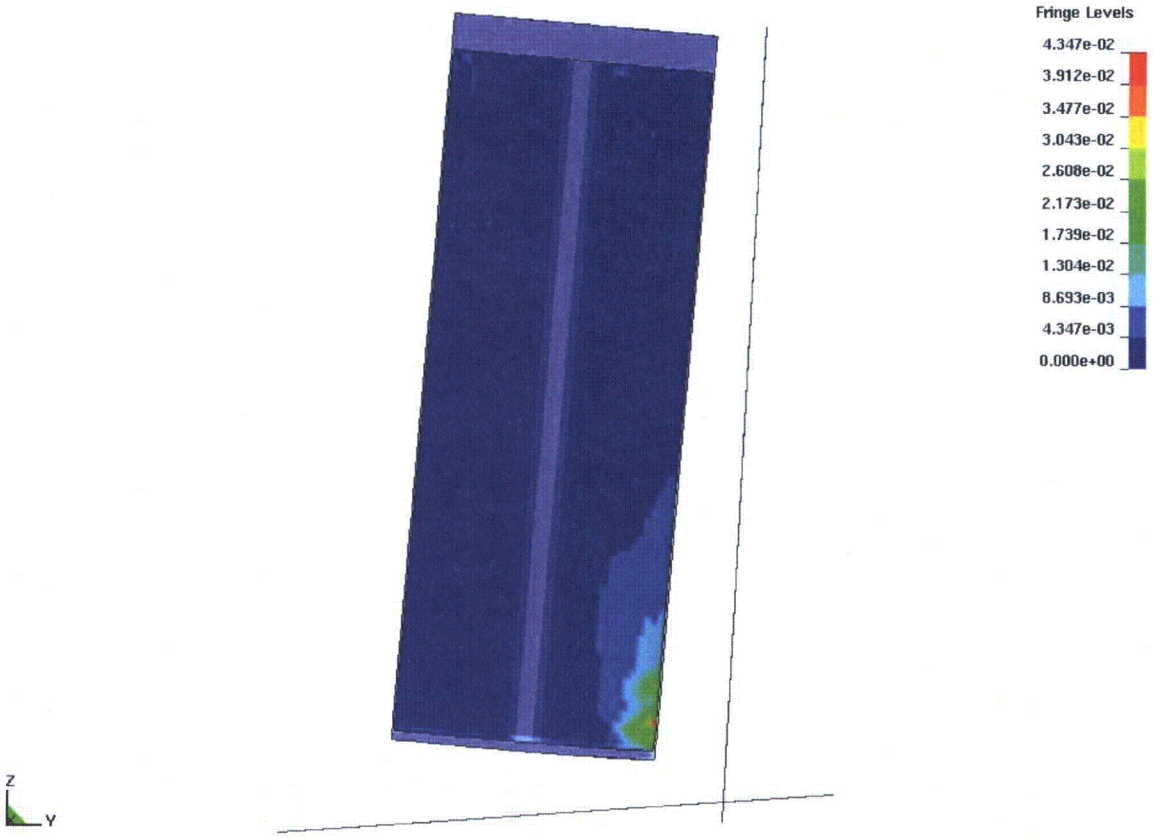

Figure 6.3.2.2-1. Max EPS for SNF Canister inside a Transportation Cask Subjected to 13.1-ft Drop with 4-degree Off-Vertical Orientation and Approximated Slapdown

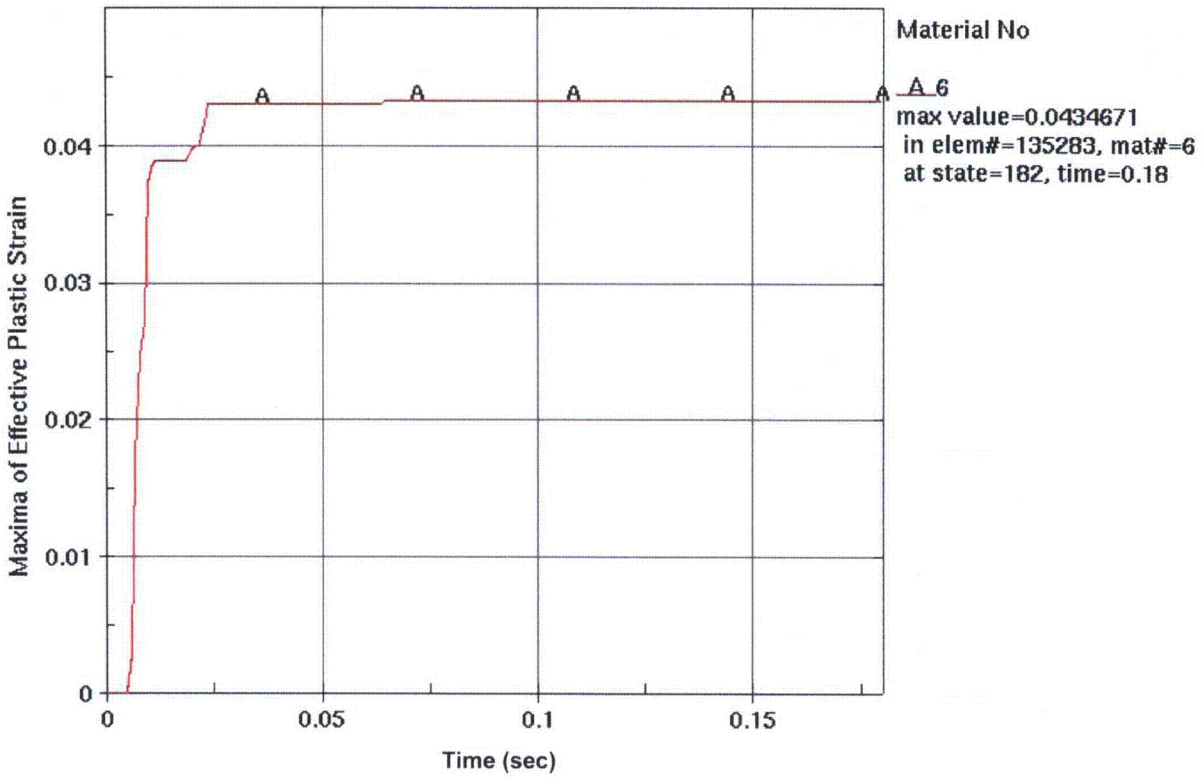

NOTE: The Max EPS history is plotted for the canister. Time is plotted in seconds (sec). The simulation starts a few milliseconds before the time of impact.

Figure 6.3.2.2-2. Max EPS History for SNF Canister inside a Transportation Cask Subjected to a 13.1-ft Drop with 4-degree Off-Vertical Orientation and Approximated Slapdown

Figure 6.3.2.2-3. Max EPS for SNF Canister inside a Transportation Cask Subjected to an Approximated Slapdown

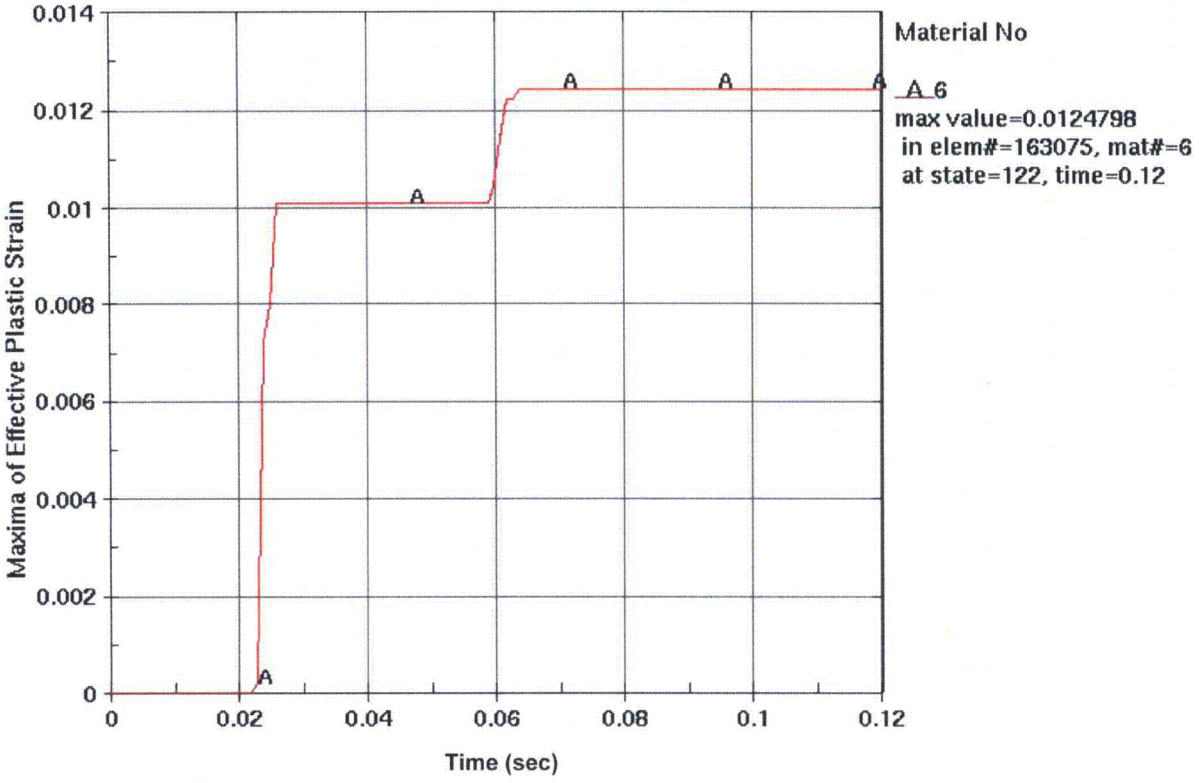

NOTE: The Max EPS history is plotted for the canister. Time is plotted in seconds (sec). The simulation starts a few milliseconds before the time of impact.

Figure 6.3.2.2-4. Max EPS History for SNF Canister inside a Transportation Cask Subjected to an Approximated Slapdown

6.3.2.3 Impact Condition 3: 6-ft Drop onto Side with 3-degree Off-Horizontal Orientation

Previous experience has shown that side impact at a slight angle is more severe than a flat impact. This is due to the initial reduced contact area at impact and subsequent slapdown on the top of the cask. Figure 6.3.2.3-1 plots Max EPS in the canister, resulting from T.IC 3, which is a 6-ft drop onto the side of the case with 3-degree off-horizontal orientation. Figure 6.3.2.3-2, which is a history plot of Max EPS for T.IC 3, shows that the Max EPS is 2.07% for the SNF canister (Table 6.3.7.6-2). For T.IC 3, the cask closure bolt strains remain purely elastic, and the Max EPS is 7.42% for the structural body of the cask (Table 6.3.7.6-2). Plastic strains in the cask (Table 6.3.7.6-2) show that plastic deformation in the shielding can absorb the majority of the rotational kinetic energy; consequently, there is little kinetic energy available for producing structural damage to the SNF canister.

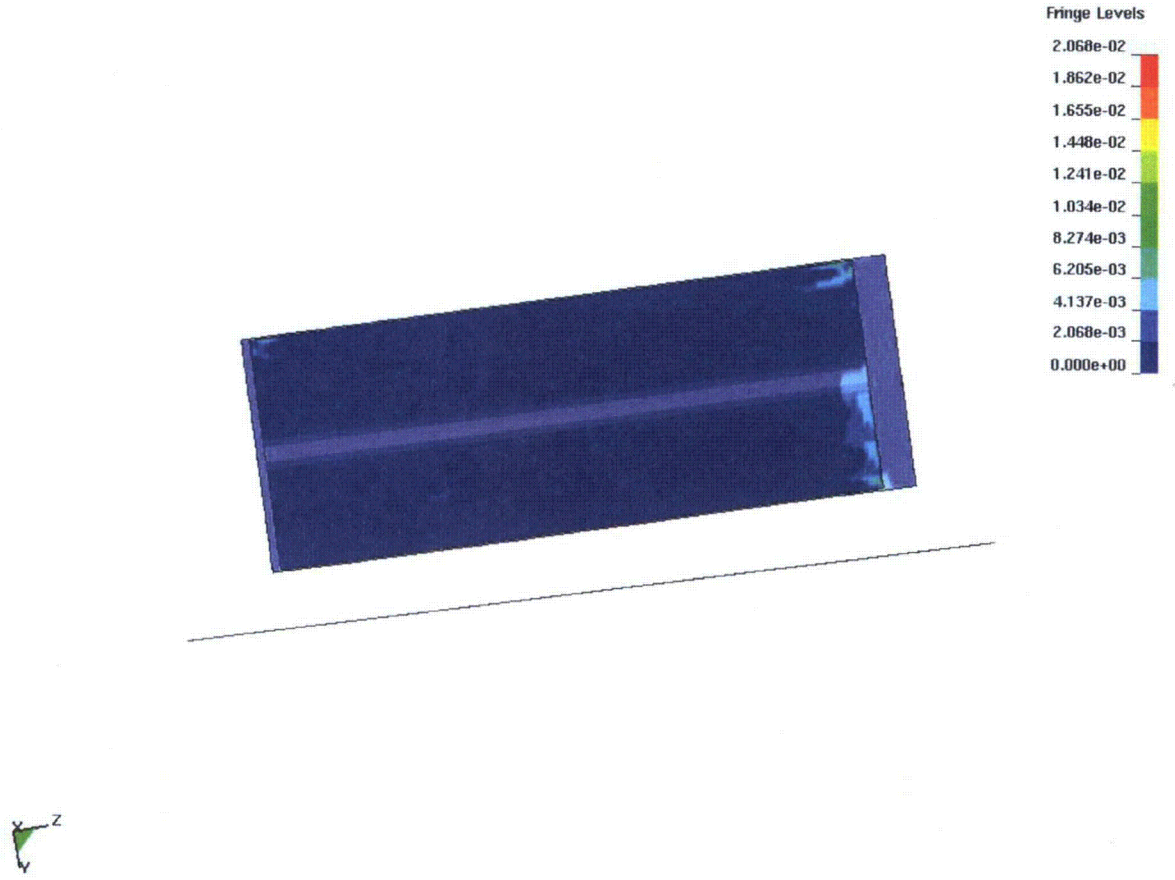

Figure 6.3.2.3-1. Max EPS for SNF Canister inside a Transportation Cask Subjected to a 6-ft Drop onto Side with 3-degree Off-Horizontal Orientation

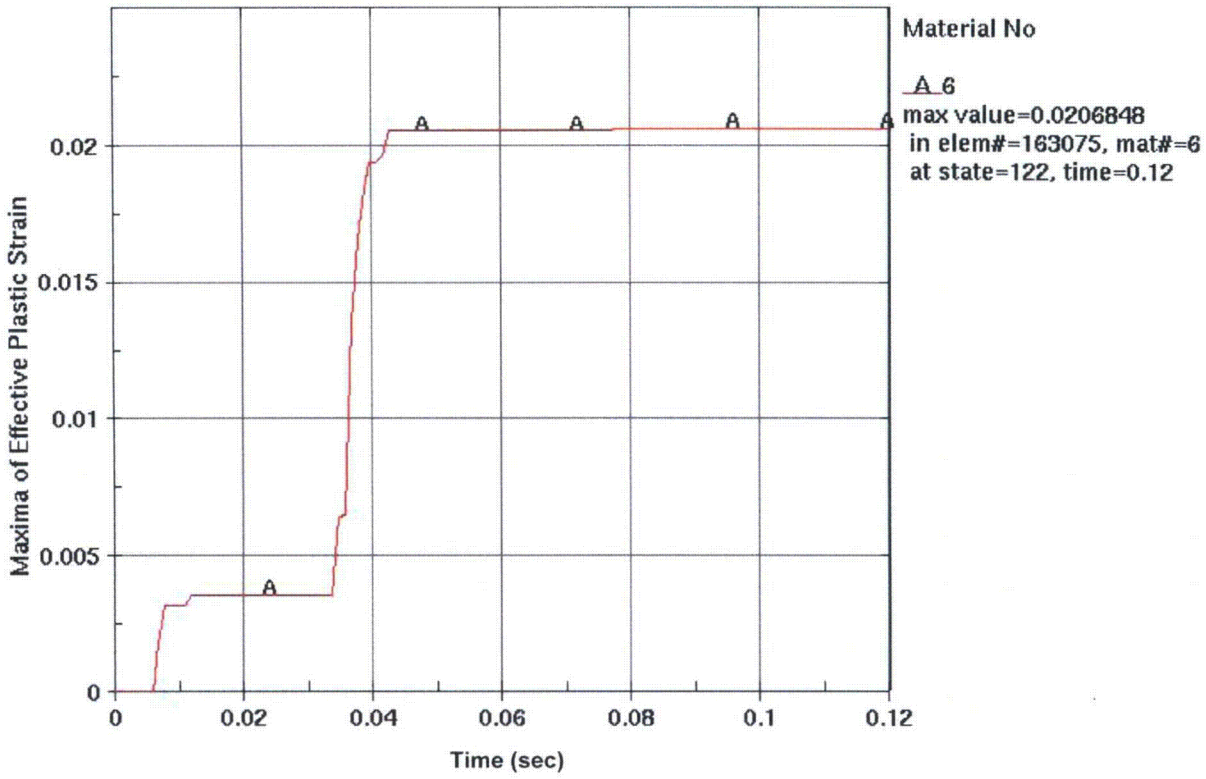

NOTE: The Max EPS history is plotted for the canister. Time is plotted in seconds (sec). The simulation starts a few milliseconds before the time of impact.

Figure 6.3.2.3-2. Max EPS History for SNF Canister inside a Transportation Cask Subjected to a 6-ft Drop onto Side with 3-degree Off-Horizontal Orientation

6.3.2.4 Impact Condition 4: 10-ft Drop of a 10-metric-ton Load onto Top of Cask

This impact condition is designed to consider plastic deformation of the canister from an axial load. The cask is very stiff in the axial direction and the path of the impact load of the rigid mass is through the cask structure. The falling mass is modeled as a rigid (unyielding) wall, oriented normal to longitudinal axis of the cask. Figure 6.3.2.4-1 plots Max EPS in the SNF canister, resulting from T.IC 4, which is a 10-ft drop of a 10-metric-ton load onto the top of the transportation cask. Figure 6.3.2.4-2, which is a history plot of Max EPS for T.IC 4, shows that the Max EPS is 0.96% for the SNF canister (Table 6.3.7.6-2). For T.IC 4, the cask closure bolt strains remain purely elastic, and the Max EPS is 1.76% for the structural body of the cask (Table 6.3.7.6-2). This was the least severe impact condition for the SNF canister of those considered in this transportation cask study.

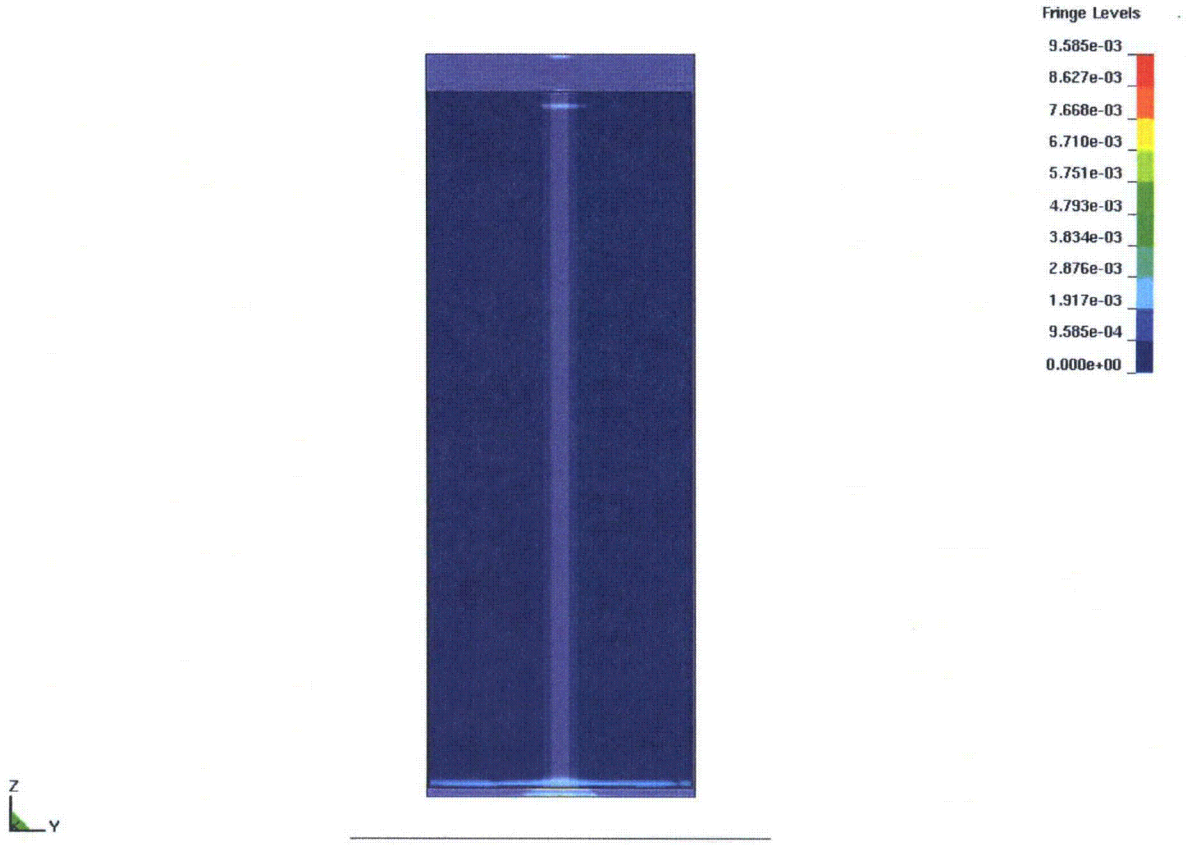

Figure 6.3.2.4-1. Max EPS for SNF Canister inside a Transportation Cask Subjected to a 10-ft Drop of a 10-metric-ton Load onto the Top of the Cask

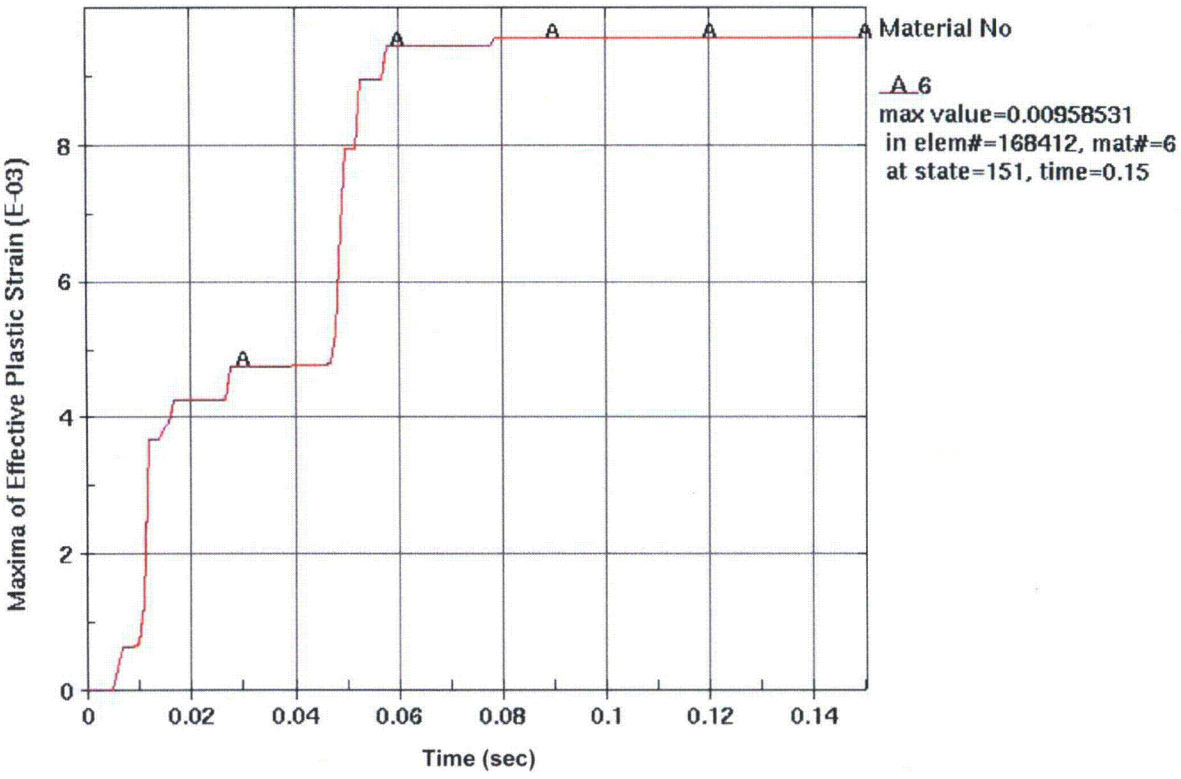

NOTE: The Max EPS history is plotted for the canister. Time is plotted in seconds (ms). The simulation starts a few milliseconds before the time of impact.

Figure 6.3.2.4-2. Max EPS History for SNF Canister inside a Transportation Cask Subjected to a 10-ft Drop of a 10-metric-ton Load onto the Top of the Cask

6.3.2.5 Impact Condition 5a, 5b, 5c, and 5d: 30-ft End Drop with 0, 4, and 45-degree Off-Vertical Orientation and with Center of Gravity over Corner of Cask

The purpose of this section is to investigate the sensitivity of the transportation cask results to impact angle for an end drop of 30 feet. Four Impact Condition (IC) cases are considered (Table 6.3.2.5-1), with T.IC 5a, 5b, and 5c having a 0, 4, and 45-degree off-vertical orientation, and for T.IC 5d, the center of gravity lies directly over the impacting corner of the cask.

Table 6.3.2.5-1. Transportation Cask Contact Angle Sensitivity Study for a 30-ft End Drop

Case Name	Impact Condition	Max EPS for Canister	Max EPS for Cask[b]
T.IC 5a	0 degree	3.55%	3.17%
T.IC 5b[a]	4 degree	5.77%	11.25%
T.IC 5c	45 degree	6.41%	70.56%
T.IC 5d	Center of gravity over cask corner	6.63%	44.88%

NOTE: [a] Same as T.IC 1c.

[b] Values of Max EPS for the cask are applicable to the structural body of the transportation cask, which excludes the shield and shield shell.

Figures 6.3.2.5-1 and 6.3.2.5-2 are the Max EPS fringe and history plots for T.IC 5a, which is a 30-ft end drop with vertical orientation. Impact Condition T.IC 5a has a Max EPS of 3.55% in the canister (Tables 6.3.2.5-1 and 6.3.7.6-2). Because T.IC 5b and T.IC.1c are the same case, Figures 6.3.2.1-5 and 6.3.2.1-6 are also the Max EPS fringe and history plots for T.IC 5b, which has a Max EPS of 5.77% in the canister. Figures 6.3.2.5-3 and 6.3.2.5-4 are the Max EPS fringe and history plots for T.IC 5c, which has an impact angle of 45 degrees. The Max EPS for T.IC 5c is 6.41% in the canister. Figures 6.3.2.5-5 and 6.3.2.5-6 are the Max EPS fringe and history plots for T.IC 5d, which has an impact with the center of gravity over the cask corner. The Max EPS for T.IC 5d is 6.63% for the canister. In spite of the wide range of contact angles, the Max EPS in the canister does not vary substantially, indicating that plastic strain in the cask (Table 6.3.2.5-1) absorbs much of the impact energy, which is particularly true for T.IC 5c and T.IC 5d (Figures 6.3.2.5-7 and 6.3.2.5-8). A close inspection of Figures 6.3.2.5-7 and 6.3.2.5-8 reveals that the region of highest strains is localized to the outer corner of the bottom plate (which is the initial point of impact) and that the maximum strain values away from the corner of the bottom lid are comparable to the Max EPS for the respective SNF canisters themselves.

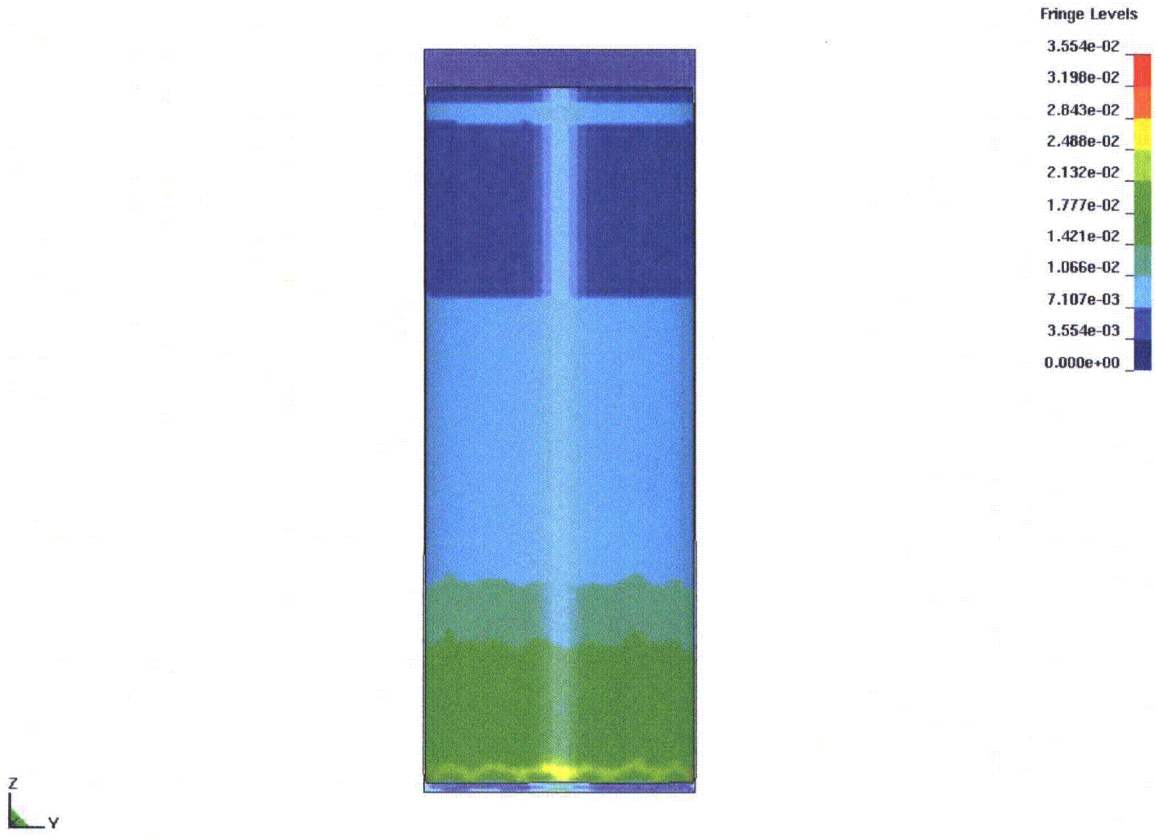

Figure 6.3.2.5-1. Max EPS for SNF Canister inside a Transportation Cask Subjected to a 30-ft End Drop with Vertical Orientation

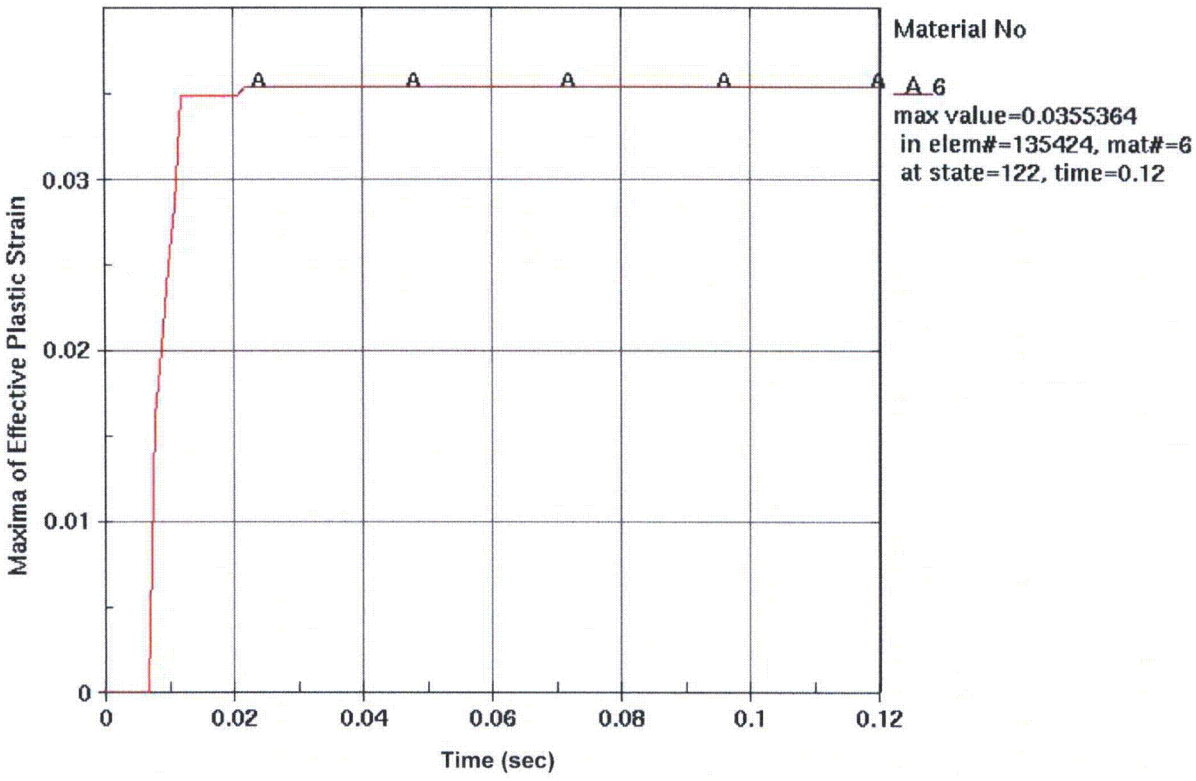

NOTE: The Max EPS history is plotted for the canister. Time is plotted in seconds (sec). The simulation starts a few milliseconds before the time of impact.

Figure 6.3.2.5-2. Max EPS History for SNF Canister inside a Transportation Cask Subjected to a 30-ft End Drop with Vertical Orientation

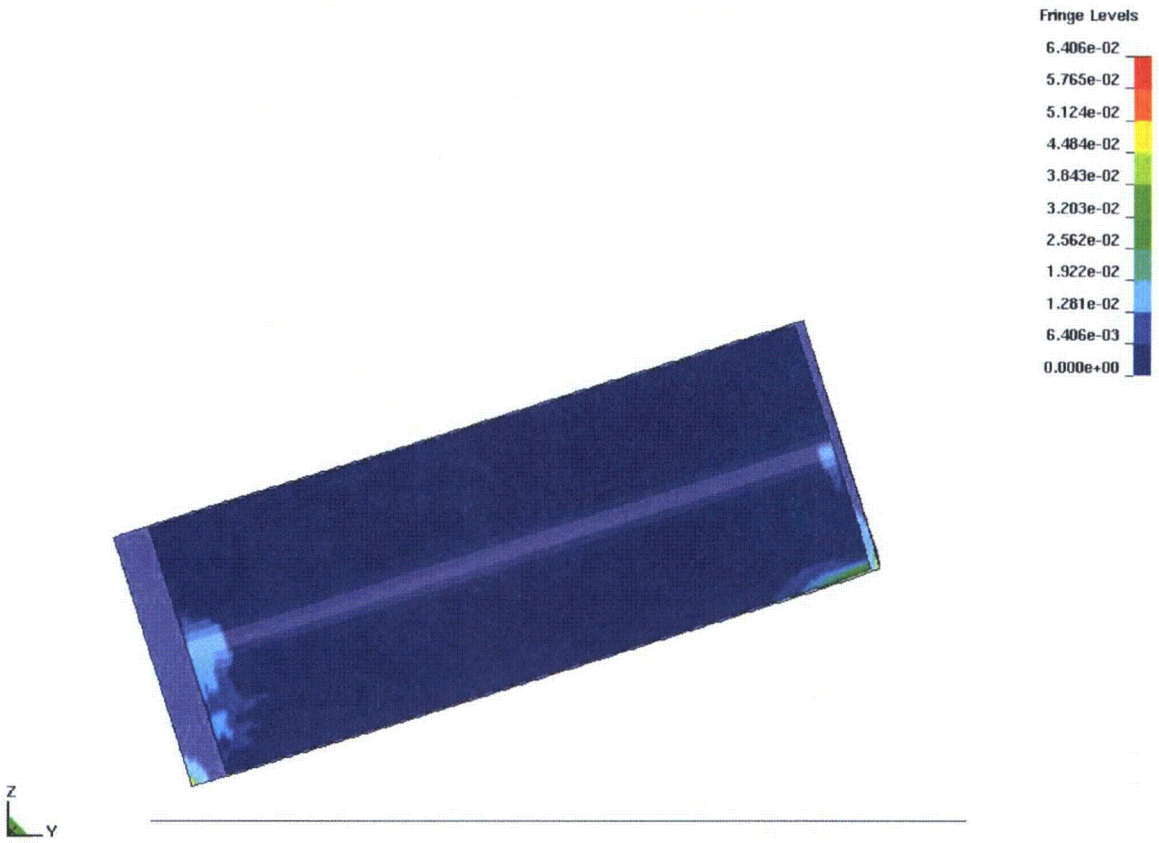

Figure 6.3.2.5-3. Max EPS for SNF Canister inside a Transportation Cask Subjected to a 30-ft End Drop with 45-degree Off-Vertical Orientation

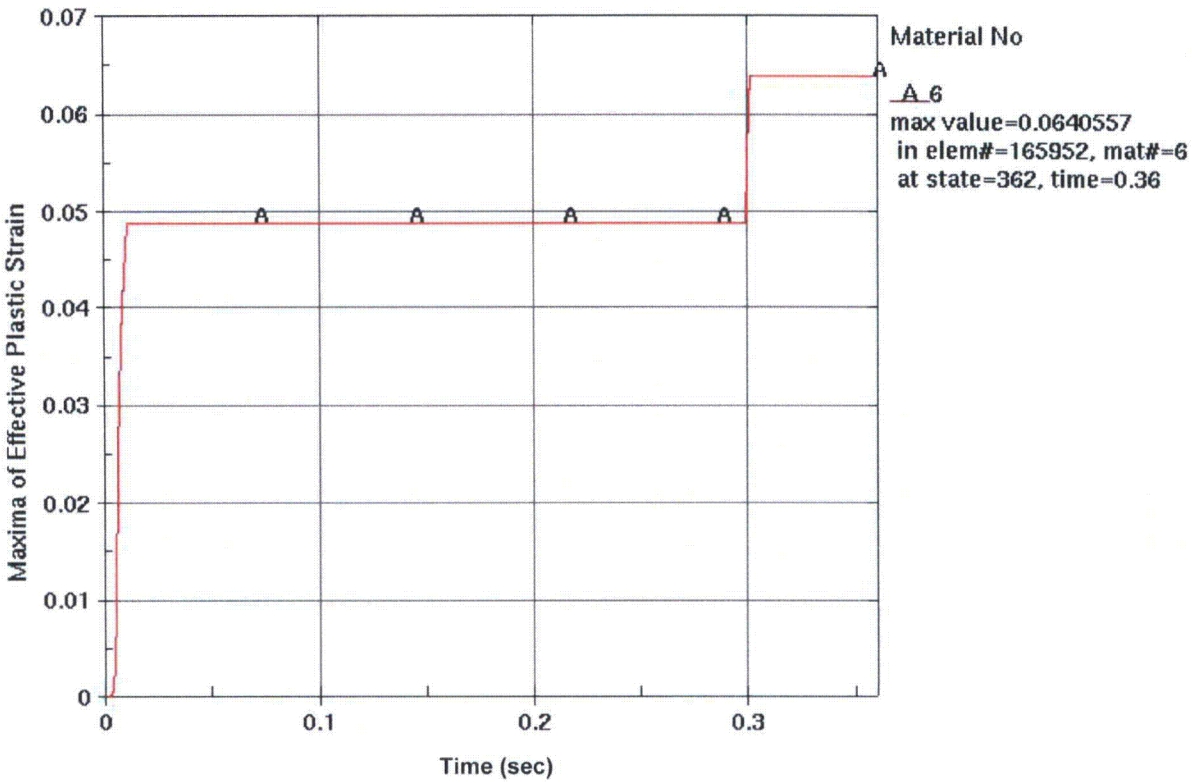

NOTE: The Max EPS history is plotted for the canister. Time is plotted in seconds (sec). The simulation starts a few milliseconds before the time of impact.

Figure 6.3.2.5-4. Max EPS History for SNF Canister inside a Transportation Cask Subjected to a 30-ft End Drop with 45-degree Off-Vertical Orientation

Figure 6.3.2.5-5. Max EPS for SNF Canister inside a Transportation Cask Subjected to a 30-ft End Drop with the Center of Gravity over the Corner of Cask

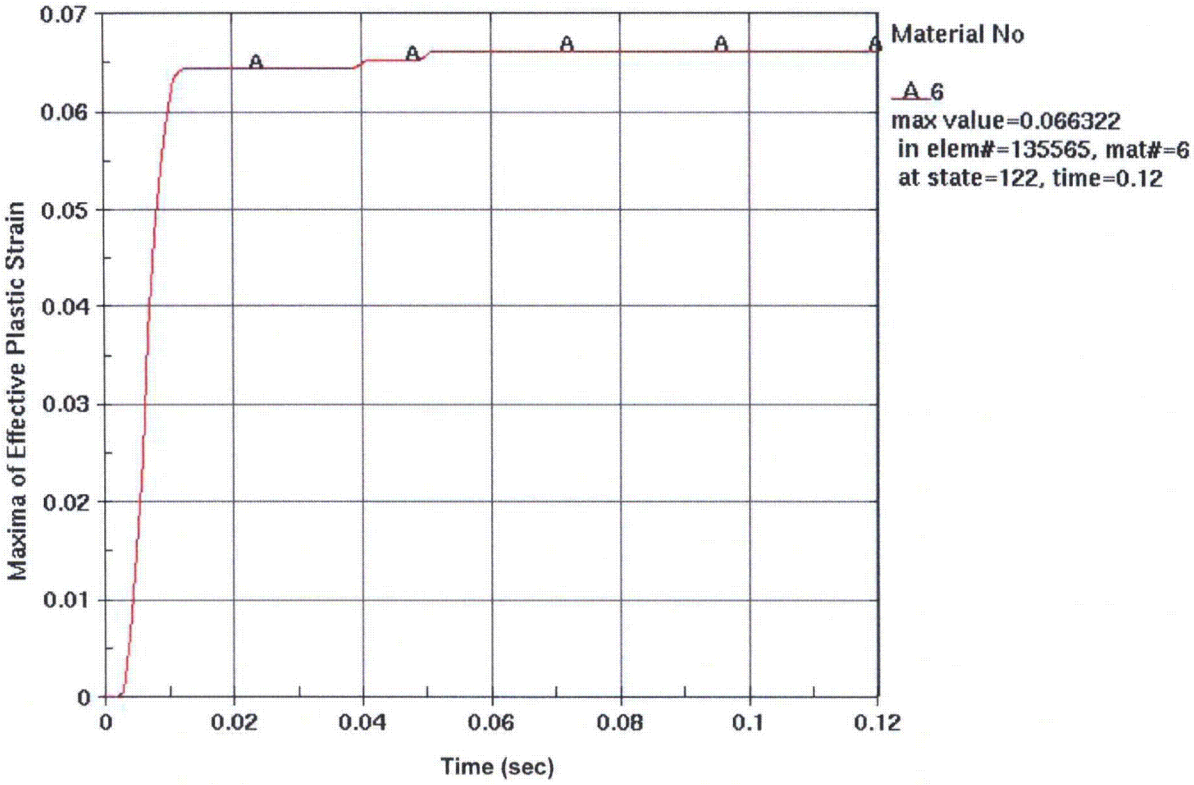

NOTE: The Max EPS history is plotted for the canister. Time is plotted in seconds (sec). The simulation starts a few milliseconds before the time of impact.

Figure 6.3.2.5-6. Max EPS History for SNF Canister inside a Transportation Cask Subjected to a 30-ft End Drop with the Center of Gravity over the Corner of Cask

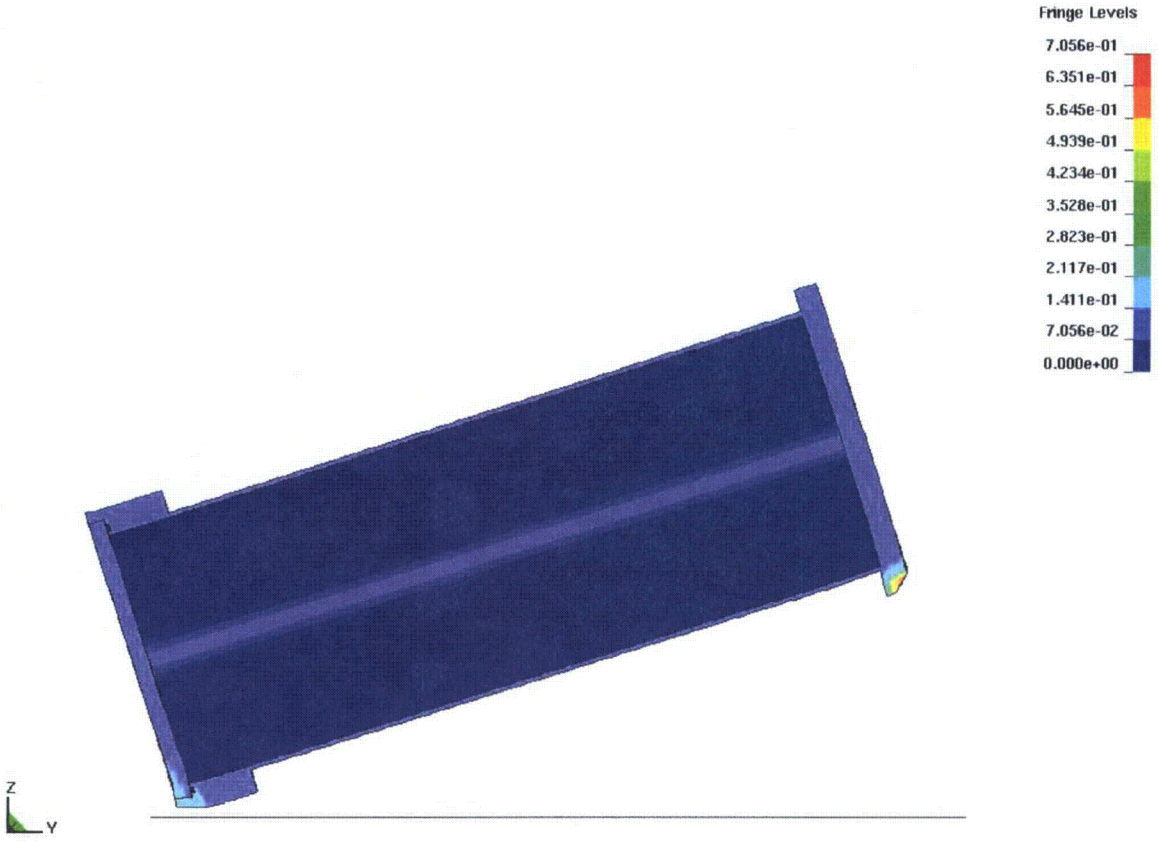

NOTE: The fringe plot shows the transportation cask at the instant of the second impact. The first impact occurred at the corner of the bottom plate (located at the lower right side of the cask in this figure), which is the region of largest strain values.

Figure 6.3.2.5-7. Max EPS for the Structural Body of the Transportation Cask Subjected to a 30-ft End Drop with 45-degree Off-Vertical Orientation

NOTE: The fringe plot shows the transportation cask at the instant of the first impact.

Figure 6.3.2.5-8. Max EPS for the Structural Body of the Transportation Cask Subjected to a 30-ft End Drop with the Center of Gravity over the Corner of Cask

6.3.3 Dual Purpose Canisters

The canister components of the model used in the dynamic impact analyses of the dual purpose canisters are shown in Figure 6.3.3-1. These components consist of a ribbed mass to simulate the SNF, plus the basket containing the SNF, and a thin-walled canister containing this ribbed mass. The corresponding finite element analysis (FEA) model is shown in Figure 6.3.3-2. The geometry and material properties of the structural components of the dual purpose canister are listed in Tables 6.3.3-1 and 6.3.3-2, respectively. The units used in the simulations of the dual purpose canisters are [L] mm, [M] kg, [t] milliseconds, [F] kN, and [P] GPa.

The meshes of the structural components of the canister and SNF basket are merged together at the joint surfaces. The contacting surface between the canister and the SNF basket is represented by a sliding interface with static and kinetic (dynamic) friction coefficients of 0.3 and 0.15, respectively, for all four Impact Condition cases (Table 6.3-3). The solid elements, which represent the canister and SNF basket components, are modeled using the LS-DYNA power-law plasticity material model, Material 18 (Ref 2.2.2).

Four "Impact Condition" cases are considered for the dual purpose canisters (Table 4.3.3-1a). The impacting surface is represented as a rigid (unyielding) surface with a static and kinetic (dynamic) coefficient of friction value of 0.2 (Table 6.3-3).

Table 6.3.3-1. Dimensions and Materials of Structural Components of Dual Purpose Canister

Structural Component	Outer Radius		Length		Wall Thickness		Material
	in	mm	in	mm	in	mm	
Top Plate	34.2	868.4	9.5000	241.30	N/A	N/A	Stainless Steel
Canister Cylinder Wall	34.2	868.4	176.96	4494.7	0.5	12.70	Stainless Steel
Canister Weldment	34.2	868.4	1.540	39.16	0.5	12.70	Stainless Steel
Bottom Plate	34.2	868.4	2.313	58.74	N/A	N/A	Stainless Steel
Fuel Basket Assembly	33.3	846.6	176.50	4483.1	N/A	N/A	Mixed

Source: Attachment 3

Table 6.3.3-2. Material Properties of Structural Components of Dual Purpose Canister

Structural Component	Density		Young's Modulus		ν^a	Strength Coefficient (K)		Hardening Exponent (n)
	lb/in^3	kg/mm^3	psi	GPa		psi	GPa	
Top Plate	0.29	8.02×10^{-6}	2.81×10^7	193.7	0.3	138800.	0.95724	0.264156
Canister Cylinder Wall	0.29	8.02×10^{-6}	2.81×10^7	193.7	0.3	138800.	0.95724	0.264156
Canister Weldment	0.29	8.02×10^{-6}	2.81×10^7	193.7	0.3	138800.	0.95724	0.264156
Bottom Plate	0.29	8.02×10^{-6}	2.81×-10^7	193.7	0.3	138800.	0.95724	0.264156
Fuel Basket Assembly	0.113	3.136×10^{-6}	1.69×10^6	11.652	0.0	8330.	0.0574	0.264156

[a] Poisson's Ratio

Source: Attachment 3

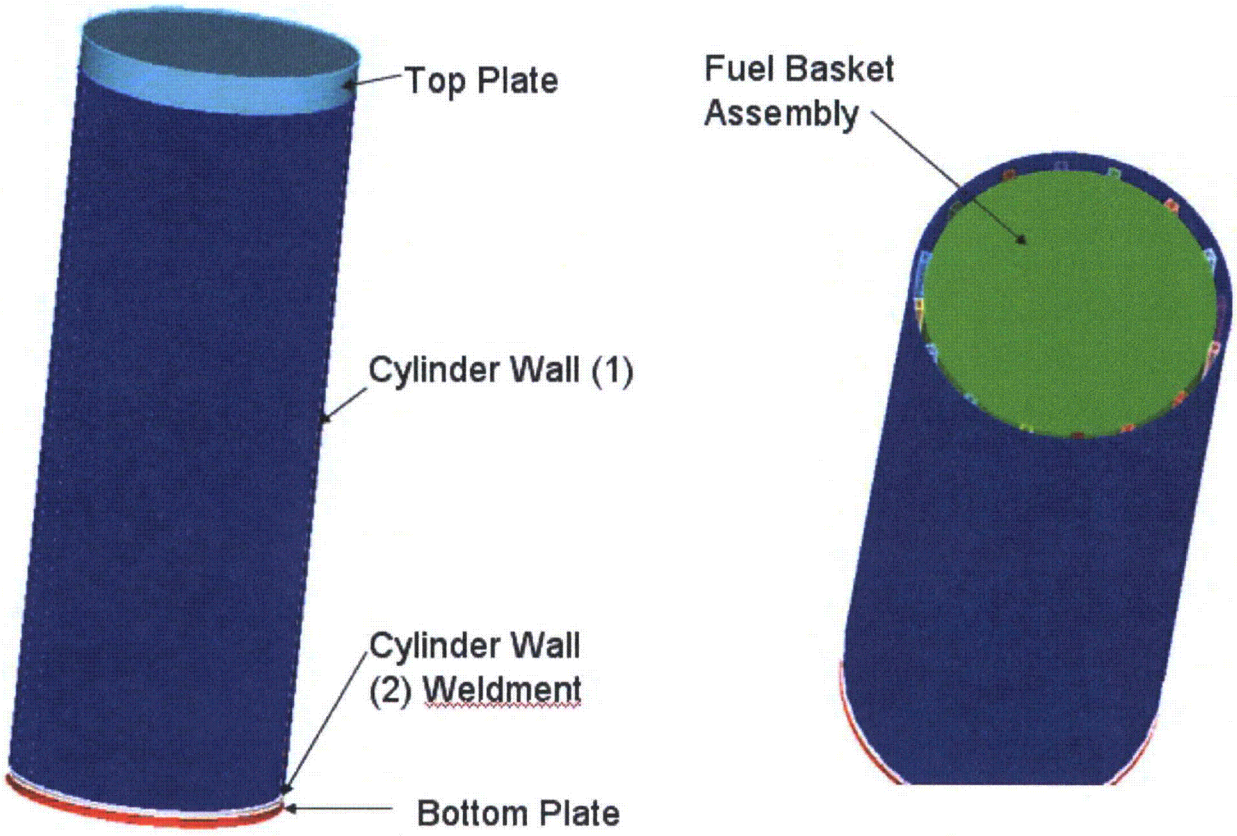

Figure 6.3.3-1. Structural Components of the Dual Purpose Canister

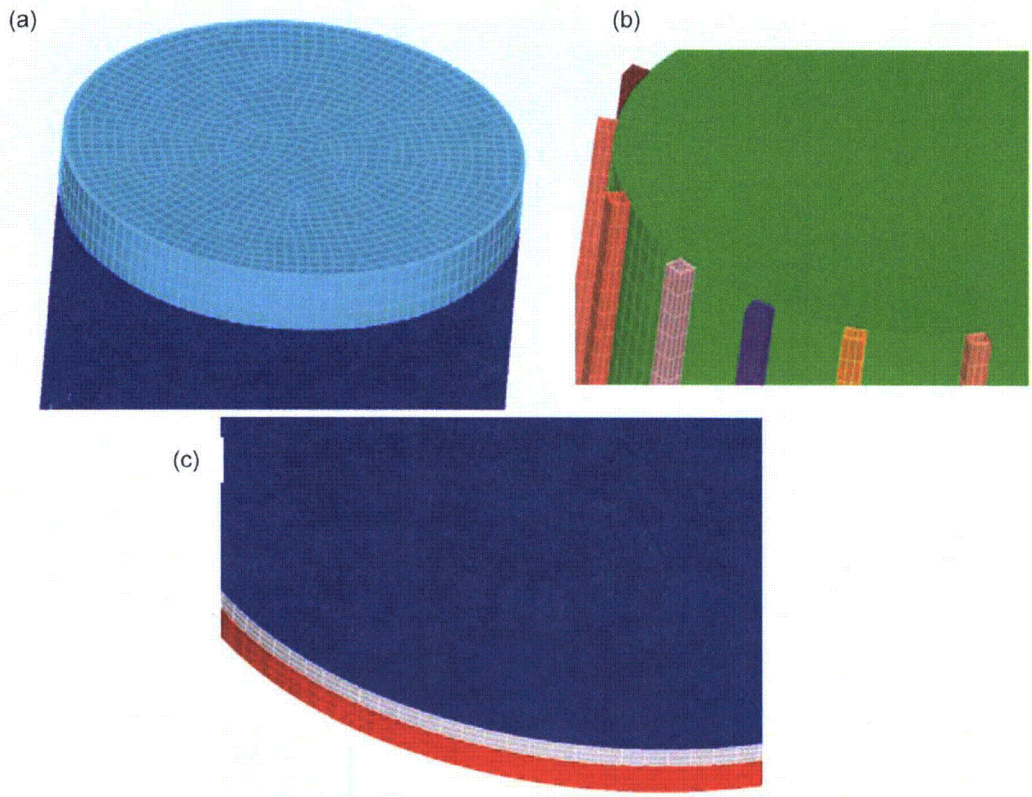

NOTE: Panel (a) is a close-up of the top plate. Panel (b) is a close-up of the SNF basket. Panel (c) is a close-up of the bottom plate.

Figure 6.3.3-2. Finite Element Analysis (FEA) Model Representation of Structural Components of the Dual Purpose Canister

6.3.3.1 Impact Condition 1a and 1b: 32.5- and 40-ft Drop onto End with Vertical Orientation

The purpose of this analysis is to simulate a dual purpose canister (DPC) in free fall from heights of 32.5 and 40 ft to the rigid (unyielding) ground. At impact, the longitudinal axis of the DPC is oriented in the vertical direction, normal to the ground. The geometry and material properties of the DPC are given in Tables 6.3.3-1 and 6.3.3-2.

The dual purpose canister has an impact velocity of 45.7 ft/sec (13.934 m/sec) for the 32.5-ft drop. Figure 6.3.3.1-1 plots the Max EPS for Impact Condition D.IC 1a. The largest value of Max EPS occurs in the bottom cylindrical wall of the canister. Figure 6.3.3.1-2 is the history plot of Max EPS in the canister for the structural components. This impact condition results in no buckling of the canister because the reaction force is uniformly distributed over the lower surface of the canister. For D.IC 1a, the Max EPS is 2.13% for the dual purpose canister (Figure 6.3.3.1-2 and Table 6.3.7.6-3).

Figure 6.3.3.1-3 plots the Max EPS for D.IC 1b, which is the same as D.IC 1a, except with a free fall of 40 ft. The largest value of Max EPS occurs in the bottom cylindrical wall of the canister. Figure 6.3.3.1-4 is the history plot of Max EPS in the canister for the structural components. For D.IC 1b, the Max EPS is 2.65% for the dual purpose canister (Figure 6.3.3.1-4 and Table 6.3.7.6-3).

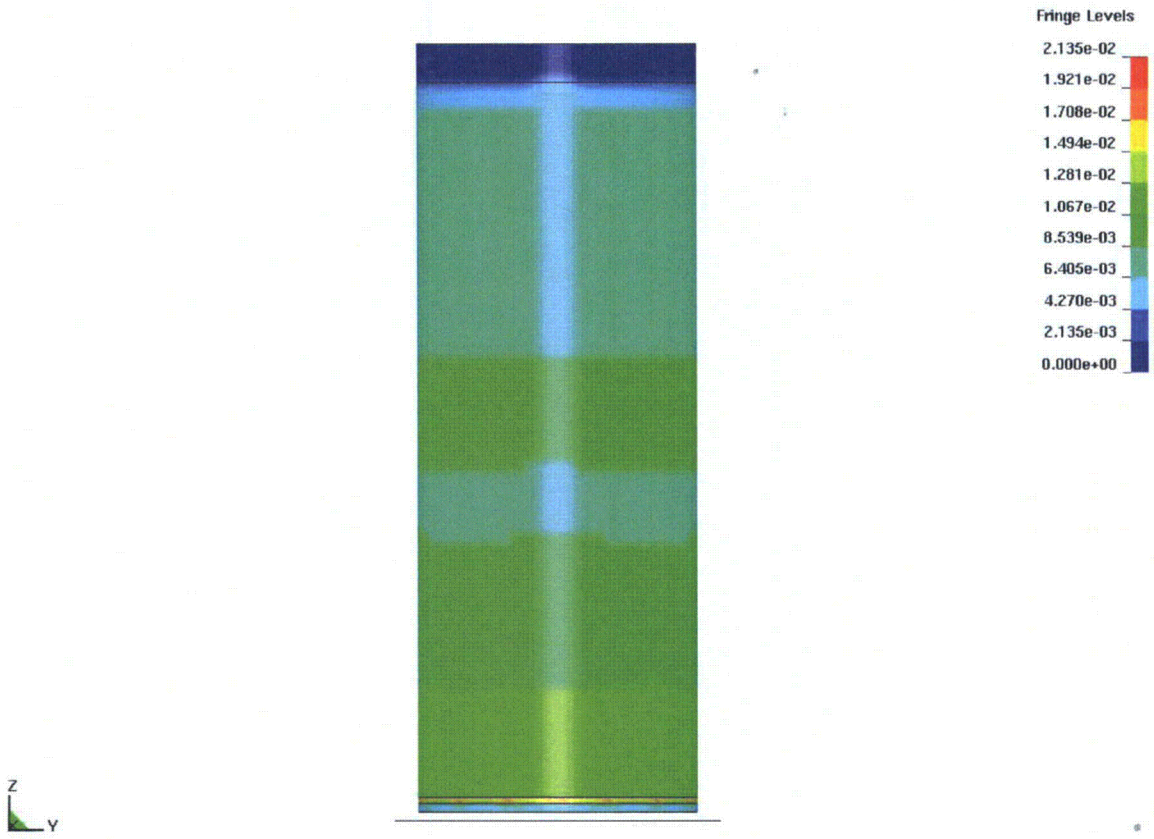

NOTE: The Max EPS is plotted for the entire canister after the time of impact.

Figure 6.3.3.1-1. Max EPS for Dual Purpose Canister Subjected to a 32.5-ft Drop onto End with Vertical Orientation

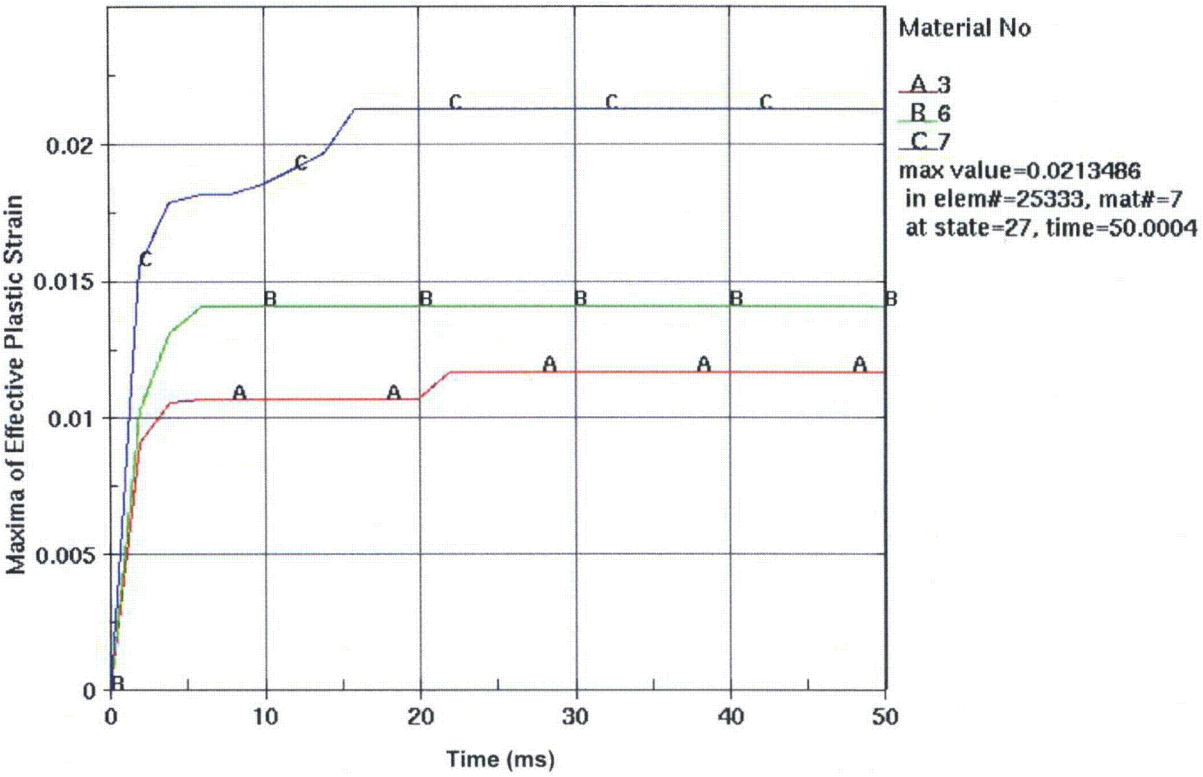

NOTE: The Max EPS histories are plotted for all structural components of the canister, except for the top plate. Time is in milliseconds (sec). The simulation starts at the time of impact.

Figure 6.3.3.1-2. Max EPS History for Dual Purpose Canister Subjected to a 32.5-ft Drop onto End with Vertical Orientation

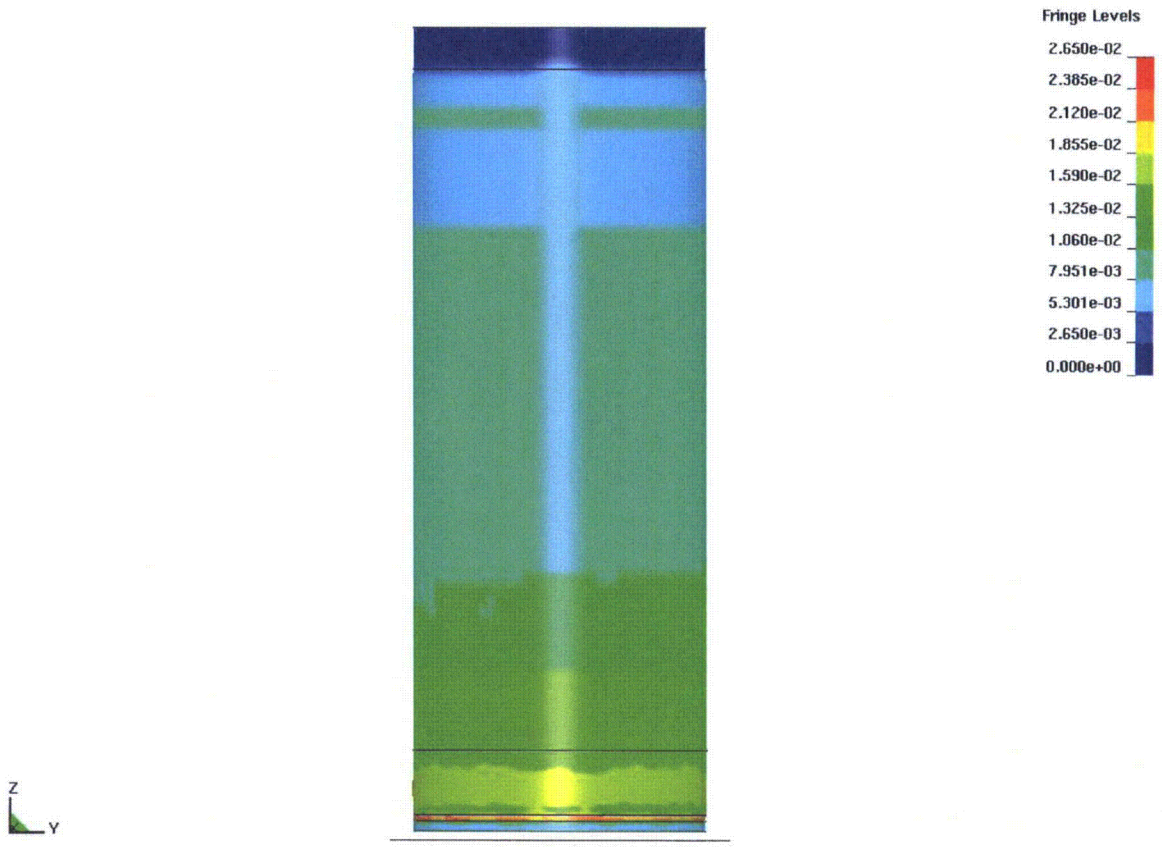

NOTE: The Max EPS is plotted for the entire canister after the time of impact.

Figure 6.3.3.1-3. Max EPS for Dual Purpose Canister Subjected to a 32.5-ft Drop onto End with Vertical Orientation

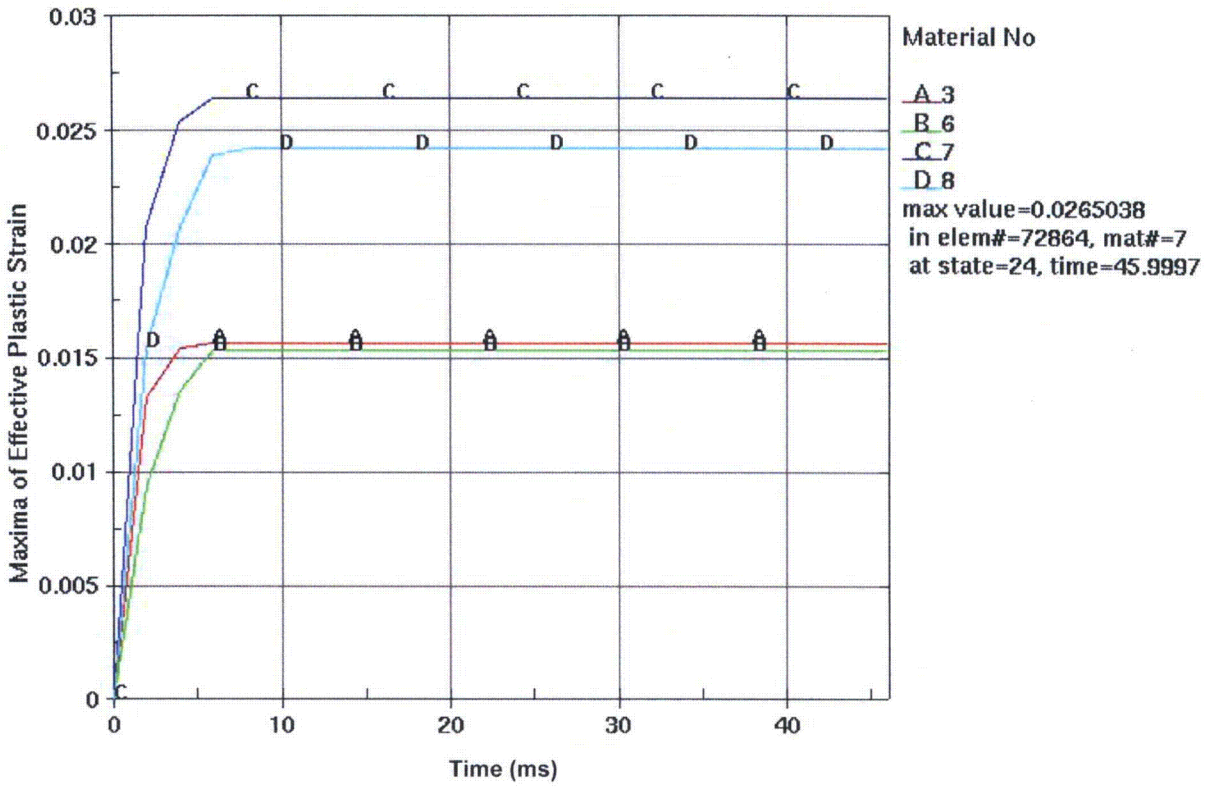

NOTE: The Max EPS histories are plotted for all structural components of the canister, except for the top plate. Time is in milliseconds (ms). The simulation starts at the time of impact.

Figure 6.3.3.1-4. Max EPS History for Dual Purpose Canister Subjected to a 40-ft Drop onto End with Vertical Orientation

6.3.3.2 Impact Condition 2a, 2b, and 2c: 23-, 10-, and 5-ft Drop onto End with 4-degree Off-Vertical Orientation

The purpose of this analysis is to simulate a dual purpose canister (DPC) in free fall from a height of 23 ft to the rigid (unyielding) ground. At impact, the longitudinal axis of the DPC is oriented in a sub-vertical direction, 4-degree off-normal to the ground. The geometry and material properties of the DPC are given in Tables 6.3.3-1 and 6.3.3-2. For the 23-ft drop, the dual purpose canister has an impact velocity of 38.45 ft/sec (11.72 m/sec).

Before discussing the details of this calculation, it is noted that this impact condition produces greater damage to the canister than does D.IC 1a or D.IC 1b, even though it has a shorter free fall height. The reason for the increased damage is the off-vertical shallow impact angle, which causes a small section of the cylinder wall to impact the rigid ground first. The off-center impact results in a large longitudinal compressive impulse, localized at the point of impact, plus a large lateral force from the SNF basket to the canister. Note that the SNF basket is free to move within the canister shell. The localized nature of the impact causes the canister shell to buckle immediately above the point of impact, as shown in Figure 6.3.3.2-1.

Figure 6.3.3.2-1 plots the Max EPS in the canister for D.IC 2a, which has a drop height of 23 ft. Figure 6.3.3.2-2 plots the Max EPS histories for the structural components of the canister. For D.IC 2a, the Max EPS is 24.19% for the canister (Figure 6.3.3.2-2 and Table 6.3.7.6-3), which corresponds to the most severe case considered in the DPC study.

Figure 6.3.3.2-3 plots the Max EPS in the canister for D.IC 2b, which has a drop height of 10 ft. Figure 6.3.3.2-4 plots the Max EPS histories for the structural components of the canister. For D.IC 2b, the Max EPS is 19.71% for the DPC (Figure 6.3.3.2-4 and Table 6.3.7.6-3). Figure 6.3.3.2-5 plots the Max EPS in the canister for D.IC 2c, which has a drop height of 5 ft. Figure 6.3.3.2-6 plots the Max EPS histories for the structural components of the canister. For D.IC 2c, the Max EPS is 15.76% for the canister (Figure 6.3.3.2-6 and Table 6.3.7.6-3).

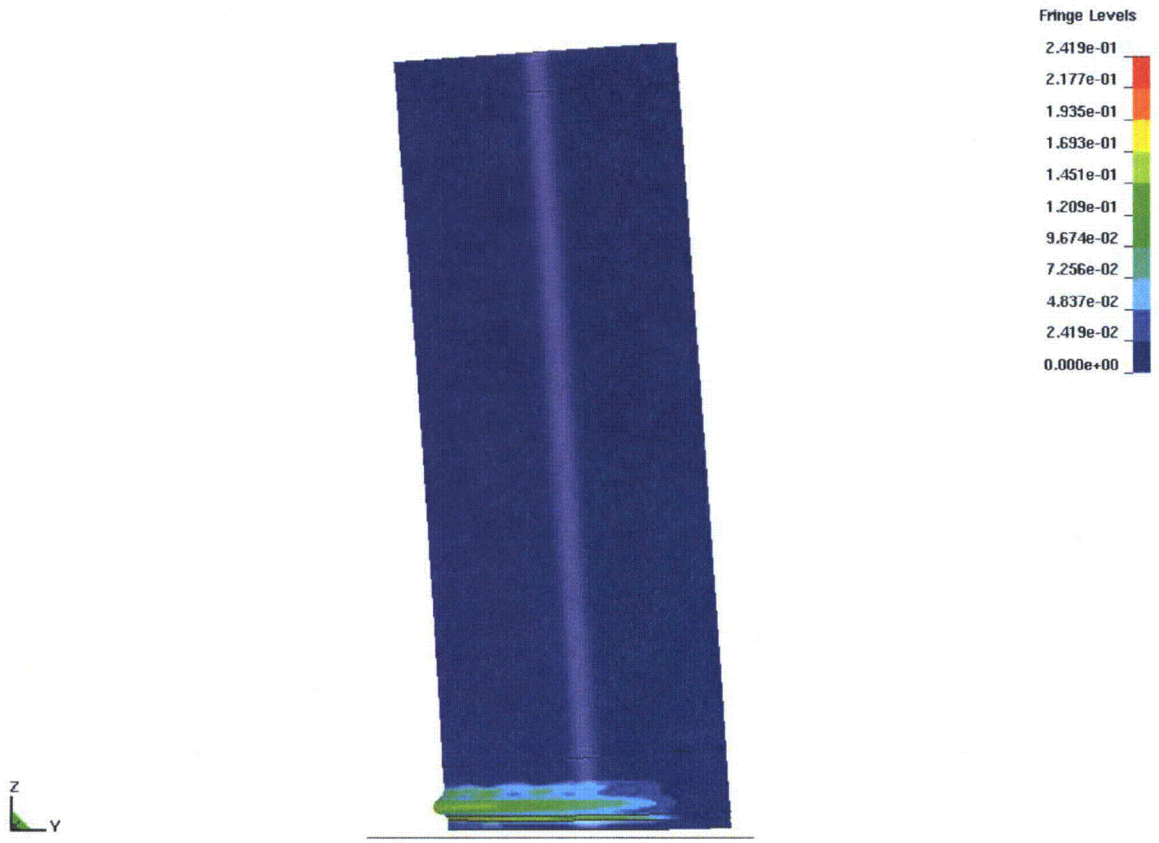

NOTE: The Max EPS is plotted for the entire canister after the time of impact.

Figure 6.3.3.2-1. Max EPS for Dual Purpose Canister Subjected to a 23-ft Drop onto End with 4-degree Off-Vertical Orientation

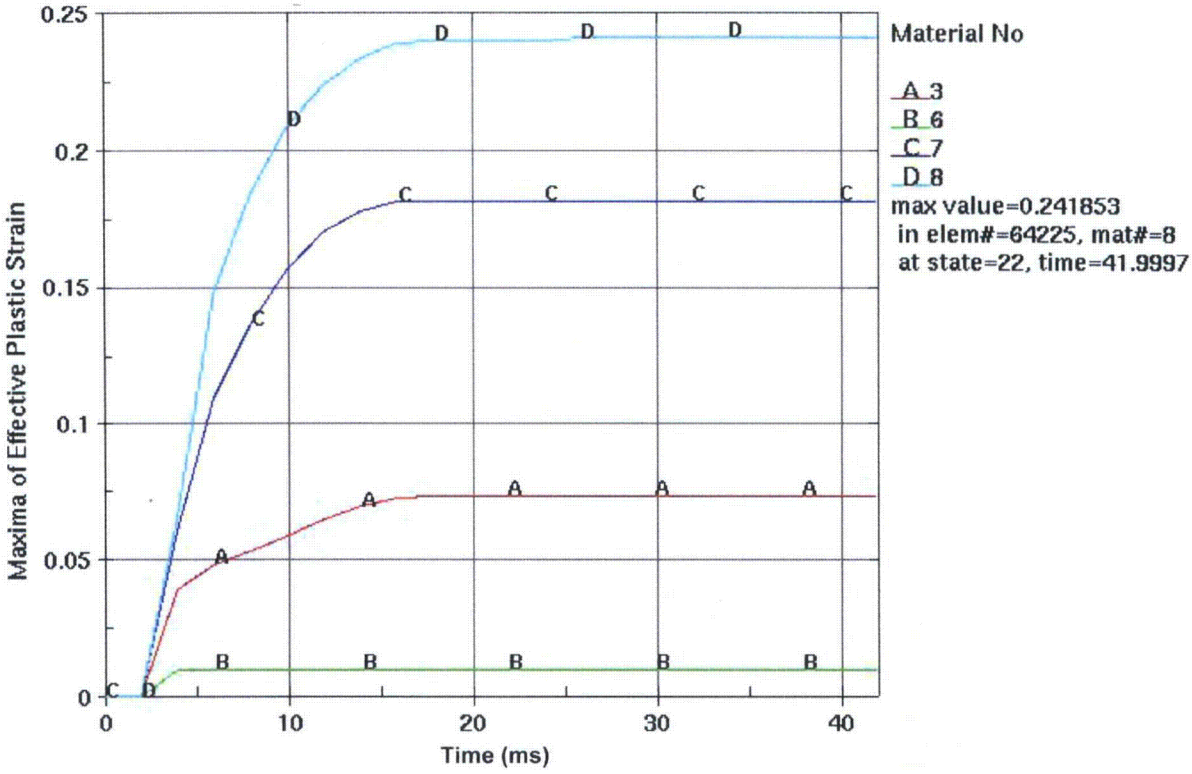

NOTE: The Max EPS histories are plotted for all structural components of the canister, except for the top plate. Time is in milliseconds (ms). The simulation starts a few milliseconds before the time of impact.

Figure 6.3.3.2-2. Max EPS History for Dual Purpose Canister Subjected to a 23-ft Drop onto End with 4-degree Off-Vertical Orientation

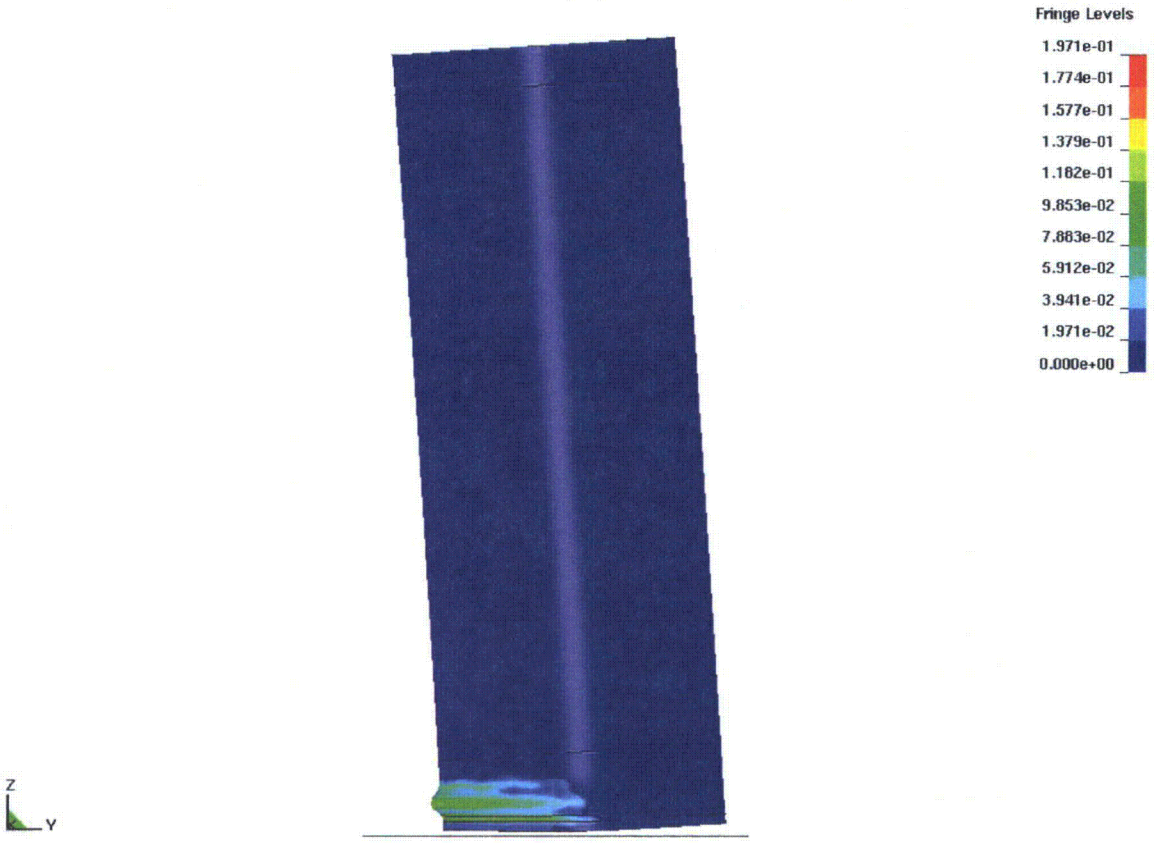

NOTE: The Max EPS is plotted for the entire canister after the time of impact.

Figure 6.3.3.2-3. Max EPS for Dual Purpose Canister Subjected to a 10-ft Drop onto End with 4-degree Off-Vertical Orientation

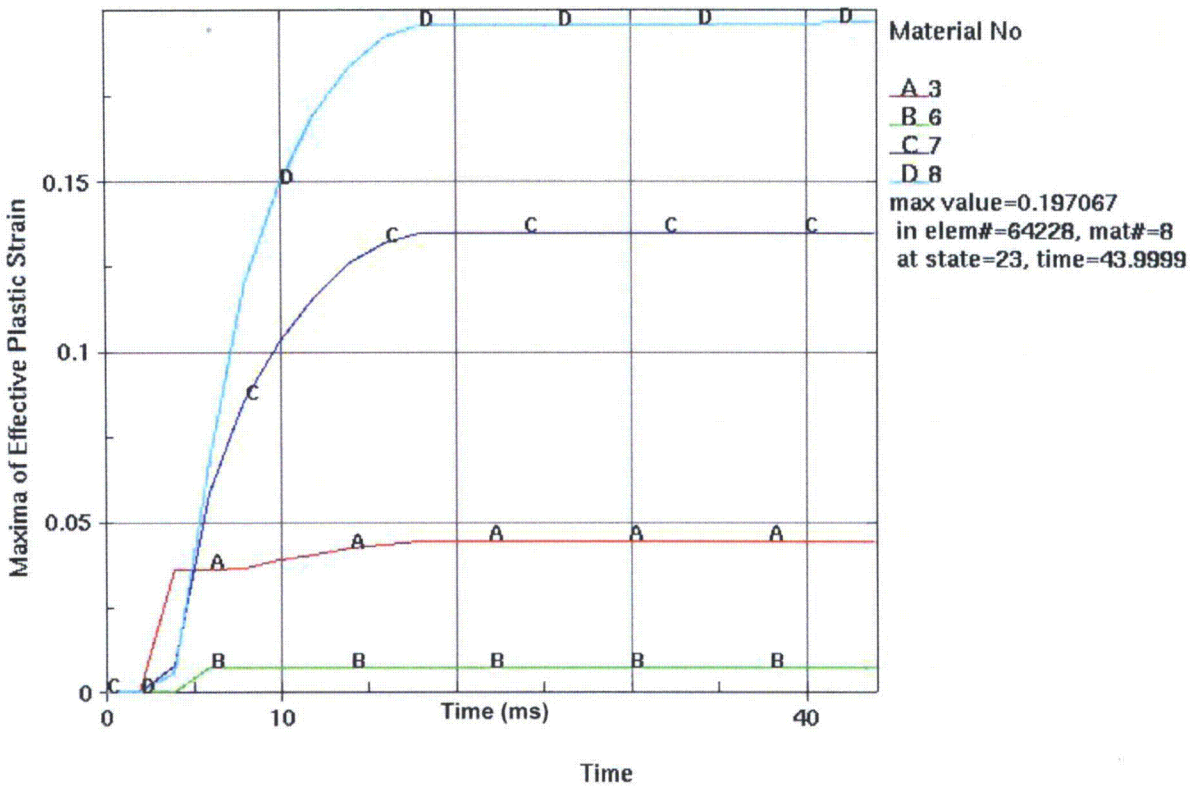

NOTE: The Max EPS histories are plotted for all structural components of the canister, except for the top plate. Time is in milliseconds (ms). The simulation starts a few milliseconds before the time of impact.

Figure 6.3.3.2-4. Max EPS History for Dual Purpose Canister Subjected to a 10-ft Drop onto End with 4-degree Off-Vertical Orientation

NOTE: The Max EPS is plotted for the entire canister after the time of impact.

Figure 6.3.3.2-5. Max EPS for Dual Purpose Canister Subjected to a 5-ft Drop onto End with 4-degree Off-Vertical Orientation

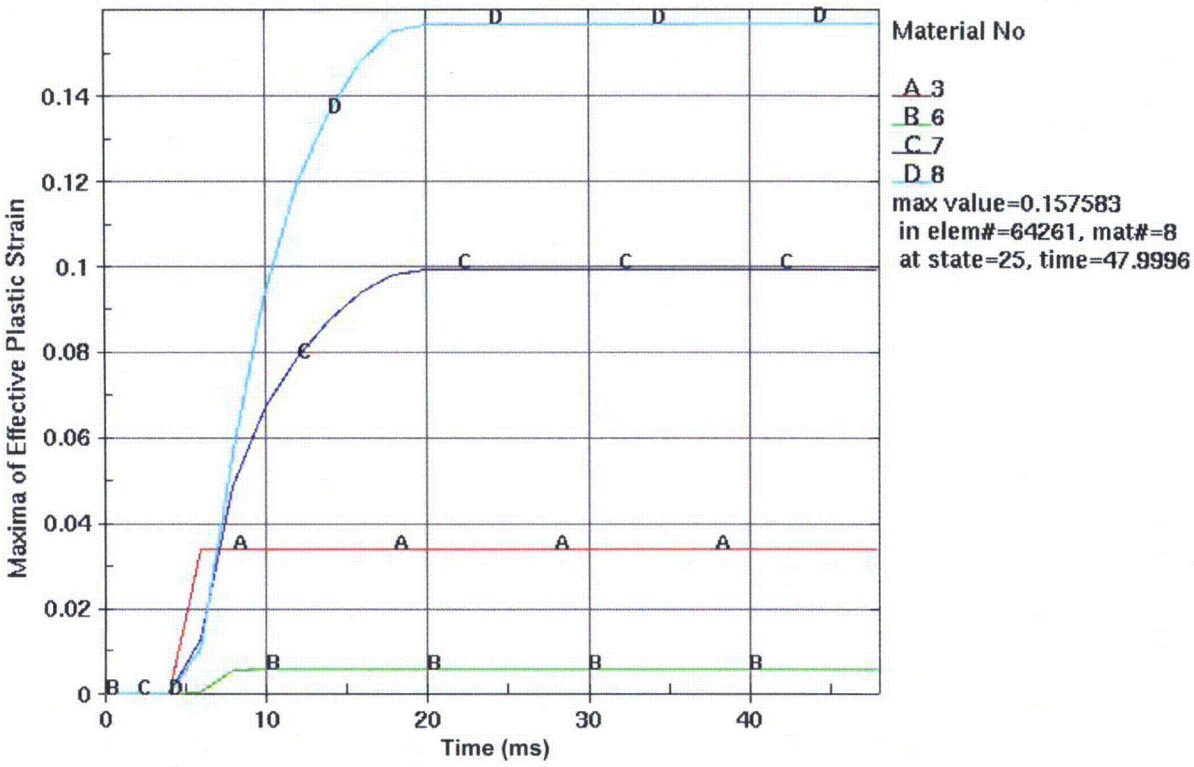

NOTE: The Max EPS histories are plotted for all structural components of the canister, except for the top plate. Time is in milliseconds (ms). The simulation starts a few milliseconds before the time of impact.

Figure 6.3.3.2-6. Max EPS History for Dual Purpose Canister Subjected to a 5-ft Drop onto End with 4-degree Off-Vertical Orientation

6.3.3.3 Impact Condition 3: 40-ft/min Horizontal Collision of Canister Side with Rigid Wall

This analysis simulates a dual purpose canister (DPC) hitting a rigid (unyielding) wall with a horizontal velocity of 40 ft/min (0.203 m/sec). At impact, the longitudinal axis of the DPC is parallel with the vertical wall. Thus, the impact load is normal to the side of the DPC. This is modeled with zero gravity (Figure 6.3.3.3-1). This simulation is intended to be representative of a horizontal collision inside a Canister Transfer Machine (CTM) bell. Compared to Impact Conditions 1 and 2, this impact condition results in much less damage. The lack of damage is also due to the stresses being evenly distributed circumferentially at the ends of the canister.

Figure 6.3.3.3-1, which plots max EPS for the entire canister after impact, shows very minor plastic strain, indicating that most of the strain in the canister is purely elastic. Figure 6.3.3.3-2 plots the Max EPS histories for the structural components of the canister. For Impact Condition 3, the Max EPS is 0.16% for the canister (Table 6.3.7.6-3).

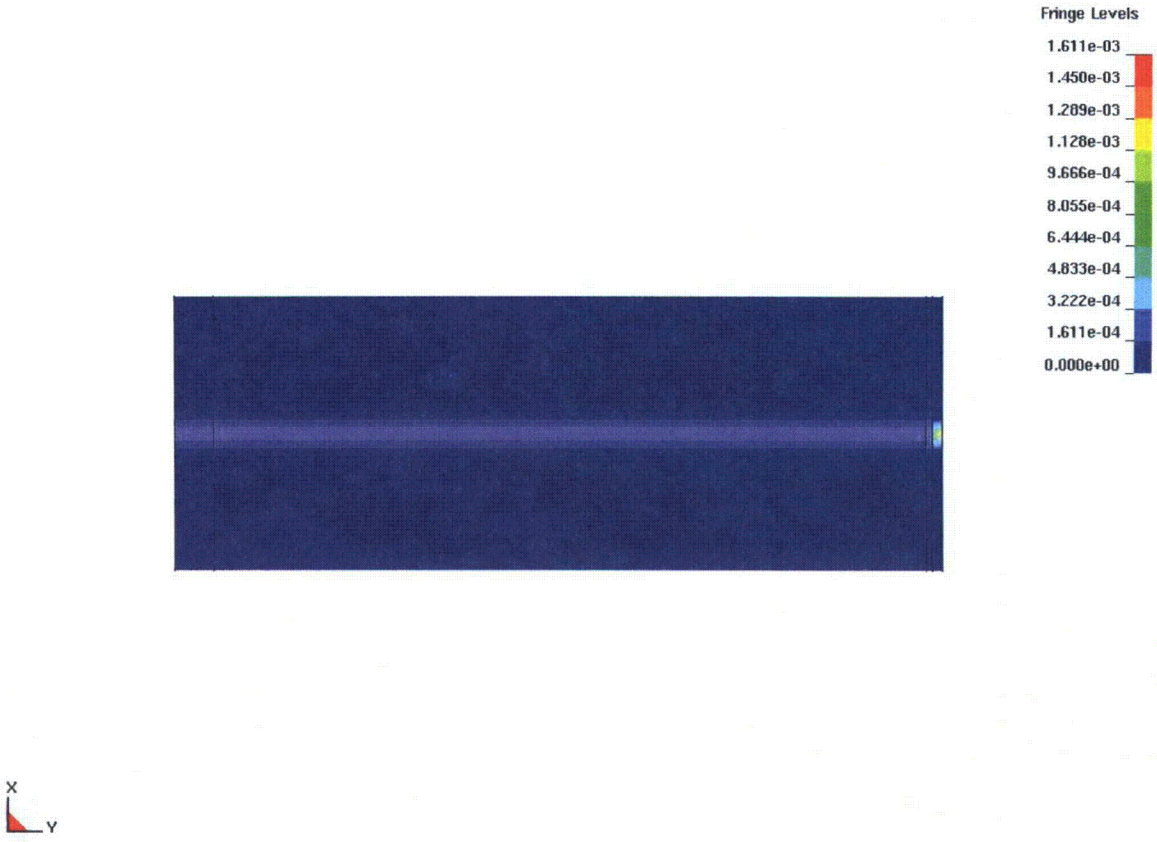

NOTE: Max EPS is plotted for the entire canister after the time of impact. The impact surface is the X-Y plane and the 40-ft/min velocity is applied in the Z direction.

Figure 6.3.3.3-1. Max EPS for Dual Purpose Canister Subjected to a 40-ft/min Horizontal Collision with a Rigid Wall

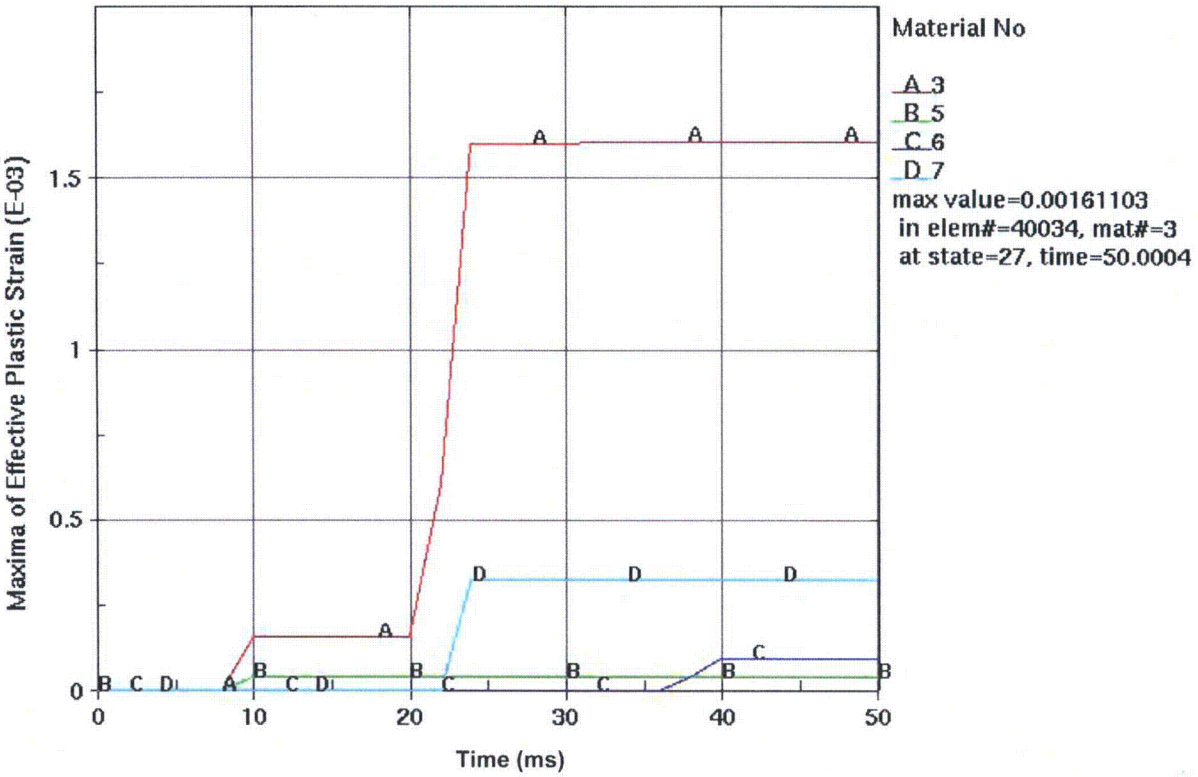

NOTE: The Max EPS histories are plotted for all structural components of the canister. Time is in milliseconds (ms).

Figure 6.3.3.3-2. Max EPS History for Dual Purpose Canister Subjected to a 40-ft/min Horizontal Collision with a Rigid Wall

6.3.3.4 Impact Condition 4: 10-ft Drop of a 10-metric-ton Load onto Top of Canister

This analysis simulates a vertical (upright) dual purpose canister (DPC) at rest on rigid (unyielding) ground. A 10-metric-ton mass freely falls 10 ft and impacts the top of the DPC. The falling mass is modeled as a rigid (unyielding) wall, oriented normal to longitudinal axis of the DPC. The geometry and material properties of the DPC are given in Tables 6.3.3-1 and 6.3.3-2. The 10-metric-ton mass has a velocity of 7.729 m/sec at the time of impact with the stationary DPC. Static and kinetic (dynamic) friction coefficients of 0.8 are applied to the contacting surfaces between the falling mass and canister (Table 6.3-3).

This impact condition results in only small plastic deformation of the canister. Since the impact load is evenly distributed in circumference, the path of the impact load of the rigid mass is through the canister wall to the rigid floor. Figure 6.3.3.4-1 plots the Max EPS, with the color pattern indicating the strain wave propagation. Figure 6.3.3.4-2 plots Max EPS histories for the respective structural components of the canister. For D.IC 4, the Max EPS is 0.75% for the dual purpose canister (Figure 6.3.3.4-2 and Table 6.3.7.6-3).

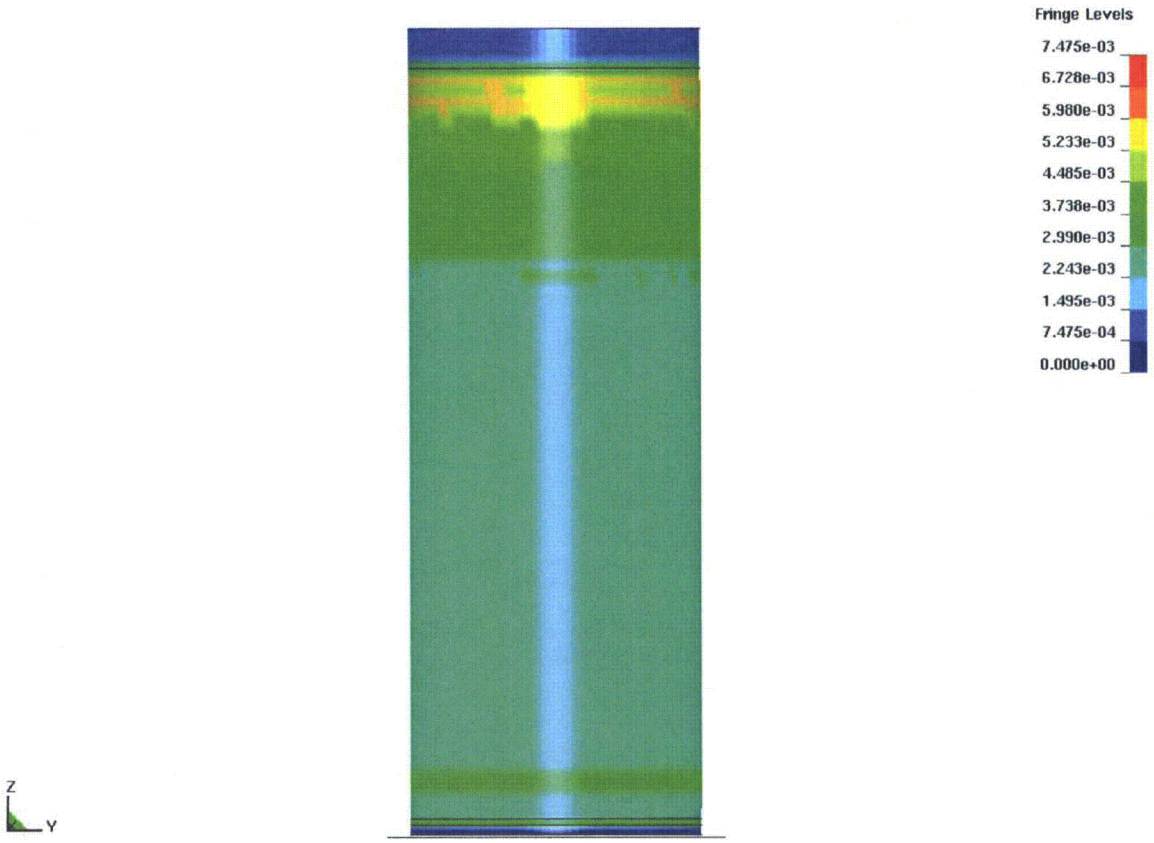

NOTE: The Max EPS is plotted for the entire canister after the time of impact.

Figure 6.3.3.4-1. Max EPS for Dual Purpose Canister (DPC) Subjected to a 10-ft Drop of a 10-metric-ton Load onto Top of Canister

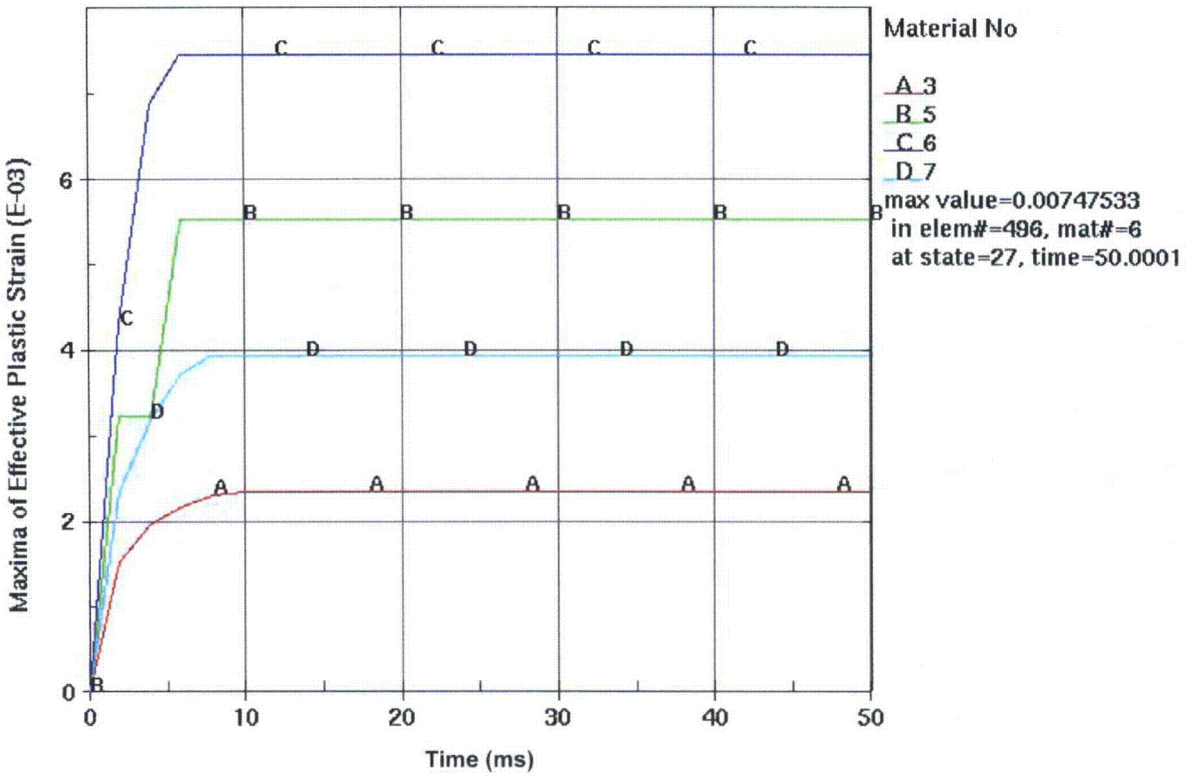

NOTE: The Max EPS histories are plotted for all structural components of the canister. Time is in milliseconds (ms). The simulation starts at the time of impact.

Figure 6.3.3.4-2. Max EPS History for Dual Purpose Canister Subjected to the Impact from a 10-ft Drop of a 10-metric-ton Mass onto Top of Canister

6.3.3.5 Sensitivity Studies for Impact Condition 2a: 23-ft End Drop with 4-degree Off-Vertical Orientation

The following sections describe an hourglass control study, a sensitivity study of friction coefficient, and a numerical mesh density study (Table 4.3.3-1b). Table 6.3.3.5-1 summarizes the sensitivity cases, along with the values of Max EPS for those cases. The results of these studies are the basis for the revised base case model that is applied to all of the DPC calculations for D.IC 2, which are described in Sections 6.3.3.2 and 6.3.3.6.

Table 6.3.3.5-1. Summary of Sensitivity Cases for Impact Condition 2a: 23-ft End Drop, with 4-degree Off-Vertical Orientation

Case Name	LS-DYNA Hour Glass Control Parameter	Friction Coefficient	Numerical Mesh Case	Max EPS	Comments[d]
H1-F1-M1	1	0.2	1	29.22%	Original base case[a]
H2-F1-M1[c]	9	0.2	1	19.37%	Hourglass sensitivity case; hourglass control parameter 9 selected as preferred
H2-F2-M1	9	0.7	1	19.60%	Friction sensitivity case; results insensitive to friction coefficient
H2-F1-M2[c]	9	0.2	2	21.88%	Element axial dimension is 1/3rd that of M1; element circumferential is 1/2 that of M1
H2-F1-M3[c]	9	0.2	3	24.19%	Element axial dimension is 1/2 that of M2; Revised base case[b]
H2-F1-M4[c]	9	0.2	4	24.18%	Element circumferential dimension is 1/2 that of M3
H2-F1-M5[c]	9	0.2	5	24.93%	Element axial dimension is 1/2 that of M4

NOTE: [a] The original base case is applied to all D.IC 1 (Section 6.3.3.1), D.IC3 (Section 6.3.3.3), and D.IC4 cases (Section 6.3.3.4).
[b] The revised base case is applied to all of the D.IC 2 cases reported in Sections 6.3.3.2 and 6.3.3.6.
[c] The five numerical mesh density sensitivity cases.
[d] The description of the element dimensions is applicable to the region of the shell where the highest effective plastic strains occur.

6.3.3.5.1 Sensitivity Study of Hourglass Control for Impact Condition 2a: 23-ft End Drop with 4-degree Off-Vertical Orientation

Hourglass control is used to control the zero energy modes (called hourglassing modes) that arise with one-point integration methods. The explicit solid elements in LS-DYNA are one-point integration elements. Undesirable hourglassing may be resisted with a viscous damping or small elastic stiffness capable of stopping the formation of anomalous modes, with a negligible affect on the stable global modes. The default hourglass control type in LS-DYNA is type 1 and is termed the standard LS-DYNA viscous form. For the original base case (Case H1-F1-M1 in Table 6.3.3.5-1), a default hourglass control type 1 was used, and hourglassing modes were observed. Use of hourglass control type 9, which is an enhanced assumed strain stiffness form for 3-D solid elements (Case H2-F1-M1 in Table 6.3.3.5-1), was found to be effective in removing these hourglassing modes.

6.3.3.5.2 Sensitivity Study of Friction Coefficient for Impact Condition 2a: 23-ft End Drop with 4-degree Off-Vertical Orientation

To investigate the sensitivity of the results to the friction coefficient, two cases are considered for D.IC 2a, which is a 23-ft end drop with 4-degree off-vertical orientation. The two friction-coefficient sensitivity cases (H2-F1-M1 and H2-F2-M1 from Table 6.3.3.5-1) utilize the LS-DYNA hourglass control type 9, which was determined in Section 6.3.3.5.1. The first case (H2-F1-M1) applies the standard value of canister-to-rigid-ground friction coefficient (0.2) applied to the DPC analyses (Table 6.3-3). The second case (H2-F2-M1) applies a value of 0.7 for the canister-to-rigid-ground friction coefficient. This relatively large difference in canister-to-rigid-ground friction coefficient results in a negligible difference in Max EPS (19.37% versus 19.60% as seen in Table 6.3.3.5-1). Therefore, the canister-to-rigid-ground friction coefficient

has a negligible influence on the value of Max EPS. Therefore, it was determined that a canister-to-rigid-ground friction coefficient value of 0.2 is reasonable for the DPC study.

6.3.3.5.3 Sensitivity Study of Numerical Mesh Density for Impact Condition 2a: 23-ft End Drop with 4-degree Off-Vertical Orientation

To investigate the sensitivity of the results to numerical mesh density, five cases are considered for D.IC 2a: which is a 23-ft end drop with 4-degree off-vertical orientation. The five cases are the second case and the last four cases listed in Table 6.3.3.5-1: H2-F1-M1, H2-F1-M2, H2-F1-M3, H2-F1-M4, and H2-F1-M5, where M1 through M5 stand for meshes 1 through 5.

The mesh sensitivity study involved reducing the element sizes in the region of the shell where the highest effective plastic strains occur. As indicated in the comments of Table 6.3.3.5-1, the numerical mesh density is progressively refined in meshes M1 through M5. The trend between Max EPS and mesh density is that Max EPS increases with mesh density, approaching a stable or asymptotic value for mesh density equal to or greater than that of mesh M3. The original mesh (M1) analysis predicted a Max EPS of 19.37%. Analysis using M2 (element size reduced from M1 by a factor of 3 in the axial direction and by a factor of 2 in the circumferential direction) predicted a Max EPS of 21.88%, which is 1.13 times greater than Max EPS for M1. Preferably, this delta should be less than 10%. Analysis using M3 (element size reduced from M2 by a factor of 2 in the axial direction) predicted a Max EPS of 24.19%, which is 1.11 times greater than Max EPS for M2. Analysis using M4 (element size reduced from M3 by a factor of 2 in the circumferential direction) predicted a Max EPS of 24.18%, nearly the same as in M3. Analysis using M5 (element size reduced from M4 by a factor of 2 in the axial direction) predicted a Max EPS of 24.93%, which is only 1.03 times greater than the Max EPS for M4 and M3, indicating that M3 has sufficient mesh density to accurately capture the maximum effective plastic strains. Therefore, it was decided to conduct the DPC analyses discussed in Sections 6.3.3.2 and 6.3.3.6 with Case H2-F1-M3 (Table 6.3.3.5-1).

6.3.3.6 Shell- and Bottom-Lid Thickness Study for Impact Condition 2a: 23-ft End Drop with 4-degree Off-Vertical Orientation

Three shell thicknesses and four bottom-lid thicknesses are considered to investigate the sensitivity of the D.IC 2a results to canister geometry. The matrix of cases is listed in Table 6.3.3.6-1. The Max EPS for each geometry case are shown as trend lines in Figure 6.3.3.6-1. Panel a in Figure 6.3.3.6-1 shows that for a given shell thickness, Max EPS increases as a function of bottom plate thickness. Panel b in Figure 6.3.3.6-1 shows that for a given bottom plate thickness, Max EPS decreases as a function of shell thickness.

Table 6.3.3.6-1. Dual Purpose Canister Shell- and Bottom-Thickness Sensitivity Study for Impact Condition 2a: 23-ft End Drop, with 4-degree Off-Vertical Orientation

Case Name	Shell Thickness (in)	Bottom-Plate Thickness (in)	Max EPS for Canister
S1-L1[a]	0.5	2.313	24.19%
S2-L1	0.75	2.313	21.52%
S3-L1	1.0	2.313	16.53%
S1-L2	0.5	0.75	23.34%
S1-L3	0.5	4.0	25.15%
S2-L3	0.75	4.0	22.57%
S3-L3	1.0	4.0	18.08%
S2-L4	0.75	8.0	24.07%
S3-L4	1.0	8.0	19.50%

NOTE: [a]This is the revised base case (Case H2-F1-M3 from Table 6.3.3.5-1).

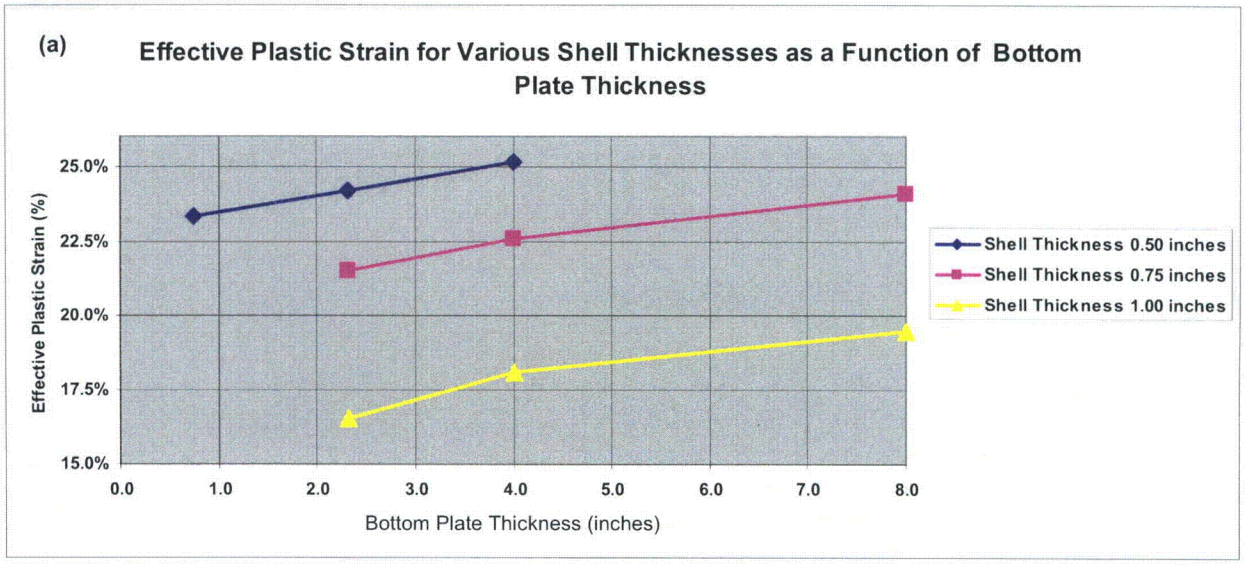

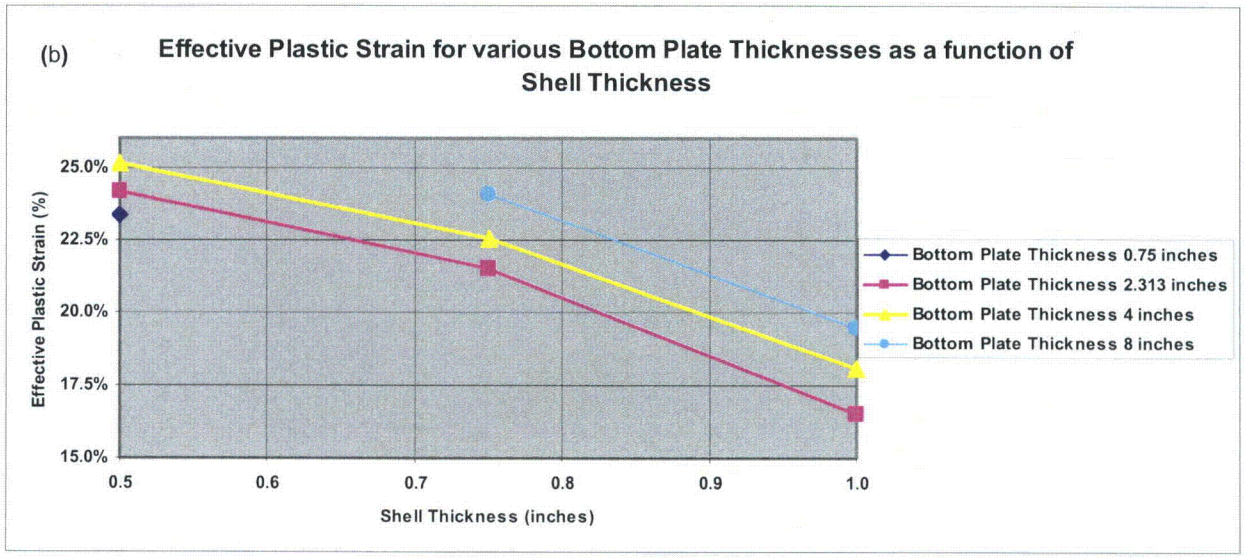

NOTE: Panel (a) plots the Max EPS as a function of bottom plate thickness for three different canister shell thicknesses. Panel (b) plots the Max EPS as a function of canister shell thickness for three different bottom plate thicknesses.

Figure 6.3.3.6-1. Max EPS Plotted as a Function of Shell Thickness and Bottom Plate Thickness for Dual Purpose Canister Subjected to a 23-ft End Drop with 4-degree Off-Vertical Orientation

6.3.4 Transportation, Aging, and Disposal Canisters

The transportation, aging, and disposal (TAD) canisters are represented by the results for the dual purpose canisters (Section 6.3.3). As discussed in Section 4.3.3.1, a single representative canister is used for the structural failure analyses of dual purpose canisters and TAD canisters.

6.3.5 DOE Spent Nuclear Fuel Canisters

The results for the DOE spent nuclear fuel (DSNF) canisters are supplied by Idaho National Laboratory (Ref. 2.2.37). One "Impact Condition" case, a 23-ft end drop with 3-degree off-vertical orientation, was considered for the DOE SNF canisters (Table 4.3.3-1a). The failure probability results are given in Table 6.3.7.6-4.

6.3.6 Multi-Canister Overpack

The results for the multi-canister overpack (MCO) are supplied by Idaho National Laboratory (Ref. 2.2.37). One "Impact Condition" case, a 23-ft end drop with 3-degree off-vertical orientation, was considered for the MCOs (Table 4.3.3-1a). The failure probability results are given in Table 6.3.7.6-5.

6.3.7 Probabilistic Steel Failure Analysis Approach

6.3.7.1 Overview

As discussed in Sections 4.3.3.2 and 4.3.3.3, representative container configurations and loading conditions were selected for the purpose of determining the conditional probability of containment failure for each scenario. Given a numerical simulation impact analysis for a configuration and load, effective strain fields or distributions throughout the container and/or transportation cask are determined. Failure of containment can occur when there is a strain component of sufficient magnitude that a through-going breakage or puncture of the container occurs. However, the LS-DYNA-calculated distribution of strains in a container for a specific impact analysis will not indicate an obvious breach. Thus, the challenge is to relate the strains obtained from an LS-DYNA simulation to the probability of failure, which is accomplished through the use of a fragility curve (Figure 6.3.7-1). The fragility curve relates the magnitude of strain (elongation) to the likelihood of failure of the container steel material.

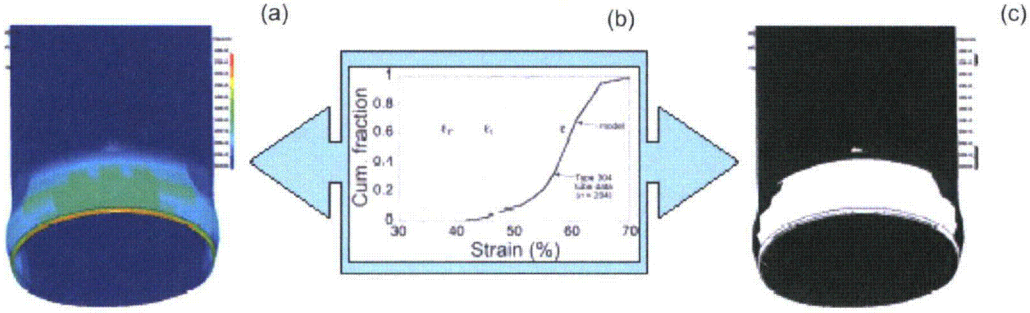

NOTE: Panel (a) shows the maximum effective plastic strain (Max EPS) distribution calculated with LS-DYNA. Panel (b) shows the fragility curve of the CDF of the probability of failure versus EPS. Panel (c) shows the resulting probability of failure.

Figure 6.3.7-1. A Schematic of Relationship between Max EPS, Fragility Curve, and Probability of Failure

6.3.7.2 Probabilistic Steel Failure Analysis Approach

The analysis approach to process strain data was developed and encoded in a MATLAB script. A probability of failure is determined from the cumulative distribution function (CDF) of capacity or fragility curve (as discussed below) from either the global maximum strain or the maximum strain values for the respective structural components, such as the lower lid of the canister.

The probability of failure is calculated based on the maximum strain for a single finite element brick, obtained from LS-DYNA simulations (Assumption 3.2.3.2). Fracture propagation takes place on the milliseconds time-scale, and thus propagates across the canister wall thickness very quickly, compared to the time frame of the LS-DYNA simulations. Furthermore, the fragility curve is obtained on the basis of a maximum average strain over the thickness of the respective specimens, which are 2-in-long stainless steel 304 coupons. Although LS-DYNA results provide multiple values of the strain through the thickness of the canister wall, it is more conservative to use the maximum strain value at a single finite element brick, rather than the average of multiple values across the thickness of the wall.

6.3.7.3 Establishment of the Fragility Curve

The distribution used to evaluate probability of canister failure as a function of strain was derived from a statistical characterization of engineering strain data of tensile failure for 204 specimens of stainless steel 304 annealed tubing (Ref. 2.2.23). This was the largest relevant set of repeated independent tests readily available for statistical analysis. Moreover, the use of tensile elongation data is more conservative than the use of compressive strain data for determining structural fragility under both tensile and compressive strain conditions. While tensile elongations are more conservative than compressive strains, they are comparable (Ref. 2.2.38).

The most common measure of ductility (Ref. 2.2.38, pp. 4-12) is the elongation in the tensile test, i.e., the *engineering strain.* Thus, if L is the gage length at a point of plastic deformation or fracture and L_o is the initial gage length, then the engineering strain is

$$S = [(L - L_o)/ L_o] \qquad \text{(Eq. 6.3.7-1)}$$

Together, with the elongation, the initial gage length must also be specified since the elongation depends on the gage length used in the tensile test. The engineering strain is not completely satisfactory, since it is based on initial length, which is continuously changing under deformation stress. A better measure of ductility is the *true strain*

$$\varepsilon = \text{Log}[S+1] = \text{Log}\,(L / L_o) \qquad \text{(Eq. 6.3.7-2)}$$

The true strain represents a sort of average strain in going from one gage length to another (Ref. 2.2.38, pp. 4-12). The true strain measure for a brick element used in the LS-DYNA calculations is the equivalent plastic strain or EPS, which is defined in Eq. 6.3.7-3.

The fragility curve, which is used for determining the probability of structural failure, can be derived by fitting a probability density function (PDF) to the ASM (1976) (Ref. 2.2.23) engineering (tensile) strain data for stainless steel 304. The tensile test data for the 204 samples

from Ref. 2.2.23 exhibit a bimodal distribution of the frequency of elongation failure, as shown in Figure 6.3.7-2. This is a histogram of 2-in. coupon minimum engineering elongation or strain at failure versus the number of specimens (frequency) that failed at a particular strain value. Both the data and their corresponding log-transform (to true strain) were found to be non-normally distributed ($p < 10^{-4}$) by the Shapiro-Wilk test (Ref. 2.2.43). However, these data were determined to be reasonably well modeled as a sample from a weighted mixture of two normal distributions, one with a mean of 46% and a standard deviation of 2.24% (weight = 7.84%), and the other with a mean of 59.3% and a standard deviation of 4.22% (weight = 92.16%). To derive independent estimation errors of the estimated mean and standard deviation for each distribution contributing to the modeled normal mixture, they were first simulated using corresponding Student-t and chi-square distributions. The goodness of fit to a 95% confidence level for the mixed PDF was assessed by the Kolmogorov-Smirnov 1 sample test (Ref. 2.2.44). This probability distribution function was then converted by integration to a cumulative distribution function (CDF) that gives the probability of failure as a function of either engineering or true strain. This analysis uses true strain values to determine the probability of failure. The fragility curve may have to be adjusted by stochastic scaling, for instance, to account for variations in material properties or weld effects that are not adequately represented in the original data set.

Figure 6.3.7-3 provides a graphical representation of the fragility curve derived from the original tensile data set. The figure also contains a fragility curve adjusted for material properties used in this analysis, as discussed below. Table 6.3.7.3-1 provides a discrete tabulation of the original and adjusted probabilities of failure as a function of true strain values. Using this table, for a given true strain value, the probability of failure can be determined for either the original or adjusted curve. The true strain value may be native or modified (e.g., due to weld effects or triaxiality factor), as discussed in Sections 6.3.7.4 and 6.3.7.5, respectively.

The original modeled fragility curve in Figure 6.3.7-3 is based on data for stainless steel 304 annealed tubing, which has a large elongation at failure (Ref. 2.2.23). There are no data for Type 304 sheet/strip stainless steel in the document, and both Type 304 round bar and Type 301 sheet/strip data sets are smaller and show even greater elongation than the tubing data.

The steels in this report are 304L un-annealed, and they will have relatively shorter elongations at failure. Hence, the base CDF model was adjusted to different steels used in typical designs and to meet the code specification of the material model used in LS-DYNA. The adjustment consisted of shifting the engineering-strain distribution by -8.3%. Thus, the initial fragility curve was shifted by 8.3% to a lower value of minimum elongation (Figure 6.3.7-3), which leads to a higher estimated probability of failure, and thus more conservative results.

The basis for the 8.3% fragility curve shift is as follows. SAE specifications (Ref. 2.2.21, page 418, footnote of Table 8-9) suggest that the minimum engineering elongation should correspond to a failure probability of 1%, which corresponds to 43.3%, based on the original engineering fragility curve. Moreover, ASTM/ASME specifications (Ref. 2.2.46, page 346, Table 5) suggest that the minimum engineering strain for S304 specification used in LS-DYNA simulations should be 35%. Therefore, the maximum fragility curve shift amounts to 43.3% minus 35%, which is equal to 8.3%. These corrections (shifts) bound the probability of failure to the higher side, and thus more conservative probability estimates are provided.

For a particular impact condition, the maximum equivalent plastic strain (Max EPS) is obtained from the LS-DYNA simulation. For every finite element brick in the mesh model, the LS-DYNA simulation calculates an EPS (as per Eq. 6.3.7-3) for the final (accumulated) strains. The global maximum value of all EPS values for a simulation is taken to be the Max EPS. The calculated Max EPS is then the true strain value used in the fragility function to determine the probability of failure for the canister in that particular simulation.

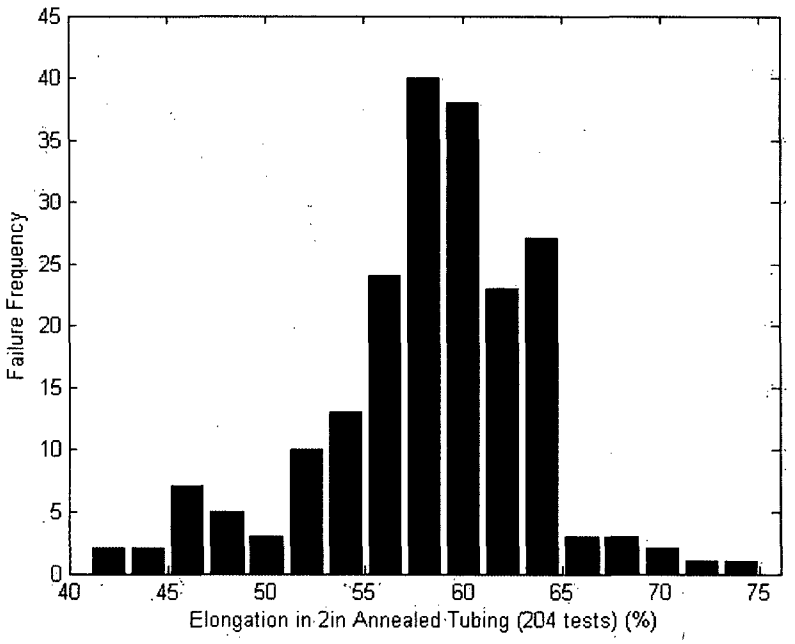

Figure 6.3.7-2. Histogram of Engineering Elongation Based on Ref. 2.2.23

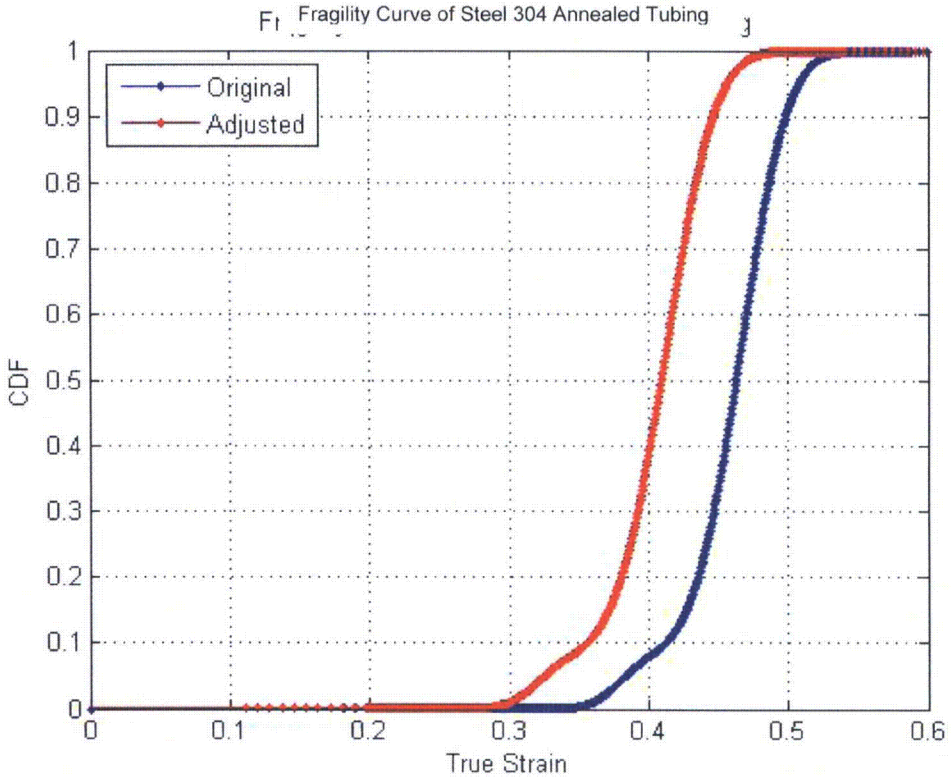

NOTE: The shifted curve is obtained by shifting the value of engineering strain for the original curve by -8.3%. The true strain is equal to ln (1 + engineering strain). For this analysis, the probability of failure is the CDF value of the failure frequency histogram (Figure 6.3.7-2), corresponding to the true strain equal to the Max EPS. The data for these CDF curves are tabulated in Table 6.3.7.3-1.

Figure 6.3.7-3. Original and Shifted Cumulative Distribution Function (CDF) of Capacity (or Fragility) Curves Plotted as a Function of True Strain

Table 6.3.7.3-1. Probability of Failure versus True Strain Tabulated for Figure 6.3.7-3

True Strain (TS)	$\frac{TS - TS_{mean}}{TS_{std}}$	Probability of Failure Original	Probability of Failure Adjusted (-8.3% shift)	True Strain (TS)	$\frac{TS - TS_{mean}}{TS_{std}}$	Probability of Failure Original	Probability of Failure Adjusted (-8.3% shift)
0.00	-1.70	0.0000E+00	1.6754E-15	0.36	0.05	1.0506E-02	1.0973E-01
0.01	-1.65	2.0924E-16	1.8688E-15	0.37	0.10	2.3978E-02	1.4282E-01
0.02	-1.60	4.1848E-16	2.0622E-15	0.38	0.15	4.3259E-02	1.9679E-01
0.03	-1.55	6.2772E-16	2.2555E-15	0.39	0.19	6.2863E-02	2.7687E-01
0.04	-1.50	8.3696E-16	2.4489E-15	0.40	0.24	7.9100E-02	3.8310E-01
0.05	-1.45	1.0462E-15	2.6422E-15	0.41	0.29	9.5539E-02	5.0814E-01
0.06	-1.41	1.2554E-15	2.8356E-15	0.42	0.34	1.2068E-01	6.3823E-01
0.07	-1.36	1.4647E-15	3.0290E-15	0.43	0.39	1.6410E-01	7.5736E-01
0.08	-1.31	1.6739E-15	3.2223E-15	0.44	0.44	2.3393E-01	8.5309E-01
0.09	-1.26	1.8832E-15	3.4157E-15	0.45	0.48	3.3371E-01	9.2036E-01
0.10	-1.21	2.0924E-15	3.6090E-15	0.46	0.53	4.5893E-01	9.6161E-01
0.11	-1.16	2.3016E-15	3.8024E-15	0.47	0.58	5.9615E-01	9.8363E-01
0.12	-1.11	2.5109E-15	2.8601E-14	0.48	0.63	7.2682E-01	9.9385E-01
0.13	-1.07	2.7201E-15	2.3645E-13	0.49	0.68	8.3454E-01	9.9797E-01
0.14	-1.02	2.9294E-15	1.6225E-12	0.50	0.73	9.1117E-01	9.9941E-01
0.15	-0.97	3.1386E-15	9.7686E-12	0.51	0.78	9.5806E-01	9.9985E-01
0.16	-0.92	3.3478E-15	5.2952E-11	0.52	0.82	9.8270E-01	9.9997E-01
0.17	-0.87	3.5571E-15	2.6233E-10	0.53	0.87	9.9379E-01	9.9999E-01
0.18	-0.82	3.7663E-15	1.2513E-09	0.54	0.92	9.9807E-01	1.0000E+00
0.19	-0.78	2.1733E-14	6.9107E-09	0.55	0.97	9.9948E-01	1.0000E+00
0.20	-0.73	2.1209E-13	2.6769E-08	0.56	1.02	9.9988E-01	1.0000E+00
0.21	-0.68	1.7358E-12	1.1600E-07	0.57	1.07	9.9998E-01	1.0000E+00
0.22	-0.63	1.1373E-11	4.8126E-07	0.58	1.11	1.0000E+00	1.0000E+00
0.23	-0.58	6.4625E-11	1.9316E-06	0.59	1.16	1.0000E+00	1.0000E+00
0.24	-0.53	4.1126E-10	7.5246E-06	0.60	1.21	1.0000E+00	1.0000E+00
0.25	-0.48	2.4773E-09	2.8566E-05	0.61	1.26	1.0000E+00	1.0000E+00
0.26	-0.44	1.2132E-08	1.0566E-04	0.62	1.31	1.0000E+00	1.0000E+00
0.27	-0.39	5.2343E-08	3.7635E-04	0.63	1.36	1.0000E+00	1.0000E+00
0.28	-0.34	2.4478E-07	1.2625E-03	0.64	1.41	1.0000E+00	1.0000E+00
0.29	-0.29	1.0945E-06	3.8474E-03	0.65	1.45	1.0000E+00	1.0000E+00
0.30	-0.24	4.7123E-06	1.0185E-02	0.66	1.50	1.0000E+00	1.0000E+00
0.31	-0.19	1.9709E-05	2.2466E-02	0.67	1.55	1.0000E+00	1.0000E+00
0.32	-0.15	7.9860E-05	4.0237E-02	0.68	1.60	1.0000E+00	1.0000E+00
0.33	-0.10	3.1104E-04	5.9110E-02	0.69	1.65	1.0000E+00	1.0000E+00
0.34	-0.05	1.1366E-03	7.5125E-02	0.70	1.70	1.0000E+00	1.0000E+00
0.35	**0.00**	**3.7379E-03**	**8.9858E-02**				

NOTE: The mean for true strain is 0.35, shown in bold. The standard deviation (std) of true strain is 0.21.
Source: Attachment 3.

6.3.7.4 Weldment Fragility Curve

The upper and lower canister lids are welded to the canister walls. The weldment areas may be subject to different mechanical properties than the native host material. Two scenarios are analyzed. Weldment areas have either (1) the same mechanical properties or (2) more brittle behavior than the native metal.

The mechanical properties of the weldment depend on the application of the weldment itself. The weldment in the best-case scenario can have the same mechanical properties as the host metal (native metal), but it is usually more brittle than the host metal. For the purposes of this study, the failure likelihood of the weldment substructure was considered to reflect weighting factors of 1.0 and 0.75 applied to estimate true strain at failure. Thus, another shift was applied to both the original and the adjusted fragility curves introduced in Section 6.3.7.3 to assess the effect of estimating the probabilities for the weldment. Failure probabilities were calculated for both cases and presented in Section 6.3.7.6.

6.3.7.5 The Relationship between Uniaxial and Triaxial Strains

The capacity function is based on tests of coupons in uniaxial tension. Cracking of stainless steel may not be determined simply by comparing the calculated Max EPS to the true strain in the fragility function (Figure 6.3.7-3) because Max EPS is calculated from a complex 3-D state of stress, while the true strain in the fragility function is determined under a 1-D state of stress. A 3-D state of stress may condition plastic flow in the material and modify the Max EPS at which failure occurs. The effective plastic strain (EPS) was calculated using the following equation (Ref. 2.2.38).

$$\mathrm{EPS} = \frac{\sqrt{2}}{3}\sqrt{(\varepsilon_1-\varepsilon_2)^2+(\varepsilon_2-\varepsilon_3)^2+(\varepsilon_1-\varepsilon_3)^2+6(\varepsilon_{12}{}^2+\varepsilon_{23}{}^2+\varepsilon_{13}{}^2)} \quad \text{(Eq. 6.3.7-3)}$$

where ε_i and ε_{ij} are the primary and secondary plastic strains in the 3-D (triaxial) space. Plastic strains are a direct output of the numerical simulations performed using LS-DYNA.

This change in ductility can be accounted for by the use of a triaxiality factor (TF), which is the ratio of normal stress to shear stress on the octahedral plane, normalized to unity for simple tension and given by the following equation (Ref. 2.2.39).

$$TF = \sqrt{2}\frac{\sigma_1+\sigma_2+\sigma_3}{\sqrt{(\sigma_1-\sigma_2)^2+(\sigma_2-\sigma_3)^2+(\sigma_1-\sigma_3)^2+6(\sigma_{12}{}^2+\sigma_{23}{}^2+\sigma_{13}{}^2)}} \quad \text{(Eq. 6.3.7-4)}$$

A value of TF greater than 1.0 is produced by a state of stress that constrains plastic flow, reduces ductility, and results in a higher likelihood of failure for a given value of EPS. A value of TF less than 1.0 is produced by a state of stress that enhances plastic flow, increases ductility and leads to a lower likelihood of failure for a given value of EPS. When TF is equal to 1.0, the state of stress is reduced to a uniaxial state. When TF is equal to 2.0, the state of stress is reduced to a biaxial state. The reduction in ductility is quantified by the ductility ratio (DR). This ratio is calculated as $DR = 2^{(1-TF)}$ for any TF greater than or equal to zero; otherwise, the ductility ratio is set to 2 (Refs. 2.2.39 and 2.2.40).

In this analysis, the cases that include the triaxiality effect, apply a ductility ratio of 0.5 (Assumption 3.2.3.4), which is based on a triaxiality factor of 2, corresponding to biaxial tension. For the purpose of determining failure probability (Figure 6.3.7-3), the Max EPS is multiplied by a factor of 2 for a ductility ratio of 0.5. This is reasonably conservative for the cylindrical-shell geometry of the respective containers. The ductility ratio of 0.5 is applied to all cases in which the triaxiality factor is included (Tables 6.3.7.6-1 through 6.3.7.6-3).

6.3.7.6 Failure Probability Results

Using the approach presented in Sections 6.3.7.3 through 6.3.7.5, canister failure probabilities for the aging overpack (AO), transportation cask (TC), and dual purpose canister (DPC) scenarios, presented in Sections 6.3.1 through 6.3.3, respectively, are determined (Tables 6.3.7.6-1 through 6.3.7.6-3). Idaho National Laboratory (Ref. 2.2.37) conducted similar structural analyses for DOE spent nuclear fuel (DSNF) and multi-canister overpack (MCO) canisters. Probability of failure for each of the components of the DSNF and MCO scenarios is calculated, based on the Max EPS results from Ref. 2.2.37, as given in Tables 6.3.7.6-4 and 6.3.7.6-5. The results in Table 6.3.7.6-4 and 6.3.7.6-5 are without consideration of triaxiality factor.

Table 6.3.7.6-1. Failure Probabilities with and without Triaxiality Factor, with and without the Fragility Curve Adjustment, for SNF Canister within Aging Overpack

Container Type/ Impact Condition[a]	Impact Condition Description	Section in Report	Max EPS[b]	Failure Probability[b]			
				Original CDF Fragility Curve w/o Adjustment		CDF Fragility Curve Adjusted for Minimum Elongation (-8.3% Shift)	
				w/o Triaxiality	w/ Triaxiality	w/o Triaxiality	w/ Triaxiality
A.IC 1	3-ft end drop, with vertical orientation	6.3.1.1	0.16%	$<1 \times 10^{-8}$	$<1 \times 10^{-8}$	$<1 \times 10^{-8}$	$<1 \times 10^{-8}$
A.IC 2	Slapdown from a vertical orientation and 2.5-mph horizontal velocity	6.3.1.2	0.82%	$<1 \times 10^{-8}$	$<1 \times 10^{-8}$	$<1 \times 10^{-8}$	$<1 \times 10^{-8}$

NOTE: [a] "A" stands for aging overpack. "IC" stands for impact condition (defined in Table 4.3.3-1a).
[b] Values of Max EPS and failure probability are applicable to the SNF canister.

Source: Attachment 3.

Table 6.3.7.6-2. Failure Probabilities with and without Triaxiality Factor, with and without the Fragility Curve Adjustment, for SNF Canister inside Transportation Cask

Container Type/ Impact Condition[a]	Impact Condition Description	Section in Report	Max EPS		Canister Failure Probability[b]			
					Original CDF Fragility Curve w/o Adjustment		CDF Fragility Curve Adjusted for Minimum Elongation (-8.3% Shift)	
			Canister[b]	Cask[c]	w/o Triaxiality	w/ Triaxiality	w/o Triaxiality	w/ Triaxiality
T.IC 1a	12-ft end drop, with 4-degree off-vertical orientation	6.3.2.1	3.53%	9.20%	$<1 \times 10^{-8}$	$<1 \times 10^{-8}$	$<1 \times 10^{-8}$	$<1 \times 10^{-8}$
T.IC 1b	13.1-ft end drop, with 4-degree off-vertical orientation	6.3.2.1	4.06%	9.37%	$<1 \times 10^{-8}$	$<1 \times 10^{-8}$	$<1 \times 10^{-8}$	$<1 \times 10^{-8}$
T.IC 1c	30-ft end drop, with 4-degree off-vertical orientation	6.3.2.1	5.77%	11.25%	$<1 \times 10^{-8}$	$<1 \times 10^{-8}$	$<1 \times 10^{-8}$	$<1 \times 10^{-8}$
T.IC 2a	13.1-ft end drop, with 4-degree off-vertical orientation, and approximated slapdown	6.3.2.2	4.35%	9.94%	$<1 \times 10^{-8}$	$<1 \times 10^{-8}$	$<1 \times 10^{-8}$	$<1 \times 10^{-8}$
T.IC 2b	Approximated slapdown from vertical orientation	6.3.2.2	1.25%	5.30%	$<1 \times 10^{-8}$	$<1 \times 10^{-8}$	$<1 \times 10^{-8}$	$<1 \times 10^{-8}$
T.IC 3	6-ft side drop, with 3-degree off-horizontal orientation	6.3.2.3	2.07%	7.42%	$<1 \times 10^{-8}$	$<1 \times 10^{-8}$	$<1 \times 10^{-8}$	$<1 \times 10^{-8}$
T.IC 4	10-ft drop of 10-metric-ton load onto top of cask	6.3.2.4	0.96%	1.76%	$<1 \times 10^{-8}$	$<1 \times 10^{-8}$	$<1 \times 10^{-8}$	$<1 \times 10^{-8}$
T.IC 5a	30-ft end drop, with vertical orientation	6.3.2.5	3.55%	3.17%	$<1 \times 10^{-8}$	$<1 \times 10^{-8}$	$<1 \times 10^{-8}$	$<1 \times 10^{-8}$
T.IC 5b	30-ft end drop, with 4-degree off-vertical orientation	6.3.2.5	5.77%	11.25%	$<1 \times 10^{-8}$	$<1 \times 10^{-8}$	$<1 \times 10^{-8}$	$<1 \times 10^{-8}$
T.IC 5c	30-ft end drop, with 45-degree off-vertical orientation	6.3.2.5	6.41%	70.56%	$<1 \times 10^{-8}$	$<1 \times 10^{-8}$	$<1 \times 10^{-8}$	$<1 \times 10^{-8}$
T.IC 5d	30-ft end drop, with center of gravity over corner (i.e., point of impact)	6.3.2.5	6.63%	44.88%	$<1 \times 10^{-8}$	$<1 \times 10^{-8}$	$<1 \times 10^{-8}$	$<1 \times 10^{-8}$

NOTE: [a] "T" stands for transportation cask. "IC" stands for impact condition (defined in Table 4.3.3-1a).
[b] Values of Max EPS and failure probability are applicable to the SNF canister.
[c] Values of Max EPS for the cask are applicable to the structural body of the transportation cask, which excludes the shield and shield shell. Note that the failure probability is not calculated for the cask by itself.

Source: Attachment 3.

Table 6.3.7.6-3. Failure Probabilities with and without Triaxiality Factor, with and without the Fragility Curve Adjustment, for Dual Purpose Canister

Container Type/ Impact Condition[a]	Impact Condition Description	Section in Report	Max EPS[b]	Canister Failure Probability[b]			
				Original CDF Fragility Curve w/o Adjustment		CDF Fragility Curve Adjusted for Minimum Elongation (-8.3% Shift)	
				w/o Triaxiality	w/ Triaxiality	w/o Triaxiality	w/ Triaxiality
D.IC 1a	32.5-ft end drop, with vertical orientation	6.3.3.1	2.13%	$<1 \times 10^{-8}$	$<1 \times 10^{-8}$	$<1 \times 10^{-8}$	$<1 \times 10^{-8}$
D.IC 1b	40-ft end drop, with vertical orientation	6.3.3.1	2.65%	$<1 \times 10^{-8}$	$<1 \times 10^{-8}$	$<1 \times 10^{-8}$	$<1 \times 10^{-8}$
D.IC 2a	23-ft end drop, with 4-degree off-vertical orientation	6.3.3.2	24.19%	$<1 \times 10^{-8}$	$\mathbf{7.71 \times 10^{-1}}$	$\mathbf{9.72 \times 10^{-6}}$	$\mathbf{9.96 \times 10^{-1}}$
D.IC 2b	10-ft end drop, with 4-degree off-vertical orientation	6.3.3.2	19.71%	$<1 \times 10^{-8}$	$\mathbf{7.01 \times 10^{-2}}$	$\mathbf{1.73 \times 10^{-8}}$	$\mathbf{3.19 \times 10^{-1}}$
D.IC 2c	5-ft end drop, with 4-degree off-vertical orientation	6.3.3.2	15.76%	$<1 \times 10^{-8}$	$\mathbf{4.10 \times 10^{-5}}$	$<1 \times 10^{-8}$	$\mathbf{3.12 \times 10^{-2}}$
D.IC 3	40-ft/min horizontal side collision	6.3.3.3	0.16%	$<1 \times 10^{-8}$	$<1 \times 10^{-8}$	$<1 \times 10^{-8}$	$<1 \times 10^{-8}$
D.IC 4	10-ft drop of 10-metric-ton load onto top of canister	6.3.3.4	0.75%	$<1 \times 10^{-8}$	$<1 \times 10^{-8}$	$<1 \times 10^{-8}$	$<1 \times 10^{-8}$
D.IC 2a S1-L1[c]	Same as D.IC 2a	6.3.3.6	24.19%	$<1 \times 10^{-8}$	$\mathbf{7.71 \times 10^{-1}}$	$\mathbf{9.72 \times 10^{-6}}$	$\mathbf{9.96 \times 10^{-1}}$
D.IC 2a S2-L1	Same as D.IC 2a	6.3.3.6	21.52%	$<1 \times 10^{-8}$	$\mathbf{1.66 \times 10^{-1}}$	$\mathbf{2.44 \times 10^{-7}}$	$\mathbf{7.62 \times 10^{-1}}$
D.IC 2a S3-L1	Same as D.IC 2a	6.3.3.6	16.53%	$<1 \times 10^{-8}$	$\mathbf{3.37 \times 10^{-4}}$	$<1 \times 10^{-8}$	$\mathbf{6.02 \times 10^{-2}}$
D.IC 2a S1-L2	Same as D.IC 2a	6.3.3.6	23.34%	$<1 \times 10^{-8}$	$\mathbf{5.52 \times 10^{-1}}$	$\mathbf{3.07 \times 10^{-6}}$	$\mathbf{9.78 \times 10^{-1}}$
D.IC 2a S1-L3	Same as D.IC 2a	6.3.3.6	25.15%	$<1 \times 10^{-8}$	$\mathbf{9.28 \times 10^{-1}}$	$\mathbf{3.48 \times 10^{-5}}$	**1.00**
D.IC 2a S2-L3	Same as D.IC 2a	6.3.3.6	22.57%	$<1 \times 10^{-8}$	$\mathbf{3.50 \times 10^{-1}}$	$\mathbf{1.07 \times 10^{-6}}$	$\mathbf{9.28 \times 10^{-1}}$
D.IC 2a S3-L3	Same as D.IC 2a	6.3.3.6	18.08%	$<1 \times 10^{-8}$	$\mathbf{1.22 \times 10^{-2}}$	$<1 \times 10^{-8}$	$\mathbf{1.14 \times 10^{-1}}$
D.IC 2a S2-L4	Same as D.IC 2a	6.3.3.6	24.07%	$<1 \times 10^{-8}$	$\mathbf{7.44 \times 10^{-1}}$	$\mathbf{8.27 \times 10^{-6}}$	$\mathbf{9.95 \times 10^{-1}}$
D.IC 2a S3-L4	Same as D.IC 2a	6.3.3.6	19.50%	$<1 \times 10^{-8}$	$\mathbf{6.29 \times 10^{-2}}$	$\mathbf{1.37 \times 10^{-8}}$	$\mathbf{2.77 \times 10^{-1}}$

NOTE: [a] D" stands for dual purpose canister. "IC" stands for impact condition (defined in Table 4.3.3-1a).
[b] Values of Max EPS and failure probability are applicable to the SNF canister.
[c] See Table 6.3.3.6-1 for definitions of S1, L1, etc.

Source: Attachment 3.

Table 6.3.7.6-4. Failure Probabilities without Triaxiality Factor, with and without Fragility Curve Adjustment, for DOE Spent Nuclear Fuel (DSNF) Canisters, Analyzed by Ref. 2.2.37

18-Inch DSNF Canister Subjected to a 3-Degree Off-Vertical Drop, 300°F (148.9°C)									
Structural Component	Max EPS[a]			Failure Probability[a]					
				Original CDF Fragility Curve w/o Adjustment			CDF Fragility Curve Adjusted for Minimum Elongation (-8.3% Shift)		
	Outside Surface	Middle	Inside Surface	Outside Surface	Middle	Inside Surface	Outside Surface	Middle	Inside Surface
Lower Head	8%	3%	6%	$<1 \times 10^{-8}$	$<1 \times 10^{-8}$	$<1 \times 10^{-8}$	$<1 \times 10^{-8}$	$<1 \times 10^{-8}$	$<1 \times 10^{-8}$
Lower-Head-to-Shell Weld	2%	2%	3%	$<1 \times 10^{-8}$	$<1 \times 10^{-8}$	$<1 \times 10^{-8}$	$<1 \times 10^{-8}$	$<1 \times 10^{-8}$	$<1 \times 10^{-8}$
Main Shell	2%	2%	3%	$<1 \times 10^{-8}$	$<1 \times 10^{-8}$	$<1 \times 10^{-8}$	$<1 \times 10^{-8}$	$<1 \times 10^{-8}$	$<1 \times 10^{-8}$
Upper-Head-to-Shell Weld	0%	0%	0%	$<1 \times 10^{-8}$	$<1 \times 10^{-8}$	$<1 \times 10^{-8}$	$<1 \times 10^{-8}$	$<1 \times 10^{-8}$	$<1 \times 10^{-8}$
Upper Head	1%	0.2%	2%	$<1 \times 10^{-8}$	$<1 \times 10^{-8}$	$<1 \times 10^{-8}$	$<1 \times 10^{-8}$	$<1 \times 10^{-8}$	$<1 \times 10^{-8}$

24-Inch DSNF Canister Subjected to a 3-Degree Off-Vertical Drop, 300°F (148.9°C)									
Structural Component	Max EPS[a]			Failure Probability[a]					
				Original CDF Fragility Curve w/o Adjustment			CDF Fragility Curve Adjusted for Minimum Elongation (-8.3% Shift)		
	Outside Surface	Middle	Inside Surface	Outside Surface	Middle	Inside Surface	Outside Surface	Middle	Inside Surface
Lower Head	2%	0.7%	1%	$<1 \times 10^{-8}$	$<1 \times 10^{-8}$	$<1 \times 10^{-8}$	$<1 \times 10^{-8}$	$<1 \times 10^{-8}$	$<1 \times 10^{-8}$
Lower-Head-to-Shell Weld	0.2%	0.3%	0.5%	$<1 \times 10^{-8}$	$<1 \times 10^{-8}$	$<1 \times 10^{-8}$	$<1 \times 10^{-8}$	$<1 \times 10^{-8}$	$<1 \times 10^{-8}$
Main Shell	0.2%	0.3%	0.5%	$<1 \times 10^{-8}$	$<1 \times 10^{-8}$	$<1 \times 10^{-8}$	$<1 \times 10^{-8}$	$<1 \times 10^{-8}$	$<1 \times 10^{-8}$
Upper-Head-to-Shell Weld	0%	0%	0%	$<1 \times 10^{-8}$	$<1 \times 10^{-8}$	$<1 \times 10^{-8}$	$<1 \times 10^{-8}$	$<1 \times 10^{-8}$	$<1 \times 10^{-8}$
Upper Head	0%	0%	0%	$<1 \times 10^{-8}$	$<1 \times 10^{-8}$	$<1 \times 10^{-8}$	$<1 \times 10^{-8}$	$<1 \times 10^{-8}$	$<1 \times 10^{-8}$

NOTE: [a]Values of Max EPS and failure probability are applicable to the specified structural component and location within the SNF canister. Note that in Ref. 2.2.37, PEEQ, which stands for peak equivalent plastic strain, is equivalent to Max EPS.

Source: Ref. 2.2.37 and Attachment 3.

Table 6.3.7.6-5. Failure Probabilities without Triaxiality Factor, with and without Fragility Curve Adjustment, for the Multi-Canister Overpack (MCO), Analyzed by Ref. 2.2.37

4 MCO Subjected to a 3-Degree Off-Vertical Drop, 70°F (21.1°C)									
Structural Component	Max EPS[a]			Failure Probability[a]					
				Original CDF Fragility Curve w/o Adjustment			CDF Fragility Curve Adjusted for Minimum Elongation (-8.3% Shift)		
	Outside Surface	Middle	Inside Surface	Outside Surface	Middle	Inside Surface	Outside Surface	Middle	Inside Surface
Bottom	35%	16%	14%	**3.74×10^{-3}**	$<1 \times 10^{-8}$	$<1 \times 10^{-8}$	**8.99×10^{-2}**	$<1 \times 10^{-8}$	$<1 \times 10^{-8}$
Bottom-to-Main Shell	21%	11%	11%	$<1 \times 10^{-8}$	$<1 \times 10^{-8}$	$<1 \times 10^{-8}$	**1.16×10^{-7}**	$<1 \times 10^{-8}$	$<1 \times 10^{-8}$
Main Shell	13%	15%	29%	$<1 \times 10^{-8}$	$<1 \times 10^{-8}$	**1.09×10^{-6}**	$<1 \times 10^{-8}$	$<1 \times 10^{-8}$	**3.85×10^{-3}**
Collar	0%	0%	0%	$<1 \times 10^{-8}$	$<1 \times 10^{-8}$	$<1 \times 10^{-8}$	$<1 \times 10^{-8}$	$<1 \times 10^{-8}$	$<1 \times 10^{-8}$
Cover	0%	0%	0%	$<1 \times 10^{-8}$	$<1 \times 10^{-8}$	$<1 \times 10^{-8}$	$<1 \times 10^{-8}$	$<1 \times 10^{-8}$	$<1 \times 10^{-8}$

NOTE: [a]Values of Max EPS and failure probability are applicable to the specified structural component and location within the SNF canister. Note that in Ref. 2.2.37, PEEQ, which stands for peak equivalent plastic strain, is equivalent to Max EPS.

Source: Ref. 2.2.37 and Attachment 3.

7. RESULTS AND CONCLUSIONS

7.1 RESERVED

7.2 SEISMIC ANALYSES OF EMPLACED WASTE PACKAGES

Results of these analyses indicate a probability of 5.0×10^{-7} that a seismic event occurring during the 100-year preclosure period causes damage leading to stress corrosion cracking for the outer corrosion barrier of the TAD-bearing waste package. The corresponding probability of damage for the codisposal waste package is 7.3×10^{-4}. Rupture of the waste package outer corrosion barriers is not predicted by the analyses for the 100-year preclosure period for both types of packages.

Results also show that there is a probability of 2.6×10^{-3} that the waste packages and/or pallets will come into contact with the drip shield, assuming it is present, due to a seismic event during the 100-year preclosure period. This is a reasonable upper bound for the probability that a seismic event prior to drip shield emplacement would displace the waste packages and pallets such that drip shield emplacement at a later time would be affected.

7.3 STRUCTURAL FAILURE ANALYSES OF CONTAINERS SUBJECT TO DROP-IMPACT LOADS

7.3.1 Aging Overpack Canisters

The maximum effective plastic strains (Max EPS) within the canister inside the aging overpack are very low (less than 1%), for both a 3-ft vertical end drop and for a tip over slapdown impact. As a result, the probability of canister failure is less than 1×10^{-8}. The Max EPS for the 3-ft vertical end drop occurs at the bottom of the canister, while the Max EPS for the tip over slapdown impact occurs at the top of the canister where the impact velocity is greatest.

Transportation Casks with SNF Canisters

The Max EPS within the canister inside the transportation casks are low for all impact conditions and have a probability of canister failure of less than 1×10^{-8}. The impact condition with the lowest Max EPS (0.96%) was the 10-ft drop of the 10 metric-ton mass on the top of the cask. The tip over slapdown impact resulted in a Max EPS of 1.25% and the 6-ft side drop at an angle of 3 degrees resulted in a Max EPS of 2.07%.

The most severe impacts were the corner drop impacts. This is shown by the increase in Max EPS for a 30-ft drop from 3.55% for an end drop, to 5.77% for a 4-degree corner drop, to 6.41% for a 45-degree corner drop, and to 6.63% for the most severe corner impact, where the center of gravity of the cask/canister is over the impact corner.

The Max EPS is also a function of drop height. As the drop height increases for the 4-degree impact orientation from 12 ft to 30 ft, the Max EPS increases from 3.53% to 5.77%.

Dual Purpose Canisters

The Max EPS within the dual purpose canister is fairly low for vertical end-drop impact conditions, resulting in a probability of canister failure of less than 1×10^{-8}. The Max EPS was 2.13% for a 32.5-ft vertical end drop and 2.65% for a 40-ft vertical end drop. For a 10-ft drop of a 10 metric-ton mass onto the top of the canister, the predicted Max EPS was 0.75%, and for a 40-ft/min horizontal collision onto the canister side, the Max EPS was 0.16%.

The most severe impacts were the 4-degree off-vertical corner drop, where the Max EPS ranged from 15.76% for a 5-ft drop to 24.19% for a 23-ft drop height. The 23-ft corner drop at a 4-degree angle was also studied with regard to the effect of changes in the canister geometry by varying the shell and bottom plate thicknesses. The geometry study showed that for a given bottom plate thickness, Max EPS decreases with increasing shell thickness. The study also showed that for a given shell thickness, Max EPS increases with increasing bottom plate thickness.

ATTACHMENT 1:RESERVED

ATTACHMENT 2: FILES FOR SEISMIC ANALYSES OF EMPLACED WASTE PACKAGES

The following is the "readme" document describing the files in the data CD for the seismic analyses.

README DOCUMENT FOR ATTACHMENT 2

- **TITLE OF DATA**: Preclosure Seismic Results for Damaged Area, Rupture, and Drip Shield Contact of TAD-bearing and Co-Disposal Waste Packages.
- **DESCRIPTION OF DATA**: The files in this attachment document damaged area, rupture, and drip shield contact assessments for TAD-bearing and Co-Disposal waste packages for preclosure seismic events for 000-PSA-MGR0-02100-000-00A.

FILE LISTING:

README_Preclosure_Seismic_Attachment_2.doc (this document)
Preclosure_Seismic_Attachment_2.zip
(1 zip file containing the 6 files listed below, which include 1 tar file that contains a total of 340 files)
Prob of Damage for CDSP Intact Internals 100 years.xls
Prob of Damage for TAD bearing Intact Internals 100 years.xls
Max Eff Strain for preclosure.xls
Prob of Contact between WP or Pallet and DS 100 years.xls
WPPallet_DS_Contact_file_listing.xls*
WPPallet_DS_Contact.tar.gz
*** Contains the file and directory listing for the tar file included in the attachment.**

Notes

1. The file listing spreadsheet includes zero-length sub-directories. Thus, there is a difference between the number of files displayed in the tar file and the number of files and subdirectories listed in the spreadsheet. There are 72 sub-directories in WPPallet_DS_Contact_file_listing.xls. Subtracting this number from the total number of files and sub-directories (412) yields 340 files. This is the number of files contained in WPPallet_DS_Contact.tar.gz.
2. File Preclosure_Seismic_Attachment_2.zip has a file length of 81,002,496 bytes. The 6 files, when extracted, require approximately 200MB of disk space. Uncompressing the compressed archive file (file with name ending with tar.gz), requires approximately 2.1GB of disk space. The contents of the compressed archive files, when extracted, require approximately 2.1GB of disk space. If all files are extracted from the ZIP file, all compressed archive files are uncompressed, and all files are extracted from the archive files, the total required space is approximately 4.5GB.

Software

- Microsoft Excel – Usage Software
- LS-PREPOST – Usage Software

Source DTNs:

MO0501BPVELEMP.001 - BOUNDED HORIZONTAL PEAK GROUND VELOCITY HAZARD AT THE REPOSITORY WASTE EMPLACEMENT LEVEL. [DIRS 172682]

MO0703PASDSTAT.001 - STATISTICAL ANALYSES FOR SEISMIC DAMAGE ABSTRACTIONS. [DIRS 182878]

LL0704PA048SPC.023 - LS-DYNA KINEMATIC DAMAGED AREA ANALYSES FOR THE TAD-BEARING WASTE PACKAGE APRIL 2007. [DIRS 180735]

LL0704PA049SPC.024 - LS-DYNA KINEMATIC DAMAGED AREA ANALYSES FOR THE 5-DHLW/DOE SNF-LONG CO-DISPOSAL WASTE PACKAGE APRIL 2007. [DIRS 180736]

Attachment File Information

The files in this attachment document damaged area, rupture, and drip shield contact assessments for TAD-bearing and Co-Disposal waste packages for preclosure seismic events for 000-PSA-MGR0-02100-000-00A. The following abbreviations are utilized in the spreadsheet files:

PGV = Peak Ground Velocity
RST = Residual Stress Threshold
TSPA = Total System Performance Assessment
TAD = Transportation, Aging, and Disposal
CDSP = Co-Disposal
WP = Waste Package

Six files are available in the ZIP file in the attachment:

File name:	Probability of Damage for CDSP Intact Internals 100 years.xls
File date/time:	10/02/2007, 5:14 PM
Description:	Calculation of the probability that a seismic event will cause damage to a CDSP waste package during the first 100 years after emplacement leading to stress corrosion cracking
File name:	Probability of Damage for TAD bearing Intact Internals 100 years.xls
File date/time:	10/02/2007, 5:14 PM
Description:	Calculation of the probability that a seismic event will cause damage to a TAD-bearing waste package during the first 100 years after emplacement leading to stress corrosion cracking
File name:	Max Eff Strain for preclosure.xls
File date/time:	09/28/2007, 3:12 PM
Description:	Determination of the bounding maximum effective strain for TAD-bearing and CDSP waste packages from impacts caused by a seismic event occurring during the first 100 years after emplacement
File name:	Prob of Contact between WP or Pallet and DS 100 years.xls
File date/time:	10/04/2007, 5:13 PM
Description:	Calculation of the probability that a seismic event will cause the waste packages and/or pallets to contact the drip shield during the first 100 years after emplacement (based on the CRV files contained in the file WPPallet_DS_Contact.tar.gz)
File name:	WPPallet_DS_Contact_file_listing.xls

File date/time: 10/05/2007, 1:47 PM
Description: File listing for waste package/pallet to drip shield contact archive file

File name: WPPallet_DS_Contact.tar.gz
File date/time: 10/05/2007, 1:28 PM
Description: Archive file (compressed) containing waste package/pallet to drip shield contact curve files

Caveat

File times are from a Windows machine, and may vary on different operating systems.

ATTACHMENT 3: FILES FOR STRUCTURAL FAILURE ANALYSES OF CONTAINERS SUBJECT TO DROP-IMPACT LOADS

The following is the "readme" document describing the files in the data CD for the seismic analyses.

README DOCUMENT FOR ATTACHMENT 3

- **TITLE OF DATA**: Preclosure Structural Results for Various Impact Conditions Applied to the Aging Overpack, the Transportation Cask, and the Dual Purpose Canister.
- **DESCRIPTION OF DATA**: The files in this attachment document inputs and results for preclosure structural impact analyses for 000-PSA-MGR0-02100-000-00A.
- **FILE LISTING:**

README_Preclosure_Structural_Attachment_3.doc (this document)
Preclosure_Structural_Attachment_3.zip
(1 zip file containing the 3 files listed below, which include 1 tar file that contains a total of 184 files)
Preclosure_Structural_Summary_of_Results.xls
Preclosure_Structural_Attachment_3.tar.gz (contains a total of 184 files)
Preclosure_Structural_Attachment_3_file_listing.xls*
SteelCDF.m
adfZ.dat

*** Contains the file and directory listing for the tar file included in the attachment.**

Notes

1. The file listing spreadsheet includes zero-length sub-directories. Thus, there is a difference between the number of files displayed in the tar file and the number of files and subdirectories listed in the spreadsheet. There are 39 sub-directories in Preclosure_Structural_Attachment_3_file_listing.xls. Subtracting this number from the total number of files and sub-directories (223) yields 184 files. This is the number of files contained in Preclosure_Structural_Attachment_3.tar.gz.
2. File Preclosure_Structural_Attachment_3.zip has a file length of 303,804,416 bytes. The 5 files, when extracted, require approximately 0.4GB of disk space. Uncompressing the compressed archive file (file with name ending with tar.gz), requires approximately 1.8GB of disk space. The contents of the compressed archive files, when extracted, require approximately 1.8GB of disk space. If all files are extracted from the ZIP file, all compressed archive files are uncompressed, and all files are extracted from the archive files, the total required space is approximately 4.3GB.

Software

- Microsoft Excel – Usage Software
- MATLAB – Usage Software
- LS-PREPOST – Usage Software
- LS-DYNA V. 971.7600.398, STN 10300-971.7600.398-00, AMD Opteron, RedHat Linux

Attachment File Information

The files in this attachment document inputs and results for preclosure structural impact analyses for 000-PSA-MGR0-02100-000-00A. NOTE: File times are from a Windows machine, and may vary on different operating systems.

Three files are available in the ZIP file in the attachment:

File name: Preclosure_Structural_Summary_of_Results.xls
File date/time: 1/14/2008, 1:35 PM
Description: Excel workbook containing a tabular summary of the impact conditions, model parameters, effective plastic strain results, and probabilities of failure for the structural impact analyses

File name: Preclosure_Structural_Attachment_3.tar.gz
File date/time: 2/14/2008, 8:34 AM
Description: Archive file (compressed) containing input and results for structural impact analyses

File name: Preclosure_Structural_Attachment_3_file_listing.xls
File date/time: 2/14/2008, 9:10 AM
Description: File listing for structural impact analysis archive file

File name: SteelCDF.m
File date/time: 1/14/2008, 3:46 PM
Description: MATLAB script for calculating probability of failure based on a maximum EPS value

File name: adfZ.dat
File date/time: 11/7/2007, 10:35AM
Description: Input data file for MATLAB Script SteelCDF.m, containing probability of failure vs. elongation (Engineering Strain

MATLAB Script Information

The MATLAB script SteelCDF.m performs the following operations:

- Reads in Probability of Failure vs. Engineering Strain curve from file adfZ.dat
- Converts curve to True Strain
- Prompts user for shift in percent of Engineering Strain curve (default 8.3%)
- Converts adjusted curve to True Strain
- Prompts user whether to use original or adjusted curve (default original)
- Plots Probability of Failure vs. True Strain curves (original and adjusted) in both linear and semi-log scales
- Calculates mean and standard deviations of the Probability and True Strain
- Prompts user for EPS value and calculates Probability of Failure

NOTE: To determine probability of failure with triaxiality factor, enter two times the Max EPS value (e.g., if Max EPS = 0.10, enter Max EPS = 0.20 for triaxiality factor)